VAAL UNIVERSITY
OF TECHNOLOGY

Adsorption of Nitrate and Fluoride anions from aqueous solutions using doped magnetite-pinecone nanocomposites.

Thesis submitted to the Vaal University of Technology
in fulfilment of the requirement for the award of
the degree of Master of Technology in
Chemistry
by

Nonhlanhla Frans

Student number: (209001283)

Promoter: Dr. A. Pholosi

Co-promoter: Prof A.E Ofomaja

Co-promoter: Dr. S. Akpotu

Date: 23 March 2022

DECLARATION

I declare that this dissertation is my work. It is being submitted for the Degree Magister Technologiae to the Department of Chemistry, Vaal University of Technology, Vanderbijlpark. It has not been submitted before for any degree or examination to any other University.

_____ on this ____23_____day of _____March_____2022

CANDIDATE

_____on this _____day of _____2021

SUPERVISOR

_____on this _____day of _____2021

CO-SUPERVISOR

DEDICATION

To loving husband Adeniyi Thompson Adewumi, my loving mother Masitimela Frans and my entire family for their support.

ACKNOWLEDGEMENTS

I sincerely wish to express my deepest appreciation and gratitude to the following for their various contributions:

- My supervisors; Prof A.E Ofomaja, Dr A. Pholosi and Dr S. Akpotu for their educative inputs and support throughout this research.
- The Vaal University of Technology through the Research Directorate for providing the research funding.
- Sasol for providing funding.
- The Applied and Computer Sciences Faculty Department of Chemistry for providing the structures necessary for the research.
- The postgraduate student's adsorption group in the research laboratory for support.
- My loving husband Adeniyi Thompson Adewumi, my loving mother Masitimela Frans and my entire family for their support.
- The almighty God for protecting me throughout my studies.

Table of Contents

LISTS OF FIGURES

LIST OF TABLES

LISTS OF ABBREVIATIONS AND SYMBOLS

q_e	Equilibrium capacity
q_t	Equilibrium capacity at time t
k_1	Pseudo-first order rate constant
k_2	Pseudo-second order rate constant
$t^{0.5}$	The time in min raised to the power of 0.5
r^2	Coefficient of determination
C_o	Initial Concentration
C_e	Equilibrium concentration
m	Mass of the adsorbent
V	Solution volume
% R	Percentage removal
h	Initial sorption rate
k_i	Intraparticle diffusion rate constant
K_a	Langmuir equilibrium constant
K_F	Freundlich capacity constant
n	Freundlich affinity constant
C_s	Saturation concentration of solute
D_1	Film diffusion coefficient
D_2	Pore diffusion coefficient
KB	Constant expressive of energy of interaction with the surface.
qe,m	Equilibrium capacity obtained by calculating from model
ΔG	Change of Gibbs free energy

ΔH	Change of enthalpy
ΔS	Change of entropy
E_a	Activation energy
t	time
PCP	Pinecone powder
MNPs	Magnetic Nano Particles
MNP-PCP	Magnetite pinecone powder nanocomposite
Mn- MNP-PCP	Manganese doped Magnetite pinecone powder nanocomposite
Ln- MNP-PCP	Lanthanum doped Magnetite pinecone powder nanocomposite
M-MNP-PCP	Metal doped Magnetite pinecone powder nanocomposite
NO_3^-	Nitrate
F^-	Fluoride
SO_4^{2-}	Sulphate
XRF	X-Ray fluorescence
FTIR	Fourier-transform infrared spectroscopy
XRD	X-ray diffraction
TGA	Thermogravimetric analysis
TEM	Transmission Electron Microscopy
ISE	Ion Selective Electrode
pH_{pzc}	pH at point zero charge
XPS	X-ray Photoelectron Spectroscopy
EDX	Electron dispersive spectroscopy
SEM	Scanning electron microscopy

PRESENTATIONS

Conferences contributions

Nonhlanhla Frans, Augustine E.Ofomaja, Agnes Pholosi. REMOVAL OF NITRATE FROM WATER USING DOPED MAGNETITE-PINECONE NANOCOMPOSITE ADSORPTIVE CAPACITY. The 4th Vaal University of Technology (VUT) Interdisciplinary Research and Postgraduate Conference, 17 October 2018 (Vanderbijlpark).

Nonhlanhla Frans, Augustine E.Ofomaja, Agnes Pholosi. REMOVAL OF NITRATE FROM WATER USING LANTHANUM DOPED MAGNETITE-PINECONE NANOCOMPOSITE. Young Water Professionals (YWP) 6th Biennial Conference, 20th -23rd of October 2019 at the Inkosi Albert Luthuli International Convention Centre (Durban ICC).

ABSTRACT

The increasing rate of pollutants, such as nitrate and fluoride from industrial and agricultural sources in the environment, especially in water bodies, is becoming alarming. Excessive nitrate and fluoride concentration in water cause environmental toxicity and hazard such as eutrophication and toxic, chronic illnesses such as methemoglobinemia. Hence, there is an urgent need to remove these pollutants from water. There have been a few successful strategies for the purification of pollutants contaminated water. Adsorption has been applied to remove pollutants from aqueous media due to its flexibility, ease of use, cost-effectiveness and ability to adsorb contaminants at low concentrations. Various adsorbents have been applied to remove nitrate and fluoride anions, and doped magnetic has shown to be effective in removing these anions.

In this study, manganese doped magnetite coated pinecone (Mn-MNP-PCP) and lanthanum doped magnetite coated pinecone (La-MNP-PCP) nanocomposite were prepared using the co-precipitation method. Fourier Transform Infra-Red (FT-IR), Scanning electron microscopy (SEM), Energy-dispersive x-ray spectroscopy (EDS), Thermo-gravimetric analysis (TGA), X-ray diffraction (XRD) were used to determine the surface groups, structure and morphology, chemical composition, thermal stability and phase determination (amorphous or crystalline) structure of the synthesised Mn-MNP-PCP and La-MNP-PCP adsorbents, respectively. In addition, batch adsorption experiments were conducted to evaluate the effects of solution pH, adsorbent dose, initial solution concentrations, contact time, adsorption kinetics, adsorption isotherm and the impact of co-existing anions on the adsorption of nitrate and fluoride ions. The mechanism of adsorption processes was also determined using equilibrium isotherm modelling results and thermodynamic parameters.

The maximum adsorption capacity of Mn-MNP-PCP and La-MNP-PCP adsorbents for nitrate adsorption was 22.8 mg/g and 37.7 mg/g at solution pH 4, while the adsorption efficiency was 45.6% and 75.4%. Fluoride removal occurred at pH 2 with the adsorption capacity of 46.2 mg/g and 44.77 mg/g with the removal efficiency of 92.4 % and 89.6% on both Mn-MNP-PCP and La-MNP-PCP adsorbents.

The optimum adsorbent dose for both Mn-MNP-PCP and La-MNP-PCP in the adsorption of nitrate and fluoride was 1 g/L. The optimum time for the uptake of nitrate and fluoride onto MNP-PCP and La-MNP-PCP was between 15 – 20 min. The competing phosphate

and sulphate ions impacted the nitrate adsorption, while the presence of carbonate and chloride had positive nitrate adsorption onto both Mn-MNP-PCP and La-MNP-PCP nanocomposites. The decrease in nitrate adsorption may be attributed to the lower affinity of Mn-MNP-PCP and La-MNP-PCP for nitrate and a competition between the nitrate ions and co-existing anions for the active sites. The presence of all competitive ions decreased the fluoride adsorption onto Mn-MNP-PCP and La-MNP-PCP nanocomposites. The multi-valent anion with higher charge density have been reported to be more readily adsorbed than monovalent anion.

The equilibrium data for nitrate and fluoride ions uptake was best described by Langmuir isotherm, which predicts the formation of ionic or covalent chemical bonds between the adsorbent and adsorbate. In the same vein, pseudo-second-order model is considerably suitable for nitrate and fluoride ions adsorption, which showed that their uptake was fast. Conclusively, La-MNP-PCP adsorbent is an effective adsorbent for nitrate adsorption, while Mn-MNP-PCP effectively trmoved fluoride ions from the aqueous solution.

CHAPTER 1

1.1 INTRODUCTION

Water pollution is a significant worldwide issue, particularly in sub-Saharan Africa, where individuals rely on groundwater for drinking (Lapworth et al., 2017). Water quality in waterways and underground has worsened because of pollution from urban, industrial and agricultural waste and contaminants (Selvakumar et al., 2017). Point and non-point pollution sources such as urban runoff and farming, improper disposal of sanitary and industrial waste, septic tank leakage, landfill leachate and animal manure, pollute water bodies such as streams, rivers, seas/oceans that end up in the underground water (Sadegh *et al*., 2017; Iriel *et al*., 2018). Due to the natural existence of these water bodies in the Earth's crust and modern human operations, particularly manufacturing and natural factors such as rain, they can enter the groundwater (Singh et al., 2020; Jain et al., 2021). These have resulted in a shortage of clean water and soil disturbances, restricting crop output and have influenced underdeveloped/developing countries or villages where they rely on groundwater for drinking (Rodriguez-Narvaez *et al*., 2017).

Surface and groundwater have been water sources for agricultural, municipal, and industrial customers over the millennia (Kookana et al., 2020). Rivers supplied hydroelectric power and cheap forms of bulk cargo transportation. They provided recreational opportunities for people based on water and water sources for wildlife and their habitats. A rise in the world's population has led to increased pollution of water bodies due to human discharges, including solid waste such as refuse dumps, sewage, industrial effluents, among others. It has also caused significantly increased pressure on natural resources, including air, water, and soil assets. The fast development of sectors, food, health care, and cars, is essential to meet people's requirements. Despite all the innovations, which are unfavourable to the setting in which we reside unless adequate management is implemented, it very challenging to maintain the quality of life.

Considering severe health problems associated with excess nitrate and fluoride concentrations in drinking water, various environmental regulatory bodies have laid down the concentration guidelines for some anions and metals, including the World Health Organisation (WHO). Concentration limits of 50, 1.5, 250, and 0.001 mg/L have been set for Nitrate, Fluoride,

Sulphate and Mercury, respectively, in drinking water. Therefore, the anion/metal ratios must be reduced to acceptable limits (Iriel *et al*., 2018; Sadegh *et al*., 2017).

The removal of these anions can be carried out through different methods. However, the commonly used treatment methods for removing excess pollutants from water include adsorption, ion exchange, reverse osmosis, electrodialysis, and denitrification (Blandin *et al*., 2016; Foroutan *et al*., 2017; Sadegh *et al*., 2017). Adsorption is recognized in wastewater treatment processes as the most efficient, promising and easy-to-use technique (Barakat, 2011). Moreover, adsorption can eliminate or minimize various types of contaminants from dilute solutions to $\mu g/dm^3$ (ppb) amounts, extending its use to control water pollution (Iriel *et al*., 2018). Although it requires highly efficient adsorbents, various artificial and natural materials have been explored as effective adsorbents to remove pollutants from water; namely magnetic nanoparticles, activated carbons, chitosan beads, polymeric resins and polymeric composites (Bhatnagar and Sillanpää, 2010). Recent advances in nanotechnology and metal oxides nanomaterial synthesis have significantly impacted fluoride and nitrate removal compared to other conventional adsorbents and processes (Al-Rashdi *et al*., 2011). These oxide nanomaterials, such as iron oxide and zinc oxide, are highly stable in adsorbing fluorides and nitrate from aqueous solutions and are rich in surface functional groups. Fluoride and nitrate adsorption are particularly favoured by the increased surface area of metal oxide nanoparticles (Suriyaraj and Selvakumar, 2016).

1.2 PROBLEM STATEMENT

The excessive release of pollutants into the environment due to industrialization and urbanization is posing a significant problem worldwide. Our water resources quality is deteriorating with each day due to the continuous addition of undesirable chemicals. If the water contamination rate and the current water usage rate continues, water demand is likely to exceed supply at some point soon. Due to their high solubility in water, anions are the most widespread groundwater contaminant globally, imposing a severe threat to human health and contributing to eutrophication. For instance, portable water-containing nitrate and sulphate concentrations due to leaches from fertilizers, household detergents and ceramics, and ceiling boards manufacturing industries can cause severe impacts on streams and human health even at trace levels. These anionic complexes have specific problems due to their toxicity and persistence in nature and have considerably influenced many environmental issues.

The need for a convenient, cheap, effective, efficient and reusable operation to improve water quality, water conservation, and water-use efficiency is a critical national priority. In the search for new technologies for removing anions from wastewater, adsorption based on various biomaterials metal binding capacities has gained prominence as a promising approach. Agricultural waste materials have been widely studied as a biomaterial for different pollutants and have shown a high affinity for heavy metal ions. However, several challenges, including low adsorption rates, low adsorption capacities, and high operating pressures applied in packed columns, limit their applications.

The research was conducted by incorporating iron nanoparticles with a biosorbent and doping the composite to produce doped magnetic bio-composite for probable removal of the contaminating ions. The application of doped magnetite nanoparticles (MNPs) as adsorbent materials in solving environmental problems has recently received significant attention due to their unique physical and chemical properties, making them superior to traditional adsorbents.

1.3 Justification

The industrialisation has led to environmental and health challenges in South Africa. Thus, remediation of anions is critical because water inadequacy in South Africa has remained disturbing. The pressure on water resources could continue to increase unless remediation measures are taken seriously to safeguard the people's health. The advantage of Agrowaste material in remediation is cost-effective, but the materials may be refined into a valuable commodity. Also, pollutant-pollutant interaction, especially in the doped magnetite nanoparticles and the effects on adsorption, provides the potential to develop cost-effective water treatment techniques in this project, the adsorption technique.

1.4 Aim

This study aimed to assess the adsorption potential of nitrate and fluoride from aqueous solutions using manganese-doped magnetite-coated pinecone (Mn-MNP-PCP) and lanthanum-doped magnetite-coated pinecone (La-MNP-PCP) nanocomposite

1.5 Objectives

The research objectives of the study were achieved through the following:

1. To synthesise and characterize La and Mn doped magnetite incorporated pinecone powder using FTIR, XRD, SEM, TGA and XPS techniques.

2. To assess the adsorption capacity of Mn-MNP-PCP and La-MNP-PCP nanocomposites on nitrate and fluoride anions with subsequent optimization
3. To carry out thermodynamic and kinetic studies of nitrate and fluoride adsorption onto Mn-MNP-PCP and La-MNP-PCP to determine the nature of adsorption.
4. To determine the effect of competing anions in the removal of nitrate and fluoride onto Mn-MNP-PCP and La-MNP-PCP.

1.6 REFERENCES

AL-RASHDI, B., SOMERFIELD, C. & HILAL, N. 2011. Heavy metals removal using adsorption and nanofiltration techniques. *Separation & Purification Reviews,* 40**,** 209-259.

BARAKAT, M. 2011. New trends in removing heavy metals from industrial wastewater. *Arabian Journal of Chemistry,* 4**,** 361-377.

BHATNAGAR, A. & SILLANPÄÄ, M. 2010. Utilization of agro-industrial and municipal waste materials as potential adsorbents for water treatment—a review. *Chemical Engineering Journal,* 157**,** 277-296.

BLANDIN, G., VERLIEFDE, A. R., COMAS, J., RODRIGUEZ-RODA, I. & LE-CLECH, P. 2016. Efficiently combining water reuse and desalination through forward osmosis—reverse osmosis (FO-RO) hybrids: a critical review. *Membranes,* 6**,** 37.

FOROUTAN, R., ESMAEILI, H., ABBASI, M., REZAKAZEMI, M. & MESBAH, M. 2017. Adsorption behavior of Cu (II) and Co (II) using chemically modified marine algae. *Environmental Technology***,** 3**,** 1-9.

IRIEL, A., BRUNEEL, S. P., SCHENONE, N. & CIRELLI, A. F. 2018. The removal of fluoride from aqueous solution by a lateritic soil adsorption: kinetic and equilibrium studies. *Ecotoxicology and Environmental Safety,* 149**,** 166-172.

JAIN, R., THAKUR, A., GARG, N. & DEVI, P. 2021. Impact of Industrial Effluents on Groundwater. *Groundwater Geochemistry: Pollution and Remediation Methods,* 10**,** 193-211.

KOOKANA, R. S., DRECHSEL, P., JAMWAL, P. & VANDERZALM, J. 2020. Urbanisation and emerging economies: Issues and potential solutions for water and food security. *Science of the Total Environment,* 732**,** 139057.

LAPWORTH, D., NKHUWA, D., OKOTTO-OKOTTO, J., PEDLEY, S., STUART, M., TIJANI, M. & WRIGHT, J. 2017. Urban groundwater quality in sub-Saharan Africa: current status and implications for water security and public health. *Hydrogeology Journal,* 25**,** 1093-1116.

RODRIGUEZ-NARVAEZ, O. M., PERALTA-HERNANDEZ, J. M., GOONETILLEKE, A. & BANDALA, E. R. 2017. Treatment technologies for emerging contaminants in water: a review. *Chemical Engineering Journal,* 323**,** 361-380.

SADEGH, H., ALI, G. A., GUPTA, V. K., MAKHLOUF, A. S. H., SHAHRYARI-GHOSHEKANDI, R., NADAGOUDA, M. N., SILLANPÄÄ, M. & MEGIEL, E. 2017. The role of nanomaterials as effective adsorbents and their applications in wastewater treatment. *Journal of Nanostructure in Chemistry,* 7**,** 1-14.

SELVAKUMAR, S., CHANDRASEKAR, N. & KUMAR, G. 2017. Hydrogeochemical characteristics and groundwater contamination in the rapid urban development areas of Coimbatore, India. *Water Resources and Industry,* 17**,** 26-33.

SINGH, J., YADAV, P., PAL, A. K. & MISHRA, V. 2020. Water pollutants: Origin and status. *Sensors in Water Pollutants Monitoring: Role of Material.* Springer, 6**,** 5-20.

SURIYARAJ, S. & SELVAKUMAR, R. 2016. Advances in nanomaterial based approaches for enhanced fluoride and nitrate removal from contaminated water. *Royal Society of Chemistry*, 13, 10565-10583.

CHAPTER 2

2. BACKGROUND INFORMATION AND LITERATURE REVIEW

This chapter reviews the literature on water pollution, wastewater remediation techniques, adsorption, and adsorbents used to remove pollutants in water systems. Furthermore, adsorption as a method is presented as an alternative method for removing anions from aqueous systems. The application of doped magnetic nanoparticles as adsorbent, their advantages and limitations is also discussed, and strategies for modifying and using modified adsorbents in water treatment. Adsorption and kinetic isotherm models used in describing experimental data were also reviewed.

2.1 WATER POLLUTION

Various industrial operations such as mining, ore refining, fertilizer production, tanning, battery and paper manufacturing are significant inorganic pollutants. These inorganic pollutants include some prevalent anionic species such as nitrogen, nitrite, cyanide, phosphate, perchlorate and fluoride (Zinicovscaia, 2016). The rivers, ponds and lakes contain wastes from human activities such as; cleaning detergents, food scraps, fertilizers, chemicals from industries, faeces, fats, wildlife and livestock waste, leakages from septic fields and pharmaceuticals (Yan et al., 2018). The discharge of toxic anions into the natural water bodies significantly affect the ecological balance and causes harm to flora and fauna (Fenwick, 2006). These inorganic pollutants may bioaccumulate in tissues over time and may have serious health consequences to animals, humans and the environment (Briffa et al., 2020).

About 70 to 80 % of all diseases in developing nations are associated with water contamination, with women and children being the most vulnerable (Prüss-Ustün et al., 2019).

Approximately 80 % of illnesses in India have been reported to be due to water contaminated with bacteria (Rao and Mamatha, 2004). Moreover, research has shown that more than 88 % of water-related illnesses, including diarrhoea, cholera and bilharzia, occur in South Africa (Fenwick, 2006). Excess nutrient supply, such as nitrogen, causes eutrophication of water bodies, resulting in decreased dissolved oxygen value (Bhatnagar and Sillanpää, 2010). Eutrophication stimulates the growth of blue-green algae, producing toxins harmful if ingested by humans and animals (Suriyaraj and Selvakumar, 2016).

The drinking water guidelines prescribed by the World Health Organization (WHO) for nitrate, fluoride, sulphate, phosphate, molybdenum, selenium, nickel, chromium and mercury are 50, 1.5, 250, 0.05, 0.01, 0.01, 0.02, 0.05 and 0.001 mg dm^{-3}, respectively (WHO, 2008; Kumar and Puri, 2012). When present in aqueous solutions, these anions are discovered to pose severe health and environmental concerns even at minute concentrations. Hence, the need to be maintained below regulatory limits. The effect of toxic anions in the water on human health includes reduced or diminished mental and central nervous function, lower energy levels, and damage to the lungs, kidneys, and liver (Shailaja and Johnson, 2007). Slow progressive muscular, physical and long-term exposure can result in degenerative neurological processes that mimic Alzheimer's disease, muscular dystrophy, Parkinson's disease, and multiple sclerosis (Zinicovscaia, 2016). Long-term contact with some anions or their minerals may cause cancer (Kostić *et al.*, 2016).

2.1.1 A concise overview of Nitrate

Predominantly sandy and well-drained soils containing shallow water tables leach nitrate into the groundwater. Most frequently, nitrates are available worldwide in polluted groundwater. Nitrate is highly soluble water; thus, it reaches the groundwater by leaching through the soil with irrigation water or rain. Environmentally, higher average temperatures indicate lower aqueous nitrate pollution. Also, precipitation affects the concentrations of nitrate in water. Nitrate is applied as a nutrient in large quantities for lawn and garden care and crop production. Nitrate contamination has become a serious environmental health hazard, particularly in developing countries where many people still rely on groundwater for domestic use (Mensinga *et al.*, 2003). The significant amount of nitrate ions implies a non-point nitrate discharge source (Sharma et al., 2016), including explosives, fertilizers, paper manufacturing, nitro organic compounds, and pharmaceuticals (Rajmohan *et al.*, 2016). Often in fertilizers, the ammonia is transformed into nitrate via nitrification, a bio-process, depicted chemically in the following equation:

$$NH_3 + 2O_2 \quad \rightarrow \quad NO_3^- + H^+ + H_2O$$

The effects of deleterious health associated with excess nitrate consumption in water induce blue-baby syndrome, otherwise called infantile methemoglobinemia (Fewtrell, 2004). The nature of infant digestive systems allows the conversion of nitrate to nitrite, the condition which

impairs the haemoglobin from transporting the oxygen. Prolong ingestion of nitrates in adults is a risk factor or causes cancer because it generates nitrosamines or their derivatives. Scientific reports have also shown that nitrate can cause abortions, immune system changes, congenital disabilities, and infection of respiratory tracts (Richard et al., 2014)

.

Moreover, the highly concentrated water-containing nitrate indicates eutrophication of water bodies, which causes gastric cancer (Mensinga *et al*., 2003). In the same manner, nitrate consumptions have adverse impacts on livestock, particularly young animals such as cattle and sheep, because rumen-associated bacteria convert nitrate to nitrite poisoning (Cockburn et al., 2013). Symptoms such as diarrhoea and abdominal pain have also been detected in animals (Rajmohan *et al.*, 2016).

2.1.2 Flouride; Source, benefits and health impact

Lack or inadequacies (in many cases) of water usage, incredibly portable water, has brought about the extensive underground exploration of the aquiver system. Fluoride is frequently discovered in areas dominated by rocks of igneous origin, such as granites (Berger et al., 2016). This highly electronegative mineral occurs as a minor part of groundwater in all forms of hydro-geological strata, including fluorspar [$3Ca_3(PO_4)_2\ Ca(F_2)$] (Shailaja and Johnson, 2007), fluorite (CaF_2) (Berger et al., 2016), and fluorapatite, $Ca_5(PO_4)_3F$ (Kimambo et al., 2019). Fluorite (CaF_2) is regarded as the primary mineral source in groundwater of dissolved F^- (Berger et al., 2016). The factors, including geo-strata nature, rock type, groundwater circulation processes, climate change, and contact time, determine the level of fluoride in groundwater (Kimambo et al., 2019).

Drinking water, bottled beverages, and salt are the primary sources of fluoride commonly consume by man (Dessalegne and Zewge, 2013). About four decades past, toothpaste contained high fluoride concentrations, including those produced for children (Erdal and Buchanan, 2005). According to the WHO quality standards, the fluoride maximum permissible limit in drinking water is ≤ 1.5 mg/L (Craig et al., 2015). However, the desirable fluoride concentration in drinking water is between 0.6 and 1.2 mg/L, the concentration range that promotes bone building but prevents dental decay (Roy and Dass, 2013). Animals and humans are exposed to fluoride in the environment through pollution of air, water, soil, food and industrial wastewater

discharges large amounts of fluoride into rivers (Singh et al., 2018). The fluoride presence in drinking water helps produce and maintain good bones and teeth when their content is within the allowed limit.

The continuing consumption of higher fluorine doses leads to skeletal and dental fluorosis, causing several physiological disorders, including mottling of the teeth, ligament calcification, bone deformities, and eventual death (Sharma et al., 2016). In addition, excess fluoride ingested may cause Alzheimer's, bladder cancer, thyroid disease, gastrointestinal bleeding and otosclerosis (Iriel *et al*., 2018). Fluoride has also been implicated in many harmful effects of fertility and pregnancy (Lv *et al*., 2007).

However, a few measures are available to prevent or eliminate high fluoride concentrations and nitrate in potable water. The measures are based on the six factors affecting the leaching of fluoride and nitrates in the backyard. Such preventive techniques include using the non-agricultural method, manure storage sites (or agricultural strategy), and the method of flood plain management. Taken together, due to the hazardous nature and high cost of removing nitrate and fluoride in drinking water supplies, especially in private and public systems, groundwater does not have the necessary water treatment setup. Therefore, an efficient and cost-effective remediation technique such as adsorption must be designed to remediate nitrate and fluoride from water.

2.2 TECHNIQUES FOR WASTEWATER TREATMENT

Different techniques have been used to remove toxic anions from water. These include reverse osmosis (Bunani *et al.*, 2015) , nanofiltration (Al-Rashdi *et al.*, 2011), precipitation (Ping *et al.*, 2008), (Ghafari *et al.*, 2008), ion exchange (Strathmann, 2010) and adsorption (Öztürk and Bektaş, 2004). However, most of these methods suffer from various limitations associated with their effectiveness, operation, costs, and secondary pollutants production. Electro-dialysis and reverse osmosis have high operational costs (Bhatnagar and Sillanpää, 2011). Specific microorganisms are required for the biological denitrification method, and the treated water requires post-treatment because of germs and metabolic substances. (Loganathan *et al.*, 2013). Most of these processes are slow and require maintenance of optimum conditions such as temperature. Adsorption, as a treatment technique has attracted the attention of most researchers and is frequently applied due to its convenience, the possibility of reusing the

adsorbent materials, cost effectiveness, simplicity of operation (Nakhli *et al.*, 2016), and production of high-quality water (Rabbani *et al.*, 2016).

2.2.1 Reverse Osmosis

The reverse osmosis technique is a pressure-driven method in which the lowest contaminants and monovalent ions in the feed are rejected by a semi-permeable membrane (Bunani *et al.*, 2015). Reverse osmosis shortcoming is due to the exclusion of the load, the physical-chemical relationships between the membrane itself, and the solvent and the solute (Malaeb and Ayoub, 2011). The membranes can either be asymmetrically containing one polymer layer or composites consisting of two or more layers (Mazlan *et al.*, 2016). Seawater purification to remove salt and many other components use reverse osmosis for drinking purposes (Blandin *et al.*, 2016). Reverse osmosis offers high removal efficiency in treating a broad range of effluents from chemical, textile, pulp and paper, oil and petrochemical sectors, food, tanning and metal processing (Malaeb and Ayoub, 2011). It improves its selectivity and effectiveness in what is known as the hybrid method when used with other separation techniques (Blandin *et al.*, 2016). However, reverse osmosis treatments require a vast quantity of water and a longer time to treat the water, making it costly adequately and energy-intensive (Ghernaout and El-Wakil, 2017). The risk of tiny leaks or deteriorating parts prevents reverse osmosis systems from being used on water treatment (Villacorte *et al.*, 2015).

2.2.2 Nanofiltration

Nanofiltration processes allow some salts to pass through the membrane. It enables monovalent ions while rejecting elevated levels of divalent cations and multivalent ions. (Hong et al., 2017). No chemicals are used, and therefore no chemicals are disposed of to the environment. The set-back issue with the nanofiltration process is that it does not remove any dissolved substances, meaning that if there are any soluble elements in water, they can not be separated from the water (Van der Bruggen and Vandecasteele, 2003).

2.2.3 Flocculation/coagulation

The flocculation/coagulation method is a chemical process that involves three steps. They include agglutinating, decanting, and eventually separating colloidal substances current in the water. The coagulation/flocculation method is a straightforward and effective wastewater treatment method commonly used and easy to use (Al-Asheh and Aidan, 2017). This technique is often used in industrial wastewater to extract suspended and dissolved solids, colloids and

organic matter (López-Maldonado *et al.*, 2014). Usually, this technique's disadvantages are the issues connected with the extreme putrescible sludge generated and the elevated operating costs of chemical additives, which could prevent complete physical-chemical alternative to wastewater therapy (Kulkarni, 2017).

2.2.4 Adsorption Technique and Application in Water treatment

The term adsorption means accumulating a substance (adsorbate) at an interface between two phases, such as solid and gas or solid and liquid (Rashed, 2013). There is an increase in the component(s) concentration on the solid stage in the adsorption process due to unbalanced attraction forces between the liquid and solid phases. The substance on which adsorption occurs is referred to as 'adsorbent'. The accumulated compound/substance at the interface is called 'adsorbate'. Due to the adsorbent's high affinity for the adsorbate species, the adsorbates are attracted and bound to the adsorbent by different mechanisms (explained schematically in **Figure 2.1)**. Adsorption is mainly used to treat industrial wastewater containing organic and inorganic pollutants (Nakhli *et al.*, 2016).

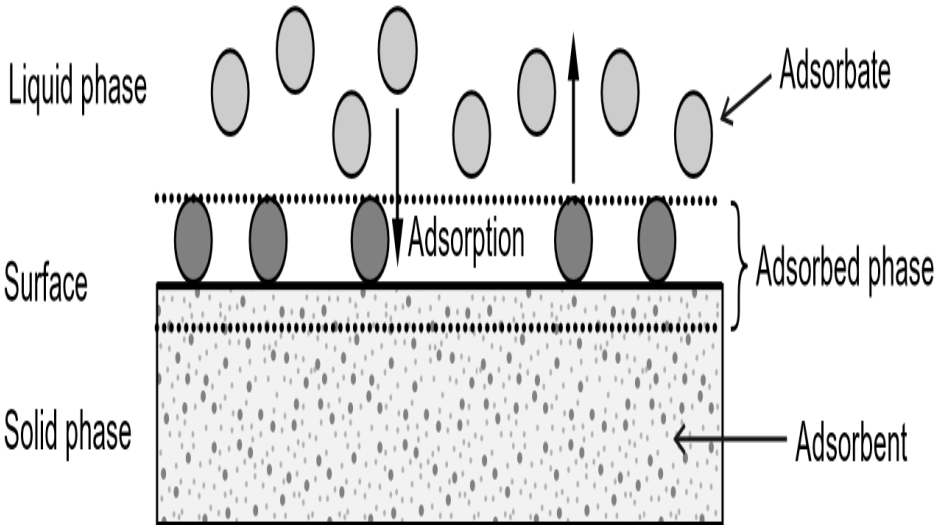

Figure 2.1: Basic terms of adsorption (Adapted from Worch, 2012)

The adsorption technique is regarded as one of the most promising wastewater treatment techniques over the last decades (Barakat, 2011). The added advantages of adsorption over other methods include the following:

1. Selective removal of metals and anions at low concentration
2. Simple design and easy operation
3. Allows the system to operate over broad pH ranges

4. Effective over wide temperature ranges
5. Conversion of a metal pollutant to a metal product
6. Provision of low capital investment and low operation cost (Soto-Rios *et al.*, 2015).

Table 2.1 shows the remediation application of adsorbents to different inorganic pollutants from wastewater.

Table 2.1: Adsorption applications in water treatment.

Application	**Adsorbent**	**Reference**
Removal of phosphate from contaminated water	Fe–Mg–La	(Yu and Chen 2015)
Removal of azo dyes and nitro compounds	$MnFe_2O_4$@SiO_2@ Ag	(Kurtan *et al.*, 2016)
Phosphate removal	Fe–Mn binary oxide	(Lu *et al.*, 2014)
Removal of arsenic from water	Zirconium oxide-coated sand	(Chaudhry *et al.*, 2017)
Removal of nitrate from water	Zinc chloride treated activated carbon	(Bhatnagar *et al.*, 2008)
Removal of fluoride and phosphate	Fe-La composite	(Wang *et al.*, 2018)
Removal of nitrate in groundwater	Magnetite nanoparticles entrapped in Ca-Alginate beads	(Cho *et al.*, 2015)

2.2.4.1 Mechanism types of Adsorption of material on a surface

There are two main adsorption process mechanisms: chemical (chemisorption) and physical (physisorption) adsorption (Bhatnagar and Sillanpää, 2010). Adsorbents possess distinct distribution of weak surface energy sites, like every other solid material, which describes the adsorption mechanism (Costanzo et al., 2012). Adsorption mechanisms are critical to the success of several chemical reaction processes, including catalytic reactions, metal-organic

phase, sensors, organic (Opto) electronics, H_2 adsorption on graphene, and (2, 2) carbon nanotube, and recent technology fields (Kachel et al., 2020). Understanding the adsorbent's structure and surface chemistry enhances the optimum design and synthesis. The chemisorption process is fundamental in heterogeneous catalysis and reactants; it is vital to control the composition and manufacture of catalysts and their evaluation.

The chemisorption technique provides many insights that allow the evaluation of adsorbent materials in design and production (Webb, 2003). In chemisorption (activated adsorption), there is a transfer/sharing of electrons between the adsorbent and the adsorbate (atoms or radicals) (Soto-Rios *et al.*, 2015). Contrastingly, physical adsorption involves the adsorption due to weak van der Waals forces (Bhatnagar and Sillanpää, 2010), which occurs very fast and reversible in any solid/liquid or solid/gas system (Yusuf *et al.*, 2017).

2.2.4.2 Factors affecting the adsorption process

The association between water contaminants and functional adsorbent groups depends not only on the existence of the adsorbent but also on the chemistry of the solution. The adsorption capacity of adsorbents is highly reliant on experimental conditions such as solution pH, initial concentration of contaminants, temperature, the concentration of adsorbents, surface area (particle size), contact time (or residence time), competing ions (effluent composition), the solubility of adsorbent wastewater, adsorbent and hydrophobic solvent affinity in the adsorption process (Bailey *et al.*, 1999; Barkakati, *et al.*, 2010).

2.2.4.2.1 pH of the medium

The solution pH determines the shift in the adsorbent's surface charge. It also affects adsorbate-adsorbent interaction by regulating the adsorbates' protonation or deprotonation (Longo and Szleifer, 2016). The possibility of desorbing pollutants from the adsorbent binding site can be accomplished under certain solution pH conditions (Wiesner et al., 2006); this activity is used to recover or regenerate adsorbents.

2.2.4.2.2 The adsorbent surface area

The degree of adsorption depends directly on the surface area of the adsorbent. Most researchers have suggested that the larger the adsorbent's surface area, the greater the adsorption range. The smaller the particle size, the larger the surface area (Yadav *et al.*, 2013; Mondal and Roy, 2018).

2.2.4.2.3 Initial pollutant concentration

A given adsorbent mass can only adsorb a fixed amount of adsorbate. Therefore, the initial adsorbate solution concentration is essential. With an increasing concentration of adsorbate, the amount of adsorbed ions decreases as the resistance to the adsorption of solute from adsorbate solution decreases with an increasing concentration of solute. Due to the enhanced driving force, the adsorption rate is enhanced (Jiang et al., 2018).

2.2.4.2.4 Temperature

Temperature dependence affects several factors in the adsorption of pollutants. The evolution of heat accompanies adsorption; accordingly, Le-Chatelier's principle posits that the magnitudes of adsorption are generally exothermic and should decrease with rising temperature (Srivastava et al., 2007). At any constant pressure, the relationship between the degree of adsorption and temperature is called adsorption isobar. A physical adsorption isobar shows a decrease in adsorption capacity

(Neto et al., 2013). The isobar of chemisorption increases adsorption capacity initially and decreases as the temperature rises (Jiang et al., 2018).

2.3 TYPES OF ADSORBENTS

An adsorbent is a primary requirement of adsorption feasibility. Adsorbents are defined as porous substances with a high surface area that can adsorb substances onto their surface by intermolecular forces (Bhatnagar and Sillanpää, 2010). Adsorbents can be of natural or synthetic origin. The natural adsorbents include; oxides, biopolymers, zeolite and clay minerals (Öztürk and Bektaş, 2004; Bhatnagar and Sillanpää, 2010; Foroutan *et al*., 2017; Tahir *et al*., 2017).

The synthesised adsorbents include; activated carbon (Huong et al.), polymeric, nanoparticles and doped metals/metal oxides (Sadegh *et al.*, 2017; Tahir *et al*., 2017; Zhang *et al*., 2017; Wang *et al.*, 2018). Some adsorbents have been used for the removal of cations and some for the removal of anions. The reason is that these adsorbents are either negatively or positively charged when immersed in water, making them attract positively/negatively charged pollutant molecules (Öztürk and Bektaş, 2004; Bhatnagar and Sillanpää, 2010; Foroutan *et al*., 2017; Tahir *et al.*, 2017).

2.3.1 Zeolites

Zeolites are made up of alkaline and alkaline earth metal hydrated aluminosilicates; they are crystalline and have infinite three-dimensional structures (Mahesh *et al.*, 2018). They may be of natural or synthetic origin, and their advantages include high surface area, adsorption, stability, ion exchange and molecular sieving (Lee and Valla, 2017). Materials from zeolites are mainly used in agriculture, water treatment, gas adsorption, industrial gas separation, aquaculture, livestock and ion exchange (Lee and Valla, 2017; Mahesh *et al.*, 2018; Shi *et al*., 2018). The use of zeolites is not likely determined by the raw mineral's cost or its inconsistency in chemical composition. Instead, the application of zeolite is dependent on its inability to remove some anions from water (Shi *et al.*, 2018). It has been used for the removal of phosphate (Ping et al., 2008) and ammonium from aqueous solution (Huang et al., 2010).

2.3.2 Activated Carbon

Activated carbon is a type of carbon with tiny, low-volume pores that boost its application surface area, such as adsorption (Bhatnagar and Sillanpää, 2010). Activated carbon is generated by multiple activation processes from different carbon-containing raw materials (Asuquo *et al.*, 2017). Activated carbon is a very useful adsorbent for water purification; however, its use in wastewater treatment is very costly (Chaturvedi and Dave, 2019). It has been used for the adsorption to remove nitrate ion and Cr(VI) from aqueous solution (Cho et al., 2011), other researchers have also used it in the removal of fluoride (Daifullah et al., 2007) and metals such as chromium and mercury (Di Natale et al., 2007).

2.3.3 Magnetic Nanoparticles Adsorbents

Magnetic nanoparticles are materials made up of a magnetic core and polymeric shell (Chomoucka *et al.*, 2010). Magnetic nanoparticles have been produced from various metals such as copper, iron, zinc, titanium, magnesium, gold, alginate and silver or magnetite oxides (Fe_3O_4), maghemite (c-Fe_2O_3), nickel ferrite ($NiFe_2O_4$) and cobalt ferrite ($CoFe_2O_4$) (Vaghari *et al.*, 2016).

Magnetic nanoparticles are commonly used in different applications such as water treatment, medical treatments, solar production and energy storage batteries (Tang and Lo, 2013; Farjadian *et al.*, 2017). The magnetic nanoparticles' distinctive magnetic characteristics facilitate the magnetisation and demagnetisation of workplace material (Tang and Lo, 2013).

Magnetic nanoparticles also show promising applications for water and wastewater treatment because of their ease of synthesis, high surface area, large amounts of active sites for interaction with metallic and organic species, separation after use by an external magnetic field and the absence of internal diffusion resistance (Qu *et al.*, 2013). However, many heavy magnetic nanoparticles have shown limitations, including non-biodegradable, low adsorption capacity, easily oxidized, toxic, carcinogenic and mutagenic even at relatively low concentrations in removing pollutants in water (Bringas *et al.*, 2006; Zhang and Itoh, 2006).

2.3.3.1 Magnetite Nanoparticle

Magnetite (Fe_3O_4) has drawn many researchers' attention because of its low toxicity and ease of fabrication. Magnetite, along with wüstite, hematite and maghemite, is a very common mineral of iron oxide and is widely mined iron ores. Magnetic nanoparticles can be defined as polymer shells and magnetic cores composed of materials (Chen et al., 2011). Magnetite nanoparticles can be easily manipulated under a magnetic field. Magnetite belongs to a family of compounds called inverse spinel ferrites. In magnetite, the octahedral (Saleh *et al.*, 2018) and tetrahedral (Td) positions of the spinel system are entirely occupied by iron ions, while there are cationic vacancies in maghemite within the octahedral position (Aghavnian *et al.*, 2015). When compared to other iron oxides, magnetite have better advantages due to its super-paramagnetic properties (Favela-Camacho et al., 2019)

Magnetite is biocompatible and finds application in many medical, molecular and polluted water treatment applications (Tian *et al.*, 2011; Tang and Lo, 2013; Hasan, 2015). Researchers have synthesized and used magnetite nanoparticles to treat water, magnetic resonance imaging, audio speaker ferrofluids, magnetic recording media and magnetic targeted drug delivery (Laurent *et al.*, 2008). The usage of magnetite nanoparticles as adsorbents in water treatment offers a convenient approach by applying external magnetic fields to separate and remove contaminants (nitrate and fluoride) (Tang and Lo, 2013, Cho *et al.*, 2015). Magnetite nanoparticles can also be reused after magnetic separation by desorbing the adsorbed contaminants (Singh *et al.*, 2011).

A significant challenge in using magnetite nanoparticles for wastewater treatment is agglomeration, air oxidation, and prone to self aggregated in aqueous systems. This mainly results from direct inter-particle interactions *via* Van der Waals forces and magnetic interactions (Geng *et al.*, 2012; Zhou *et al.*, 2013). This challenge can be overcome by

modifying or dispersing the surface of doped magnetic nanoparticles covered with biosorbents such as organic layers (surfactants or polymers) or metallic elements (gold or platinum), metal oxides (aluminium oxide), graphene and pinecone powder (Ofomaja et al., 2010, Geng et al., 2012).

2.3.3.2 Pinecone powder

Pinecones are waste products from pine trees (the dominant tree species in South African plantations), used for decoration, agricultural waste, and wood for coffin-making (Stafford, 2016). Pinecones have a composition of almost 44 wt. cellulose percent, 27 wt. hemicellulose percent, and 22 wt. lignin percent (Rambabu *et al.*, 2016). The pinecone cell walls are made up of polar functional groups such as aldehydes, alcohols, carboxylic phenolics, ketones and other groups forming active sorption sites (Dawood *et al.*, 2011). These functional groups form active sites for the sorption of pollutants. They are known to have a porous surface area (Ofomaja *et al.*, 2010) and have the merit to disperse agglomerated doped magnetite nanoparticles (Cho *et al.*, 2015). However, the high lignin and cellulose content on the pinecone's cell wall limits its ability to disperse the agglomerated particles (Saavedra et al., 2020). In addition, alkaline, such as sodium hydroxide solution, has effectively modified their surface (Ofomaja *et al.*, 2010). Besides using pinecone as a dispersant, it has also been used as an adsorbent in removing water pollutants such as; arsenites (Ouma et al., 2018) and 2-nitrophenol (Kupeta et al., 2018).

2.3.3.3 Nanoparticles Doping

Literature study demonstrates that multi-metal or insertion of dopant elements has been applied to improve properties such as efficiency in detecting and removing wastewater toxins and shortening water treatment periods compared to single metal oxides (Gupta et al., 2010, Bolyard, 2012). Magnetite and other adsorbents have been widely doped, among others, with La (Kong et al., 2019) and Mn (Yang et al., 2019).

i. Manganese-Iron Oxide Nanoparticle (Mn-MNP)

Manganese element is one of the most abundant metals generally occurring with iron in the Earth's crust and is one of the least toxic elements (Frisbie et al., 2012). Manganese is an element of many mineral types under a broad spectrum of chemical and temperature circumstances and is never discovered naturally in its pure (elemental) form (Maynard, 2010). Manganese occurs in many oxidation states in natural systems, and those containing Mn^{2+},

Mn^{4+} or Mn^{7+} are the most environmentally and biologically essential manganese compounds (Najafpour *et al.*, 2016). Manganese oxides also exhibit a considerable variety of atomic architectures, many of which can easily accommodate a broad range of other metal cations. Manganese and iron oxides are renowned for their anion and different toxic metals affinity (Delaney *et al.*, 2011). Manganese has been the subject of tremendous attention as a transition metal with distinctive properties, catalytic activity and an outstanding ability to treat wastewater. The doping of manganese has been shown to improve the adsorbent materials' surface area and pore size, such as magnetite, to favour adsorption processes. The properties help the adsorption processes and increase removal potential for anions, due to their unique large, specific surface area, well-defined pore size and form, post-grafting functional groups, organic dyes and toxic metal ions (Chen et al., 2011, Yang et al., 2019).

Manganese-Iron Oxide Nanoparticle (Mn-MNP-PCP) with excellent magnetic features is one of the most prevalent smooth spinel magnetic ferrites. Mn-MNP-PCP is partly a reverse spinal ferrite with elevated magnetic permeability, high electrical resistance and low losses (Islam, 2016). Manganese-Iron Oxide ($MnFe_3O_4$) Nanoparticle has gained special attention for temperature-dependent antiferromagnetic and super-paramagnetic behaviours in multiple technological areas of material science (Fouad *et al*., 2008; Gupta *et al.*, 2010; Delaney *et al*., 2011). $MnFe_3O_4$ magnetic nanoparticles have been reported as an excellent adsorbent in water treatment (Fouad et al., 2008; Lv et al., 2009; Kurtan et al., 2016).

ii. Lanthanum-Iron Oxide Nanoparticle (La-MNP)

Lanthanum (La) metal is the first element of the lanthanides (or lanthanoides), a series of 15 metals from lanthanum to lutetium with 57 to 71 atomic numbers (Herrmann *et al.*, 2016). Lanthanum predominantly exists in the stable oxidation of +3; the free ion lanthanum (La^{3+}) species is considered the most bioavailable and has strong sensitivity (Moermond *et al.*, 2001). In addition, lanthanum has a low solubility as a rare earth metal and an oxide and has been categorized as non-toxic (Yu and Chen, 2015). In particular, lanthanum is a widely used rare-earth metal with a high adsorption capacity for fluoride and nitrate (Nagaraj et al., 2017; Huong et al., 2019).

The lanthanum type sorbent has demonstrated high anionic contaminant adsorption capacity and environmental friendliness. Doping lanthanum onto magnetite has been shown to influence the final magnetite properties and has several advantages, including high separation efficiency, short time, low energy consumption, and high selectivity (Huong et al.,

2019). A few lanthanum adsorbents such as lanthanum hydroxide and iron-lanthanum doped material have been developed for water removal of phosphate, fluoride and nitrate (Yu and Chen, 2015). Lanthanum-doped spinel cobalt ferrite ($CoFe_2O_4$) nanoparticles were used to remove contaminants from effluents (Akika et al., 2018). Lanthanum has also shown a high affinity for removing pollutants such as arsenate and fluoride (Jais *et al.*, 2016).

2.4 ADSORPTION ISOTHERMS AND KINETICS STUDIES

Kinetic models and adsorption isotherms are applied to determine the potential of adsorbents. Firstly, the time dependence on adsorption processes are established and secondly, the adsorption isotherm modelling (Iriel et al., 2018; Okoli and Ofomaja, 2018).

2.4.1 Adsorption Isotherm

Quantitatively, an adsorbent's adsorption capacity for a targeted water pollutant essentially provides detailed knowledge of the adsorption mechanism. Adsorption isotherms, however, shed further light on the technique of adsorption. Therefore, the connection between the adsorbed pollutant amount and its solution concentration at temperature, T, describes adsorption's isotherms. Examples of isotherm include; Langmuir, Freundlich, Dubinin-Radushkevich, Redlich-Peterson, and Temkin. The linear form of Langmuir and Freundlich's equations are widely used (Hashemzadeh et al., 2018).

2.4.1.1 Langmuir Isotherm

a) Langmuir isotherm is a type of monolayer adsorption.
b) It is compatible with the monolayer spread on the adsorbent,
c) It is an equilibrium model
d) All adsorption sites are equally probable, and
e) It is a second order reaction.

The general Langmuir expression is given as follows:

$$q_e = q_m \frac{K_L C_e}{1+K_L C_e} \qquad (2.1)$$

Where q_e is the equilibrium adsorption capacity (mg/g), C_e is the equilibrium adsorbate concentration (mg/L), the Langmuir constants: q_m (mg/g) and K_L (L/mg) are the respective single layer coverage capacity and parameter of adsorption energy.

2.4.1.2 Linear Isotherm

The expression of linear isotherm is of the form:

$$q_{e=K_P.C_e} \quad (2.2)$$

Q_e is the adsorption capacity at equilibrium (mg/g), K_p, the adsorbate's partition coefficient. and C_e = equilibrium concentration of adsorbate (mg/L).

2.4.1.3 Freundlich Isotherm

It is empirical and commonly used to describe multilayer adsorption with the interaction between adsorbed molecules on a heterogeneous surface.

Freundlich expression is given below:

$$q_e=K_F C_e^{1/n} \quad (2.3)$$

Where q_e is the amount of adsorbed adsorbate in mg/g, C_e is the equilibrium adsorbate concentration in mg/L, K_F ((mg/g)/(mg/L)n), and n are the Freundlich equation parameters. n indicates the adsorption's energy or intensity and suggests the favourability and capacity of the adsorbent-adsorbate system.

2.4.1.4 Brunauer, Emmett and Teller (Komarneni et al.) Isotherm

It is stated that the various layers generated during physical adsorption do not transmigrate. There is equal adsorption energy in the layers except for the first layer

$$q_e = \frac{q_s C_{BET} C_e}{(C_s - C_e)[1+(C_{BET}-1)\left(\frac{C_e}{C_s}\right)]} \quad (2.4)$$

Where C_{BET} is the BET isotherm constant (L/mg), Cs is the concentration of adsorbate monolayer saturation (mg/L), qs is the theoretical isotherm saturation capacity (mg/g) and q_e is the equilibrium adsorption capacity (mg/g) when $C_e << C_S$, $K_B >> 1$ and $K_{ad} = K_B/Cs$ BET, the isotherm approaches Langmuir isotherm.

2.4.2 Adsorption Kinetics

Recognizing the adsorption kinetics and determining the phenomenological coefficients that characterize sorbate transport within sorbents is of concern. Kinetics addresses change in chemical characteristics over time and are mainly concerned with change rates. For many aspects of surface chemistry, from an understanding of adsorption/desorption mechanisms to more, adsorption kinetics' growth is essential (Dąbrowski, 2001). Different kinetic models, including pseudo-first-order, Ritchie, pseudo-second-order, intraparticle diffusion models, have been used to study or examine several reaction orders for the adsorption process (Iriel et al., 2018; Simonin, 2016).

2.4.2.1 Pseudo-first-order

Lagergren recommended a rate equation for solutes' sorption from a liquid solution (Lagergren, 1898). This pseudo-first-order rate equation is:

$$\frac{d_q}{d_t} = k_1(q_e - q) \quad (2.5)$$

Where q (mg/g) and qe (mg/g) are the adsorption capacity of the adsorbent at any time and at equilibrium, and k_1 (min^{-1}) is the rate constant of the first-order sorption.

The integrated form for the boundary conditions $t = 0$ to $t = t$ and $q = 0$ to $q = q$, gives:

$$ln\frac{(q_e - q)}{q_e} = -k_1 t \quad (2.6)$$

q and qe are the grams of solute sorbed per gram of sorbent at any time and equilibrium, and $k1$ is the rate constant of the first-order sorption.

2.4.2.2 Pseudo-second-order

The kinetics can also be calculated using Ho and McKay (1999) second-order pseudo mechanism equation to investigate the constants of absorption adsorption mechanisms, which can be written as follows:

$$\frac{d_q}{d_t} = k_1(q_e - q)^2 \quad (2.7)$$

Qe and q (mg/g) are the adsorption capacities at equilibrium and time t. ks (g/mg/min) is the constant rate.

Integrating the equation for the boundary conditions $t = 0$ to $t = t$ and $q = 0$ to $q = q$, gives:

$$\frac{t}{q} = \frac{1}{k_2 q_e^2} \quad (2.8)$$

The plot of *t/q* versus *t* gives a straight line with a slope of $1/k_2 qe^2$ and an intercept of $1/qe$. Thus, from the slope and intercept, respectively, the gram of solute sorbed per gram of sorbent at equilibrium (q_e) and sorption rate constant (k_2) could be evaluated.

2.4.2.3 Ritchie kinetic model

The Ritchie equation for the isotherm of kinetic adsorption was derived based on the theory explaining the gas kinetics of adsorption on energetically heterogeneous solid surfaces(Ritchie, 1977). The model is expressed as follows:

$$\frac{1}{q} = \frac{1}{k_r q_e t} + \frac{1}{q_e} \quad (2.9)$$

Where *kr* (1/min) is the rate constant, *q* (mg/g) indicates adsorption capacity at time *t* (Cui et al.), and *qe* (mg/g) is adsorption capacity at equilibrium. A *1/q* versus *1/t* linear plot gives magnitudes of *qe* and *kr* from the intercept and slope.

2.4.2.4 Intraparticle diffusion

According to the intraparticle diffusion relation, a plot of adsorption capacity versus the square root of time produces a straight line if it controls the adsorption process. However, intra-particle diffusion has the rate-limiting step when the lane passes through the origin (Sutherland & Venkobachar, 2010; Aryal & Liakopoulou-Kyriakides, 2011). A significant correlation coefficient for the intraparticle diffusion model suggests that adsorption occurs in the adsorbent pores (Aryal & Liakopoulou-Kyriakides, 2011). The model is described by Equation 2.10

$$q_t = k_{id} t^{0.5} C \quad (2.10)$$

The k_{id} ($mg.g^{-1}$ $min^{-0.5}$) is the intraparticle diffusion rate constant, and *C* is the intercept reflecting the thickness of the boundary layer.

2.5 CONCLUSION

An extensive literature study was performed to explore magnetite nanoparticles adsorptive ability to remove anion pollutants. Literature also shows that in water treatment, multi-metal or doped metal oxides have attracted considerable attention. However, adsorption has drawn most researchers' attention and has been frequently used owing to its comfort, the ability to reuse adsorbent products, cost-effectiveness, and operational simplicity.

2.6 REFERENCES

AGHAVNIAN, T., MOUSSY, J.B., STANESCU, D., BELKHOU, R., JEDRECY, N., MAGNAN, H., OHRESSER, P., ARRIO, M.A., SAINCTAVIT, P. & BARBIER, A. 2015. Determination of the cation site distribution of the spinel in multiferroic CoFe2O4/BaTiO3 layers by X-ray photoelectron spectroscopy. *Journal of Electron Spectroscopy and Related Phenomena, 202,* 16-21.

AKIKA, F., BENAMIRA, M., LAHMAR, H., TIBERA, A., CHABI, R., AVRAMOVA, I., SUZER, Ş. & TRARI, M. 2018. Structural and optical properties of Cu-substitution of NiAl2O4 and their photocatalytic activity towards Congo red under solar light irradiation. *Journal of Photochemistry and Photobiology A: Chemistry,* 364**,** 542-550.

AL-ASHEH, S. & AIDAN, A. 2017. Operating conditions of coagulation-flocculation process for high turbidity ceramic wastewater. *Journal of Water and Environmental Nanotechnology,* 2**,** 80-87.

AL-RASHDI, B., SOMERFIELD, C. & HILAL, N. 2011. Heavy metals removal using adsorption and nanofiltration techniques. *Separation & Purification Reviews,* 40**,** 209-259.

ARYAL, M., & LIAKOPOULOU-KYRIAKIDES, M. (2011). Equilibrium, kinetics and thermodynamic studies on phosphate biosorption from aqueous solutions by Fe(III)-treated Staphylococus xylosus biomass: Common ion effect. *Colloids Surfaces A Physicochem. Eng. Asp.* 387. p.43–49

ASUQUO, E., MARTIN, A., NZEREM, P., SIPERSTEIN, F. & FAN, X. 2017. Adsorption of Cd (II) and Pb (II) ions from aqueous solutions using mesoporous activated carbon adsorbent: Equilibrium, kinetics and characterisation studies. *Journal of Environmental Chemical Engineering,* 5**,** 679-698.

BAILEY, S.E., OLIN, T.J., BRICKA, R.M. & ADRIAN, D.D. 1999. A review of potentially low-cost sorbents for heavy metals. *Water research, 33*(11), 2469-2479.

BARAKAT, M. 2011. New trends in removing heavy metals from industrial wastewater. *Arabian Journal of Chemistry,* 4**,** 361-377.

BARKAKATI, P., BEGUM, A., DAS, M.L. & RAO, P.G. 2010. Adsorptive separation of Ginsenoside from aqueous solution by polymeric resins: Equilibrium, kinetic and thermodynamic studies. *Chemical Engineering Journal*, *161*(1-2), 34-45.

BERGER, T., MATHURIN, F. A., DRAKE, H. & ÅSTRÖM, M. E. 2016. Fluoride abundance and controls in fresh groundwater in Quaternary deposits and bedrock fractures in an area with fluoride-rich granitoid rocks. *Science of the Total Environment,* 569**,** 948-960.

BHATNAGAR, A., JI, M., CHOI, Y. H., JUNG, W., LEE, S. H., KIM, S. J., LEE, G., SUK, H., KIM, H. S. & MIN, B. 2008. Removal of nitrate from water by adsorption onto zinc chloride treated activated carbon. *Separation Science and Technology,* 43**,** 886-907.

BHATNAGAR, A. & SILLANPÄÄ, M. 2010. Utilization of agro-industrial and municipal waste materials as potential adsorbents for water treatment—a review. *Chemical Engineering Journal,* 157**,** 277-296.

BHATNAGAR, A. & SILLANPÄÄ, M. 2011. A review of emerging adsorbents for nitrate removal from water. *Chemical Engineering Journal,* 168**,** 493-504.

BLANDIN, G., VERLIEFDE, A. R., COMAS, J., RODRIGUEZ-RODA, I. & LE-CLECH, P. 2016. Efficiently combining water reuse and desalination through forward osmosis—reverse osmosis (FO-RO) hybrids: a critical review. *Membranes,* 6**,** 37.

BOLYARD, S. C. 2012. Fate of Coated Zinc Oxide in Municipal Solid Waste Landfills.

BRIFFA, J., SINAGRA, E. & BLUNDELL, R. 2020. Heavy metal pollution in the environment and their toxicological effects on humans. *Heliyon,* 6**,** 46-91.

BRINGAS, E., SAN ROMÁN, M. F. & ORTIZ, I. 2006. Separation and recovery of anionic pollutants by the emulsion pertraction technology. Remediation of polluted groundwaters with Cr (VI). *Industrial & Engineering Chemistry Research,* 45**,** 4295-4303.

BUNANI, S., YÖRÜKOĞLU, E., YÜKSEL, Ü., KABAY, N., YÜKSEL, M. & SERT, G. 2015. Application of reverse osmosis for reuse of secondary treated urban wastewater in agricultural irrigation. *Desalination,* 364**,** 68-74.

CHATURVEDI, S. & DAVE, P. N. 2019. Water purification using nanotechnology an emerging opportunities. *Chemical Methodologies,* 3**,** 115-144.

CHAUDHRY, S. A., KHAN, T. A. & ALI, I. 2017. Zirconium oxide-coated sand-based batch and column adsorptive removal of arsenic from water: Isotherm, kinetic and thermodynamic studies. *Egyptian Journal of Petroleum,* 26**,** 553-563.

CHEN, H., CHU, P. K., HE, J., HU, T. & YANG, M. 2011. Porous magnetic manganese oxide nanostructures: Synthesis and their application in water treatment. *Journal of Colloid and Interface Science,* 359**,** 68-74.

CHO, D.-W., CHON, C.-M., KIM, Y., JEON, B.-H., SCHWARTZ, F. W., LEE, E.-S. & SONG, H. 2011. Adsorption of nitrate and Cr (VI) by cationic polymer-modified granular activated carbon. *Chemical Engineering Journal,* 175**,** 298-305.

CHO, D.-W., SONG, H., KIM, B., SCHWARTZ, F. W. & JEON, B.-H. 2015. Reduction of nitrate in groundwater by Fe (0)/Magnetite nanoparticles entrapped in Ca-Alginate beads. *Water, Air, & Soil Pollution,* 226**,** 206.

CHOMOUCKA, J., DRBOHLAVOVA, J., HUSKA, D., ADAM, V., KIZEK, R. & HUBALEK, J. 2010. Magnetic nanoparticles and targeted drug delivery. *Pharmacological Research,* 62**,** 144-149.

COCKBURN, A., BRAMBILLA, G., FERNÁNDEZ, M.-L., ARCELLA, D., BORDAJANDI, L. R., COTTRILL, B., VAN PETEGHEM, C. & DORNE, J.-L. 2013. Nitrite in feed: from animal health to human health. *Toxicology and applied pharmacology,* 270**,** 209-217.

COSTANZO, F., SILVESTRELLI, P. L. & ANCILOTTO, F. 2012. Physisorption, diffusion, and chemisorption pathways of H2 molecule on graphene and on (2, 2) carbon nanotube by first principles calculations. *Journal of chemical theory and computation,* 8**,** 1288-1294.

CRAIG, L., LUTZ, A., BERRY, K. A. & YANG, W. 2015. Recommendations for fluoride limits in drinking water based on estimated daily fluoride intake in the Upper East Region, Ghana. *Science of the Total Environment,* 532**,** 127-137.

CUI, H.-J., SHI, J.-W., YUAN, B. & FU, M.-L. 2013. Synthesis of porous magnetic ferrite nanowires containing Mn and their application in water treatment. *Journal of Materials Chemistry A,* 1**,** 5902-5907.

DĄBROWSKI, A. 2001. Adsorption—from theory to practice. *Advances in colloid and interface science,* 93**,** 135-224.

DAIFULLAH, A., YAKOUT, S. & ELREEFY, S. 2007. Adsorption of fluoride in aqueous solutions using KMnO4-modified activated carbon derived from steam pyrolysis of rice straw. *Journal of Hazardous Materials,* 147**,** 633-643.

DAWOOD, S. & SEN, T.K. 2012. Removal of anionic dye Congo red from aqueous solution by raw pine and acid-treated pine cone powder as adsorbent: equilibrium, thermodynamic, kinetics, mechanism and process design. *Water research, 46*(6), 1933-1946.

DI NATALE, F., LANCIA, A., MOLINO, A. & MUSMARRA, D. 2007. Removal of chromium ions form aqueous solutions by adsorption on activated carbon and char. *Journal of Hazardous Materials,* 145**,** 381-390.

DELANEY, P., MCMANAMON, C., HANRAHAN, J. P., COPLEY, M. P., HOLMES, J. D. & MORRIS, M. A. 2011. Development of chemically engineered porous metal oxides for phosphate removal. *Journal of Hazardous Materials,* 185**,** 382-391.

DESSALEGNE, M. & ZEWGE, F. 2013. Daily dietary fluoride intake in rural villages of the Ethiopian Rift Valley. *Toxicological & Environmental Chemistry,* 95**,** 1056-1068.

ERDAL, S. & BUCHANAN, S. N. 2005. A quantitative look at fluorosis, fluoride exposure, and intake in children using a health risk assessment approach. *Environmental health perspectives,* 113**,** 111-117.

FARJADIAN, F., MORADI, S. & HOSSEINI, M. 2017. Thin chitosan films containing super-paramagnetic nanoparticles with contrasting capability in magnetic resonance imaging. *Journal of Materials Science: Materials in Medicine,* 28**,** 47.

FAVELA-CAMACHO, S. E., SAMANIEGO-BENÍTEZ, E. J., GODÍNEZ-GARCÍA, A., AVILÉS-ARELLANO, L. M. & PÉREZ-ROBLES, J. F. 2019. How to decrease the agglomeration of magnetite nanoparticles and increase their stability using surface properties. *Colloids and Surfaces A: Physicochemical and Engineering Aspects*, 574**,** 29-35.

FENWICK, A. 2006. Waterborne infectious diseases—could they be consigned to history? *Science,* 313**,** 1077-1081.

FEWTRELL, L. 2004. Drinking-water nitrate, methemoglobinemia, and global burden of disease: a discussion. *Environmental health perspectives,* 112**,** 1371-1374.

FOROUTAN, R., ESMAEILI, H., ABBASI, M., REZAKAZEMI, M. & MESBAH, M. 2017. Adsorption behavior of Cu (II) and Co (II) using chemically modified marine algae. *Environmental Technology, 11***,** 1-9.

FOUAD, O., HALIM, K. A. & RASHAD, M. 2008. Catalytic oxidation of CO over synthesized nickel ferrite nanoparticles from fly ash. *Topics in Catalysis,* 47**,** 61-65.

FRISBIE, S. H., MITCHELL, E. J., DUSTIN, H., MAYNARD, D. M. & SARKAR, B. 2012. World Health Organization discontinues its drinking-water guideline for manganese. *Environmental Health Perspectives,* 120**,** 775.

GENG, Z., LIN, Y., YU, X., SHEN, Q., MA, L., LI, Z., PAN, N. & WANG, X. 2012. Highly efficient dye adsorption and removal: a functional hybrid of reduced graphene oxide–Fe_3O_4 nanoparticles as an easily regenerative adsorbent. *Journal of Materials Chemistry,* 22**,** 3527-3535.

GHAFARI, S., HASAN, M. & AROUA, M. K. 2008. Bio-electrochemical removal of nitrate from water and wastewater—a review. *Bioresource Technology,* 99**,** 3965-3974.

GHERNAOUT, D. & EL-WAKIL, A. 2017. Requiring Reverse Osmosis Membranes Modifications—An Overview. *American Journal of Chemical Engineering,* 5**,** 81-88.

GUPTA, K., MAITY, A. & GHOSH, U. C. 2010. Manganese associated nanoparticles agglomerate of iron (III) oxide: synthesis, characterization and arsenic (III) sorption behavior with mechanism. *Journal of hazardous materials,* 184**,** 832-842.

HASAN, S. 2015. A review on nanoparticles: their synthesis and types. *Research Journal of Recent Sciences* _____ *ISSN,* 2277**,** 2502.

HASHEMZADEH, M., NILCHI, A., HASSANI, A. & SABERI, R. 2018. Synthesis of novel surface-modified hematite nanoparticles for the removal of cobalt-60 radiocations from aqueous solution. *International Journal of Environmental Science and Technology, 7***,** 1-18.

HERRMANN, H., NOLDE, J., BERGER, S. & HEISE, S. 2016. Aquatic ecotoxicity of lanthanum–A review and an attempt to derive water and sediment quality criteria. *Ecotoxicology and Environmental Safety,* 124**,** 213-238.

HO, Y.S. & MCKAY, G. 1999. Pseudo-second order model for sorption processes. *Process biochemistry, 34*(5), 451-465.

HONG, S., CONSTANS, C., SURMANI MARTINS, M. V., SEOW, Y. C., GUEVARA CARRIÓ, J. A. & GARAJ, S. 2017. Scalable graphene-based membranes for ionic sieving with ultrahigh charge selectivity. *Nano Letters,* 17**,** 728-732.

HUANG, H., XIAO, X., YAN, B. & YANG, L. 2010. Ammonium removal from aqueous solutions by using natural Chinese (Chende) zeolite as adsorbent. *Journal of Hazardous materials*, 175**,** 247-252.

HUONG, P. T., JITAE, K., GIANG, B. L., NGUYEN, T. D. & THANG, P. Q. 2019. Novel lanthanum-modified activated carbon derived from pine cone biomass as ecofriendly bio-sorbent for removal of phosphate and nitrate in wastewater. *Rendiconti Lincei. Scienze Fisiche e Naturali,* 30**,** 637-647.

IRIEL, A., BRUNEEL, S. P., SCHENONE, N. & CIRELLI, A. F. 2018. The removal of fluoride from aqueous solution by a lateritic soil adsorption: kinetic and equilibrium studies. *Ecotoxicology and Environmental Safety,* 149**,** 166-172.

ISLAM, N. 2016. Investigation of structural and magnetic properties of Gd substituted Mn-Ni-Zn ferrites. 4**,** 1-147.

JAIS, F. M., IBRAHIM, S., YOON, Y. & JANG, M. 2016. Enhanced arsenate removal by lanthanum and nano–magnetite composite incorporated palm shell waste–based activated carbon. *Separation and Purification Technology,* 169**,** 93-102.

JIANG, Y., CAI, W., TU, W. & ZHU, M. 2018. Facile Cross-Link Method To Synthesize Magnetic Fe_3O_4@ SiO_2–Chitosan with High Adsorption Capacity toward Hexavalent Chromium. *Journal of Chemical & Engineering Data,* 64**,** 226-233.

KACHEL, S. R., KLEIN, B. P., MORBEC, J. M., SCHÖNIGER, M., HUTTER, M., SCHMID, M., KRATZER, P., MEYER, B., TONNER, R. & GOTTFRIED, J. M. 2020. Chemisorption and Physisorption at the Metal/Organic Interface: Bond Energies of Naphthalene and Azulene on Coinage Metal Surfaces. *The Journal of Physical Chemistry C,* 124**,** 8257-8268.

KIMAMBO, V., BHATTACHARYA, P., MTALO, F., MTAMBA, J. & AHMAD, A. 2019. Fluoride occurrence in groundwater systems at global scale and status of defluoridation–state of the art. *Groundwater for Sustainable Development,* 9**,** 100-223.

KOMARNENI, S., FREGEAU, E., BREVAL, E. & ROY, R. 1988. Hydrothermal preparation of ultrafine ferrites and their sintering. *Journal of the American Ceramic Society,* 71**,** 11-23.

KONG, L., TIAN, Y., PANG, Z., HUANG, X., LI, M., YANG, R., LI, N., ZHANG, J. & ZUO, W. 2019. Synchronous phosphate and fluoride removal from water by 3D rice-like

lanthanum-doped La@ MgAl nanocomposites. *Chemical Engineering Journal,* 371**,** 893-902.

KOSTIĆ, A. Ž., PANTELIĆ, N. Đ., KALUĐEROVIĆ, L. M., JONAŠ, J. P., DOJČINOVIĆ, B. P. & POPOVIĆ-DJORDJEVIĆ, J. B. 2016. Physicochemical Properties of Waters in Southern Banat (Serbia); Potential Leaching of Some Trace Elements from Ground and Human Health Risk. *Exposure and Health,* 8**,** 227-238.

KULKARNI, S. J. 2017. Coagulation for Wastewater Treatment: A Review on Investigations and Studies. *International Journal of Scientific Research in Science and Technology,* 2**,** 501-505.

KUMAR, M. & PURI, A. 2012. A review of permissible limits of drinking water. *Indian Journal of Occupational and Environmental Medicine,* 16**,** 40.

KUPETA, A., NAIDOO, E. & OFOMAJA, A. 2018. Kinetics and equilibrium study of 2-nitrophenol adsorption onto polyurethane cross-linked pine cone biomass. *Journal of Cleaner Production,* 179**,** 191-209.

KURNIAWAN, T. A., CHAN, G. Y., LO, W.-H. & BABEL, S. 2006. Physico–chemical treatment techniques for wastewater laden with heavy metals. *Chemical Engineering Journal,* 118**,** 83-98.

KURTAN, U., AMIR, M., YıLDıZ, A. & BAYKAL, A. 2016. Synthesis of magnetically recyclable $MnFe_2O_4$@ SiO_2@ Ag nanocatalyst: its high catalytic performances for azo dyes and nitro compounds reduction. *Applied Surface Science,* 376**,** 16-25.

LAGERGREN, S. 1898. Kungliga svenska vetenskapsakademiens. *Handlingar,* 24**,** 1-39.

LAURENT, S., FORGE, D., PORT, M., ROCH, A., ROBIC, C., VANDER ELST, L. & MULLER, R.N. 2008. Magnetic iron oxide nanoparticles: synthesis, stabilization, vectorization, physicochemical characterizations, and biological applications. *Chemical reviews*, *108*(6), 2064-2110.

LEE, K. X. & VALLA, J. A. 2017. Investigation of metal-exchanged mesoporous Y zeolites for the adsorptive desulfurization of liquid fuels. *Applied Catalysis B: Environmental,* 201**,** 359-369.

LOGANATHAN, P., VIGNESWARAN, S. & KANDASAMY, J. 2013. Enhanced removal of nitrate from water using surface modification of adsorbents–a review. *Journal of Environmental Management,* 131**,** 363-374.

LONGO, G. S. & SZLEIFER, I. 2016. Adsorption and protonation of peptides and proteins in pH responsive gels. *Journal of Physics D: Applied Physics,* 49**,** 323001.

LÓPEZ-MALDONADO, E., OROPEZA-GUZMAN, M., JURADO-BAIZAVAL, J. & OCHOA-TERÁN, A. 2014. Coagulation–flocculation mechanisms in wastewater treatment plants through zeta potential measurements. *Journal of Hazardous Materials,* 279**,** 1-10.

LU, J., LIU, H., ZHAO, X., JEFFERSON, W., CHENG, F. & QU, J. 2014. Phosphate removal from water using freshly formed Fe–Mn binary oxide: adsorption behaviors and mechanisms. *Colloids and Surfaces A: Physicochemical and Engineering Aspects,* 455**,** 11-18.

LV, L., HE, J., WEI, M., EVANS, D. & ZHOU, Z. 2007. Treatment of high fluoride concentration water by MgAl-CO3 layered double hydroxides: Kinetic and equilibrium studies. *Water Research,* 41**,** 1534-1542.

LV, S., CHEN, X., YE, Y., YIN, S., CHENG, J. & XIA, M. 2009. Rice hull/MnFe 2 O 4 composite: preparation, characterization and its rapid microwave-assisted COD removal for organic wastewater. *Journal of Hazardous Materials,* 171**,** 634-639.

MAHESH, M., THOMAS, J., KUMAR, K. A., BHOPLE, B. S., SARESH, N., VAID, S. K. & SAHU, S. K. 2018. Zeolite Farming: A Sustainable Agricultural Prospective. *Int. J. Curr. Microbiol. App. Sci,* 7**,** 2912-2924.

MALAEB, L. & AYOUB, G. M. 2011. Reverse osmosis technology for water treatment: state of the art review. *Desalination,* 267**,** 1-8.

MAYNARD, J. B. 2010. The chemistry of manganese ores through time: a signal of increasing diversity of earth-surface environments. *Economic Geology,* 105**,** 535-552.

MAZLAN, N. M., PESHEV, D. & LIVINGSTON, A. G. 2016. Energy consumption for desalination—A comparison of forward osmosis with reverse osmosis, and the potential for perfect membranes. *Desalination,* 377**,** 138-151.

MENSINGA, T. T., SPEIJERS, G. J. & MEULENBELT, J. 2003. Health implications of exposure to environmental nitrogenous compounds. *Toxicological reviews,* 22**,** 41-51.

MOERMOND, C. T., TIJINK, J., VAN WEZEL, A. P. & KOELMANS, A. A. 2001. Distribution, speciation, and bioavailability of lanthanides in the Rhine-Meuse estuary, The Netherlands. *Environmental Toxicology and Chemistry,* 20**,** 1916-1926.

MONDAL, N. K. & ROY, A. 2018. Potentiality of a fruit peel (banana peel) toward abatement of fluoride from synthetic and underground water samples collected from fluoride affected villages of Birbhum district. *Applied Water Science,* 8**,** 90.

M. 2017. Investigation of lanthanum impregnated cellulose, derived from biomass, as an adsorbent for the removal of fluoride from drinking water. *Carbohydrate Polymers,* 176**,** 402-410.

NAJAFPOUR, M. M., RENGER, G., HOŁYŃSKA, M., MOGHADDAM, A. N., ARO, E.-M., CARPENTIER, R., NISHIHARA, H., EATON-RYE, J. J., SHEN, J.-R. & ALLAKHVERDIEV, S. I. 2016. Manganese compounds as water-oxidizing catalysts: from the natural water-oxidizing complex to nanosized manganese oxide structures. *Chemical Review* 116**,** 2886-2936.

NAKHLI, A., BERGAOUI, M., AGUIR, C., KHALFAOUI, M., M'HENNI, M. F. & BEN LAMINE, A. 2016. Adsorption thermodynamics in the framework of the statistical physics formalism: basic blue 41 adsorption onto Posidonia biomass. *Desalination and Water Treatment,* 57**,** 12730-12742.

NETO, V. D. O. S., RAULINO, G. S. C., PAULO DE TARSO, C. F., ARAÚJO-SILVA, M. A. & DO NASCIMENTO, R. F. 2013. Equilibrium and kinetic studies in adsorption of toxic metal ions for wastewater treatment. *viewpoints,* 7**,** 8.

OFOMAJA, A., NAIDOO, E. & MODISE, S. 2010. Surface modification of pine cone powder and its application for removal of Cu (II) from wastewater. *Desalination and Water Treatment,* 19**,** 275-285.

OGATA, F., IMAI, D. & KAWASAKI, N. 2015. Adsorption of nitrate and nitrite ions onto carbonaceous material produced from soybean in a binary solution system. *Journal of Environmental Chemical Engineering,* 3**,** 155-161.

OKOLI, C. P. & OFOMAJA, A. E. 2018. Degree of time dependency of kinetic coefficient as a function of adsorbate concentration; new insights from adsorption of tetracycline onto monodispersed starch-stabilized magnetic nanocomposite. *Journal of Environmental Management,* 218**,** 139-147.

OUMA, I. L., NAIDOO, E. B. & OFOMAJA, A. E. 2018. Thermodynamic, kinetic and spectroscopic investigation of arsenite adsorption mechanism on pine cone-magnetite composite. *Journal of Environmental Chemical Engineering,* 6**,** 5409-5419.

ÖZTÜRK, N. & BEKTAŞ, T. E. 2004. Nitrate removal from aqueous solution by adsorption onto various materials. *Journal of Hazardous Materials,* 112**,** 155-162.

PING, N., HANS-JÖRG, B., BING, L., XIWU, L. & ZHANG, Y. 2008. Phosphate removal from wastewater by model-La (III) zeolite adsorbents. *Journal of Environmental Sciences,* 20**,** 670-674.

PRÜSS-USTÜN, A., WOLF, J., BARTRAM, J., CLASEN, T., CUMMING, O., FREEMAN, M. C., GORDON, B., HUNTER, P. R., MEDLICOTT, K. & JOHNSTON, R. 2019. Burden of disease from inadequate water, sanitation and hygiene for selected adverse health outcomes: an updated analysis with a focus on low-and middle-income countries. *International journal of hygiene and environmental health,* 222**,** 765-777.

QU, X., ALVAREZ, P. J. & LI, Q. 2013. Applications of nanotechnology in water and wastewater treatment. *Water Research,* 47**,** 3931-3946.

RABBANI, D., MAHMOUDKASHI, N., MEHDIZAD, F. & SHATERIAN, M. 2016. Green approach to wastewater treatment by application of Rosa damascena waste as nano-biosorbent. *Journal of Environmental Science and Technology,* 9**,** 121-130.

RAJMOHAN, K., GOPINATH, M. & CHETTY, R. 2016. Review on challenges and opportunities in the removal of nitrate from wastewater using electrochemical method. *Journal of Environmental Biology,* 37**,** 1519.

RAMBABU, N., PANTHAPULAKKAL, S., SAIN, M. & DALAI, A. 2016. Production of nanocellulose fibers from pinecone biomass: evaluation and optimization of chemical and mechanical treatment conditions on mechanical properties of nanocellulose films. *Industrial Crops and Products,* 83**,** 746-754.

RAO, S. M. & MAMATHA, P. 2004. Water quality in sustainable water management. *Current Science***,** 942-947.

RASHED, M. N. 2013. Adsorption technique for the removal of organic pollutants from water and wastewater. *Organic pollutants-monitoring, risk and treatment,* 7**,** 167-194.

RICHARD, A. M., DIAZ, J. H. & KAYE, A. D. 2014. Reexamining the risks of drinking-water nitrates on public health. *Ochsner Journal,* 14**,** 392-398.

RITCHIE, A. 1977. Alternative to the Elovich equation for the kinetics of adsorption of gases on solids. *Journal of the Chemical Society, Faraday Transactions 1: Physical Chemistry in Condensed Phases,* 73**,** 1650-1653.

ROY, S. & DASS, G. 2013. Fluoride contamination in drinking water–a review. *Resour. Environ,* 3**,** 53-58.

SAAVEDRA RIOS, C.D.M., SIMONIN, L., GEYER, A.D., MATEI GHIMBEU, C. & DUPONT, C. 2020. Unraveling the properties of biomass-derived hard carbons upon thermal treatment for a practical application in na-ion batteries. *Energies, 13*(14), 3513.

SADEGH, H., ALI, G. A., GUPTA, V. K., MAKHLOUF, A. S. H., SHAHRYARI-GHOSHEKANDI, R., NADAGOUDA, M. N., SILLANPÄÄ, M. & MEGIEL, E. 2017. The role of nanomaterials as effective adsorbents and their applications in wastewater treatment. *Journal of Nanostructure in Chemistry,* 7**,** 1-14.

SALEH, T. A., ADIO, S. O., ASIF, M. & DAFALLA, H. 2018. Statistical analysis of phenols adsorption on diethylenetriamine-modified activated carbon. *Journal of Cleaner Production,* 182**,** 960-968.

SHAILAJA, K. & JOHNSON, M. E. C. 2007. Fluorides in groundwater and its impact on health. *Journal of environmental biology,* 28**,** 331-332.

SHARMA, C., MAHAJAN, A. & KUMAR GARG, U. 2016. Fluoride and nitrate in groundwater of south-western Punjab, India—occurrence, distribution and statistical analysis. *Desalination and Water Treatment,* 57**,** 3928-3939.

SHI, J., YANG, Z., DAI, H., LU, X., PENG, L., TAN, X., SHI, L. & FAHIM, R. 2018. Preparation and application of modified zeolites as adsorbents in wastewater treatment. *Water Science and Technology***,** wst, 20**,** 182-249.

SIMONIN, J.-P. 2016. On the comparison of pseudo-first order and pseudo-second order rate laws in the modeling of adsorption kinetics. *Chemical Engineering Journal,* 300**,** 254-263.

SINGH, G., KUMARI, B., SINAM, G., KUMAR, N. & MALLICK, S. 2018. Fluoride distribution and contamination in the water, soil and plants continuum and its remedial technologies, an Indian perspective–a review. *Environmental Pollution,* 239**,** 95-108.

SINGH, S., BARICK, K. & BAHADUR, D. 2011. Surface engineered magnetic nanoparticles for removal of toxic metal ions and bacterial pathogens. *Journal of Hazardous Materials,* 192**,** 1539-1547.

SOTO-RIOS, P. C., NAKANO, K., LEON-ROMERO, M., AIKAWA, Y., ARAI, S. & NISHIMURA, O. 2015. Differences in the removal mechanisms of Undaria pinnatifida

and Phragmites australis as biomaterials for lead removal. *Water Science and Technology,* 72**,** 1226-1233.

SRIVASTAVA, V. C., MALL, I. D. & MISHRA, I. M. 2007. Adsorption thermodynamics and isosteric heat of adsorption of toxic metal ions onto bagasse fly ash (BFA) and rice husk ash (RHA). *Chemical Engineering Journal,* 132**,** 267-278.

STAFFORD, F. 2016. *The Long, Long Life of Trees*, Yale University Press.

STRATHMANN, H. 2010. Ion-exchange membrane processes in water treatment. *Sustainability Science and Engineering,* 2**,** 141-199.

SURIYARAJ, S. & SELVAKUMAR, R. 2016. Advances in nanomaterial based approaches for enhanced fluoride and nitrate removal from contaminated water. *Royal Society of Chemistry*, 13, 10565-10583.

SUTHERLAND, C., & VENKOBACHAR, C. (2010). A Diffusion-Chemisorption Kinetic Model for Simulating Biosorption Using Forest Macro-Fungus, Fomes Fasciatus. *Int. Res. J. Plant Sci.* 1. p.107–117s

TAHIR, N., BHATTI, H. N., IQBAL, M. & NOREEN, S. 2017. Biopolymers composites with peanut hull waste biomass and application for Crystal Violet adsorption. *International Journal of Biological Macromolecules,* 94**,** 210-220.

TANG, S. C. & LO, I. M. 2013. Magnetic nanoparticles: essential factors for sustainable environmental applications. *Water Research,* 47**,** 2613-2632.

TIAN, Y., WU, M., LIN, X., HUANG, P. & HUANG, Y. 2011. Synthesis of magnetic wheat straw for arsenic adsorption. *Journal of Hazardous Materials,* 193**,** 10-16.

VAGHARI, H., JAFARIZADEH-MALMIRI, H., MOHAMMADLOU, M., BERENJIAN, A., ANARJAN, N., JAFARI, N. & NASIRI, S. 2016. Application of magnetic nanoparticles in smart enzyme immobilization. *Biotechnology Letters,* 38**,** 223-233.

VAN DER BRUGGEN, B. & VANDECASTEELE, C. 2003. Removal of pollutants from surface water and groundwater by nanofiltration: overview of possible applications in the drinking water industry. *Environmental Pollution,* 122**,** 435-445.

VILLACORTE, L. O., TABATABAI, S. A. A., ANDERSON, D. M., AMY, G. L., SCHIPPERS, J. C. & KENNEDY, M. D. 2015. Seawater reverse osmosis desalination and (harmful) algal blooms. *Desalination,* 360**,** 61-80.

WANG, J., WU, L., LI, J., TANG, D. & ZHANG, G. 2018. Simultaneous and efficient removal of fluoride and phosphate by Fe-La composite: Adsorption kinetics and mechanism. *Journal of Alloys and Compounds,* 753**,** 422-432.

WEBB, P. A. 2003. An introduction to chemical adsorption analytical techniques and methods. *MIC Tech. Publ.,* 13**,** 1-4.

WIESNER, A. D., KATZ, L. E. & CHEN, C.-C. 2006. The impact of ionic strength and background electrolyte on pH measurements in metal ion adsorption experiments. *Journal of colloid and interface science,* 301**,** 329-332.

WHO, 2008. *Guidelines for drinking-water quality: second addendum. Vol. 1, Recommendations*. World Health Organization.

WORCH, E. 2012. Adsorption Technology in Water Treatment Fundamentals, Processes, and Modeling, 2012 Walter de Gruyter GmbH & Co. *KG, Berlin/Boston,* 5**,** 3.

YADAV, A. K., ABBASSI, R., GUPTA, A. & DADASHZADEH, M. 2013. Removal of fluoride from aqueous solution and groundwater by wheat straw, sawdust and activated bagasse carbon of sugarcane. *Ecological Engineering,* 52**,** 211-218.

YAN, X., LIU, M., ZHONG, J., GUO, J. & WU, W. 2018. How human activities affect heavy metal contamination of soil and sediment in a long-term reclaimed area of the Liaohe River Delta, North China. *Sustainability,* 10**,** 338.

YANG, Z.-H., CAO, J., CHEN, Y.-P., LI, X., XIONG, W.-P., ZHOU, Y.-Y., ZHOU, C.-Y., XU, R. & ZHANG, Y.-R. 2019. Mn-doped zirconium metal-organic framework as an effective adsorbent for removal of tetracycline and Cr (VI) from aqueous solution. *Microporous and Mesoporous Materials,* 277**,** 277-285.

YU, Y. & CHEN, J. P. 2015. Key factors for optimum performance in phosphate removal from contaminated water by a Fe–Mg–La tri-metal composite sorbent. *Journal of Colloid and Interface Science,* 445**,** 303-311.

YUSUF, M., KHAN, M. A., OTERO, M., ABDULLAH, E., HOSOMI, M., TERADA, A. & RIYA, S. 2017. Synthesis of CTAB intercalated graphene and its application for the adsorption of AR265 and AO7 dyes from water. *Journal of Colloid and Interface Science,* 493**,** 51-61.

ZHANG, C., LI, Y., WANG, F., YU, Z., WEI, J., YANG, Z., MA, C., LI, Z., XU, Z. & ZENG, G. 2017. Performance of magnetic zirconium-iron oxide nanoparticle in the removal of phosphate from aqueous solution. *Applied Surface Science,* 396**,** 1783-1792.

ZHANG, F.-S. & ITOH, H. 2006. Photocatalytic oxidation and removal of arsenite from water using slag-iron oxide-TiO_2 adsorbent. *Chemosphere,* 65**,** 125-131.

ZHOU, L., DENG, H., WAN, J., SHI, J. & SU, T. 2013. A solvothermal method to produce RGO-Fe 3 O 4 hybrid composite for fast chromium removal from aqueous solution. *Applied Surface Science,* 283**,** 1024-1031.

ZINICOVSCAIA, I. 2016. Conventional methods of wastewater treatment. *Cyanobacteria for bioremediation of wastewaters, 11***,** 17-25.

CHAPTER 3

3. EXPERIMENTAL METHODOLOGY

3.1 INTRODUCTION

The chapter is broken down into three sections. The first section explains the co-precipitation method of preparing the doped magnetite pinecone powder nano-particles adsorbent. The second section involves characterization of the prepared lanthanum and manganese doped magnetite pinecone nano-particles using Fourier transform infrared instrument (FTIR), thermogravimetric analysis (TGA), X-ray diffraction (XRD), scanning electron microscope (SEM) and electron dispersive X-ray spectroscopy (EDX). Experiments are also presented to determine acidic groups and pH_{pzc} with solid addition method. The last sections describe the application of doped magnetite pinecone adsorbents (La-MNP-PCP and Mn-MNP-PCP) to remove nitrate and fluoride from aqueous solution. The batch adsorption studies and kinetic studies were also determined.

3.2 EXPERIMENTAL

3.2.1 Chemicals and reagents

Ferric chloride ($FeCl_3 \cdot 6H_2O$), manganese sulphate (Mn_2SO_4> 99 %), lanthanum chloride ($LaCl_3.7H_2O$> 99 %), ethanol 99% and were purchased from Sigma-Aldrich. Ferrous sulphate ($FeSO_4 \cdot 7H_2O$> 99 %), sodium hydroxide pellets (NaOH) and ammonium hydroxide (NH_4OH) were supplied by Labchem (South Africa). Sodium nitrate ($NaNO_3$) and sodium fluoride (NaF).. Some of the materials used in this study include weighing Scale, pH meter, sieves, pulveriser, vacuum pump, vacuum oven, plastic containers, weighing scale, reflux apparatus. All the reagents used in this study were analytical grade and were used without further purification.

Nitrate standard solution 1000 mg/L: A stock solution of 1000 mg/L nitrate was prepared by measuring 3.6 g of oven dried KNO_3 Dissolve 3.6 g of KNO_3 in 250 mL of ultrapure water. Poured solution into a 500 mL graduated cylinder and filled the cylinder to the 500 mL line with distilled water. Carefully swirled to mix. Poured into a jar and label as 1000 mg/L nitrate solution. Put the date on the label.

Nitrate standard solution 100 mg/L: A stock solution of 100 mg/L nitrate was prepared by measuring 0.36 g of oven dried KNO_3 Dissolve 0.36 g of KNO_3 in 250 mL of ultrapure water. Poured solution into a 500 mL graduated cylinder and filled the cylinder to the 500 mL line with distilled water. Carefully swirled to mix. Poured into a jar and label as 100 mg/L nitrate solution. Put the date on the label.

Nitrate standard solution 50 mg/L: A stock solution of 50 mg/L nitrate was prepared by measuring 0.18 g of oven dried KNO_3 Dissolve 0.18 g of KNO_3 in 250 mL of ultrapure water. Poured solution into a 500 mL graduated cylinder and filled the cylinder to the 500 mL line with distilled water. Carefully swirled to mix. Poured into a jar and label as 50 mg/L nitrate solution. Put the date on the label.

Fluoride standard solution 1000 mg/L: To prepare this standard solution, filled out a quater of a 1 liter volumetric flask with ultrapure water and added 2.21 grams of analytical grade sodium fluoride (NaF) reagent. Swirled the volumetric flask gently to dissolve the reagent and filled to the mark with distilled water. Caped and upend the volumetric flask several times to mix the solution. Put the date on the label.

Fluoride standard solution 100 mg/L: To prepare this standard solution, filled out a quater of a 1 liter volumetric flask with ultrapure water and added 0.221 grams of analytical grade sodium fluoride (NaF) reagent. Swirled the volumetric flask gently to dissolve the reagent and filled to the mark with distilled water. Caped and upend the volumetric flask several times to mix the solution. Put the date on the label.

Fluoride standard solution 50 mg/L: To prepare this standard solution, filled out a quater of a 1 liter volumetric flask with ultrapure water and added 0.110 grams of analytical grade sodium fluoride (NaF) reagent. Swirled the volumetric flask gently to dissolve the reagent and filled to the mark with distilled water. Caped and upend the volumetric flask several times to mix the solution. Put the date on the label.

3.2.2 Pine tree cones collection

Pine cones were collected from the Vaal University of Technology, Vanderbijlpark Campus, South Africa. The cones scales were peeled off and washed with water to remove impurities such as sand

and leaves. The washed scales were dried in the oven at 90 ^{o}C for 24 h. The scales were dry-milled by a ball mill pulveriser, sieved, and particles between 90 and 45 µm were collected and applied (Ofomaja *et al*., 2010).

3.2.3 Treatment of Pinecone with NaOH

A weighed amount of 50 g of the milled pinecone powder was transferred into a 1000 mL beaker containing 500 mL of 0.15 mol/L sodium hydroxide solution. The mixture was stirred for 18 h at 500 rpm, washed with water until the water is clear and dried at 60^{o} C for 24h (Ofomaja *et al*., 2010).

3.2.3 Preparation of Manganese-doped PCP-Fe_3O_4 (Mn-MNP-PCP) adsorbent

A weighed amount of 3.1 g $FeCl_3 \cdot 6H_2O$, 2.1 g $FeSO_4 \cdot 7H_2O$ and 0.5 g Mn $(SO_4)_2$ was dissolved in round flask containing 100 mL water and heated to 60 ^{o}C using a hot plate. An amount of 1.5 g of pinecone powder was added to the manganese-iron solution. A 30 mL solution of ammonium hydroxide (25%) was added rapidly and sequentially to a residue. The solution was stirred for 30 min and cooled to a room temperature. The filtered precipitates were washed with ultrapure water to a neutral pH, then washed with 250 mL of ethanol (99%). The solution was then centrifuged at 60 rpm for 60 seconds, and the suspended solids (Mn-MNP-PCP) were dried in a vacuum oven at 60 ^{o}C.

3.2.4 Preparation of Lanthanum-doped PCP-Fe_3O_4 (La-MNP-PCP) adsorbent

About 100 mL solution containing 3.1 g $FeCl_3 \cdot 6H_2O$, 2.1 g $FeSO_4 \cdot 7H_2O$ and 0.5 g $La(NO_3)_3$ was prepared with water and heated to 60 ^{o}C. The mixture was thoroughly mixed with 1.5 g of pinecone powder, followed by 30 mL ammonium hydroxide (25%) solution was added rapidly and sequentially. The mixture was stirred for 30 min and cooled to room temperature. The solution was filtered, and the residue obtained was washed several times with ultrapure water until reaching a neutral pH. The solution was further washed with 250 mL ethanol (99%), centrifuged at 60 rpm for 60 sec, and the suspended solids (MNP-PCP) were dried at 60 ^{o}C overnight. An amount of 0.8 g of freshly prepared MNP-PCP was dispersed in a mixture of 12.5 mL ultrapure water, 12.5 mL cyclohexanol and 1 mL NaOH (2 M) followed by sonication for 30 min. Then, 1.6 g of lanthanum chloride heptahydrate ($LaCl_3.7H_2O$) was added into the mixture under vigorous stirring for 30 min. The mixture was incubated at 100 ^{o}C for five days to produce La-MNP-PCP. Finally, the product

was washed several times with ethanol, followed by acetone, methanol and excess ultrapure water, then oven-dried at 80 ^{o}C in a vacuum oven for 24 h (Nodeh *et al*., 2017).

3.3 CHARACTERIZATION OF ADSORBENTS

3.3.1 Fourier Transform Infrared (FTIR):

Fourier Transform Infrared Spectrometer (Perkin-Elmer infrared spectrophotometer) was conducted to elucidate functional groups present in the MNP-PCP, Mn-MNP-PCP and La-MNP-PCP before and after nitrate and fluoride adsorption. The analysis were done using a Perkin-Elmer (USA) FTIR Spectra 400 spectrometer in the range 650-4000 cm^{-1}.

3.3.2 Thermogravimetric Analysis (TGA):

The Thermal analyser (Perkin Elmer STA 6000) was used to measure the weight loss change sample's weight loss as a function of temperature. This instrument can obtain DSC and TGA measurements simultaneously. The MNP-PCP, Mn-MNP-PCP and La-MNP-PCP adsorbents were weighed into quartz crucibles. Thermal scans were performed from 30 to 700 °C at a heating rate of 10 ^{o}C/min using empty crucible as a reference.

3.3.3 X-ray Diffraction (XRD):

The phase and structural propertiesof the adsorbents were analyzed by X-ray diffraction. XRD patterns were obtained with an X'Pert PRO X-ray diffractometer (PANalytical, PW3040/60 XRD; CuKα anode; λ = 0.154 nm). The samples were gently consolidated in an aluminium holder and scanned at 45 kV and 40 mA from 10 ^{o}C to 90 ^{o}C the exposure time for each sample was 20 min and a step size of 0.02. The diffraction patterns were analyzed using X'Pert High Score software (version 2.2.0) and plotted using Origin Pro 7.0.

3.3.4 Scanning Electron Microscope (SEM)-Energy Dispersive Spectroscopy EDX

The Scanning Electron Microscope was used to investigate the structural morphology and shape nature images of Mn-MNP-PCP and La-MNP-PCP adsorbents (before and after adsorption) using JEOL JSM-6500F FE-SEM. A cast resin stub was produced for each Mn-MNP-PCP and La-MNP-PCP adsorbents (before and after adsorption) sample received. The stubs were polished and gold coated. Imaging was done at different magnification to provide a representative overview of each

sample. Energy Dispersive spectroscopy was also taken to determine the elemental composition of the Mn-MNP-PCP and La-MNP-PCP adsorbents (before and after adsorption).

3.3.5 X-ray Photoelectron Spectroscopy XPS

X-ray photoelectron spectroscopy (XPS) analysis was carried out on PHI 5000 scanning ESCA microprobe with a 100 μm diameter monochromatic Al Kα x-ray beam (hν = 1486.6 eV) generated by a 25 W, 15 kV electron beam to analyze different binding energy peaks. Multipack version 9 software was utilized to analyse the spectra to identify the chemical compounds and their electronic states using Gaussian–Lorentz fits.

3.3.6 pH at point zero charge

The solid addition method was used to determine the pH at point zero charge (pH_{pzc}) of the Mn-MNP-PCP and La-MNP-PCP adsorbents (Ofomaja *et al.*, 2014). To a series of 100 mL conical flasks, 45 mL of 0.01 $mol.dm^{-3}$ of a KNO_3 solution of known concentration was transferred. The solution's pH values were adjusted from pH 2 to 12 by adding either 0.010 $mol.dm^{-3}$ of HCl or NaOH. The total volume of the solution in each flask was made up to 50 mL by adding KNO_3 of the same strength. The solution's pH_i values were accurately noted, and 0.1 g of Mn-MNP-PCP and La-MNP-PCP adsorbents were added to each volumetric flask, which was securely instantly capped. The suspension was shaken and allowed to equilibrate for 48 h with intermittent manual shaking. The pH value of the supplements liquids was noted. The difference between the initial and the final pH values ($\Delta pH = pH_i - pH_f$) was plotted against the pH_i. The point of intersection of the resulting curve at which $\Delta pH = 0$ gave the pH_{pzc}.

3.4 EXPERIMENTAL PROCESS FOR THE REMOVAL OF NITRATE AND FLUORIDE IONS USING Mn-MNP-PCP and La-MNP-PCP ADSORBENTS

Batch sorption experiments for nitrate and fluoride ion using Mn-MNP-PCP and La-MNP-PCP adsorbents were conducted to determine the optimum adsorbent dose, solution pH, temperature, adsorbent concentration and equilibrium time, to generate adsorption equilibrium data and kinetics data. The concentrations of nitrate/fluoride ion left in the solutions were analysed by ion-selective

electrode meter (HANNA HI5522-01 ISE). The amount of nitrate/fluoride ion adsorbed onto the adsorbent was calculated using the following equation:

$$q = \frac{C_i - C_f}{m} \text{x } V \quad (3.1)$$

The amount (%) of nitrate and fluoride adsorbed/removed onto the adsorbent was calculated using the following equation:

$$q\% = \frac{C_f}{C_i} \quad (3.2)$$

Where, q is the amount of adsorbed nitrate/fluoride (mg/g), C_i is the initial concentration (mg/L), C_f is the equilibrium concentration (mg/L), *V* is the solvent volume (*L*), and m is the mass of the adsorbent sample (g).

3.4.1 Effect of solution pH

The effect of initial solution pH on the nitrate and fluoride adsorption was studied in a batch adsorption system in which 100 mL of 50 mg/L of nitrate and fluoride ion was added to 250 mL beakers, and the initial solution pH varied from 2.0 to 12.0 using 0.01 mol/L of either HCl or NaOH solution. An amount of 0.1 g of Mn-MNP-PCP and/or La-MNP-PCP adsorbents were added to each beaker and agitated for 2 h with Radleys Tornado overhead stirring system at 25 °C at 195 rpm. The solution was then filtered through a 0.45 mm filter paper to stop adsorption. The nitrate and fluoride concentrations in the supernatant solutions were analysed by (nitrate and fluoride) ion-selective electrode meter (HANNA HI5522-01 ISE).

3.4.2 Effect of adsorbent dosage

The effect of biosorbent dose on the equilibrium uptake of was investigated by adding the biosorbents masses of 0.05; 0.10; 0.50; 1.0; and 1.5 g to five 250 mL beakers containing 100 mL of 100 mg/L solutions at optimum pH. The flasks were shaken at 195 rpm and 26 °C for 2 h. The equilibrium concentration of nitrate and fluoride remaining in solution was determined by ion-selective electrode meter (HANNA HI5522-01 ISE). The amount of nitrate/fluoride adsorbed was calculated using Eq. (3.1).

3.4.3 Effect of initial adsorbate concentration

Different concentrations of 100 ml nitrate/fluoride ion solutions (10, 25, 50, 75 and 100 mg/L) at optimum pH were added to a weighed adsorbent masses 0.1 g. The sample solutions were stirred with Radleys Tornado overhead stirring system at 26 °C for 2 h at 195 rpm and filtered. The concentrations of nitrate/fluoride in the supernatant solutions were analysed by ion-selective electrode meter (HANNA HI0000 ISE).

3.4.4 Effect of contact time at different concentrations

Different concentrations of 100 ml nitrate/fluoride ion solutions (10, 20, 40, 60 and 100 mg/L) at optimum pH were added to a weighed adsorbent mass of 0.1 g. The nitrate or fluoride ISE probe was inserted in the solution while monitoring and collecting the concentration reading (in mg/L) at selected time intervals (0.5; 1; 2; 3; 5; 20; 30; 60 and 120 min). The amount of nitrate/fluoride adsorbed was calculated using Eq. (3.1).

3.4.5 Effect of temperatures at different concentrations

A weighed amounts of 0.1 g of adsorbents were mixed with 100 ml of each nitrate/fluoride batch sample (10, 20, 40, 60 and 100 mg/L) solutions prepared at optimum pH. The solutions were agitated with a maintained solution temperature of 25, 30, 35, 40 and 45 °C with Radleys Tornado overhead stirring System at 195 rpm for 1 h and filtered. The concentrations of nitrate/fluoride in the supernatant solutions were analysed by ion-selective electrode meter (HANNA HI5522-01 ISE), and nitrate/fluoride adsorbed was calculated using Eq. (3.1).

3.4.6 Temperature Kinetics

Weighed amounts of 0.1 g adsorbent were added to 100 mL, 100 mg/L concentration of nitrate/fluoride batch sample solutions prepared at optimum pH. The solutions were agitated with a maintained solution temperature of 25, 30, 35, 40 and 45 °C with Radleys Tornado overhead stirring system at 195 rpm. The ISE probe was inserted in the solution while monitoring and collecting the concentration reading (in mg/L) at selected time intervals. The concentrations of nitrate/fluoride in the supernatant solutions were analysed by (nitrate and fluoride) ion-selective electrode meter (HANNA HI5522-01 ISE), and the amount of nitrate/fluoride adsorbed was calculated using Eq. (3.1).

3.4.7 Effect of co-existing (competing) anions

Effect of co-existing anions was conducted to evaluate the influence of competing anions by adding 0.1 mol/dm^3 concentrations of co-existing anions sodium chloride (NaCl), sodium sulphate (Na_2SO_4), sodium carbonate (Na_2CO_3) and sodium phosphate (Na_3PO_4),) in 100 mL nitrate/fluoride solution (fixed nitrate/fluoride concentration of 100 mg/dm^3) for 2 hat room temperature at optimum pH and adsorbent mass of 0.1 g. At the end of experiments, the loaded adsorbent was separated from the solution through a 0.45 mm filter paper. To minimize minor interferences of other competing ions, Ionic Strength Adjustment Buffer (ISAB) was prepared by dissolving 10.5 g Potassium Sulphate (A.R. grade) and 3.11g of silver sulphate in 800 mL de-ionised water. Then 25 mL of 0.1 M sulphuric acid was added and makeup to 1000 mL. The residual nitrate/fluoride concentration was added to a special ISAB in equal volumes (1:1), (nico2000, 2015, Feb 11). The concentrations of nitrate/fluoride in the solutions were analysed by using (nitrate and fluoride) ion-selective electrode meter (HANNA HI5522-01 ISE) and the amount of nitrate/fluoride adsorbed was calculated using Eq. (3.1).

3.5 REFERENCE

NICO2000. 2015, Feb 11. *Method for determining the concentration of nitrate (NO_3^-) in aqueous solutions* [Online]. Available: http://www.nico2000.net/analytical/nitrate.htm [Accessed Oct 08 2017].

NODEH, H. R., SERESHTI, H., AFSHARIAN, E. Z. & NOURI, N. 2017. Enhanced removal of phosphate and nitrate ions from aqueous media using nanosized lanthanum hydrous doped on magnetic graphene nanocomposite. *Journal of Environmental Management,* 197**,** 265-274.

OFOMAJA, A., NAIDOO, E. & MODISE, S. 2010. Surface modification of pine cone powder and its application for removal of Cu (II) from wastewater. *Desalination and Water Treatment,* 19**,** 275-285.

CHAPTER 4

4 RESULTS AND DISCUSSION (CHARACTERIZATION OF THE ADSORBENT MATERIALS)

4.1 INTRODUCTION

This chapter covers the synthesis and characterisation of the magnetite coated pinecone powder nanocomposites (MNP-PCP), manganese doped magnetite coated pinecone (Mn-MNP-PCP) and lanthanum doped magnetite coated pinecone (La-MNP-PCP). The synthesised adsorbent materials (MNP-PCP, Mn-MNP-PCP and La-MNP-PCP) were characterised using various analytical techniques to determine their composition, crystallinity and morphology. Surface functional groups of the synthesised adsorbent materials (MNP-PCP, Mn-MNP-PCP and La-MNP-PCP) were elucidated using analytical techniques such as Fourier Transform Infrared Spectroscopy (FTIR). Other techniques such as X-ray diffraction (XRD) analysis were conducted for phase determination (amorphous or crystalline), and surface morphology was determined using scanning electron microscopy (SEM). The thermal stabilities were determined using thermogravimetric analysis (TGA) technique. The characterisation results showed the nanocomposites were correctly synthesised.

4.2 FOURIER TRANSFORMED INFRARED (FTIR) SPECTROSCOPY

FTIR analysis was conducted to study the different functional groups present in MNP-PCP, Mn-MNP-PCP and La-MNP-PCP materials and determine functional groups present on the magnetite coated pine and to understand its interaction with manganese and lanthanum. The analysis were done using a Perkin-Elmer (USA) FTIR Spectra 400 spectrometer in the range 650-4000 cm^{-1}, and the results are shown in Figure 4.1. The broad bands appearing at 3480 – 3300 cm^{-1} are assigned as –OH bond stretching of polyphenols, peak at 1641 cm^{-1}, and C=O stretching of carboxylic acid or ester in all the MNP-PCP material (Shahid et al., 2018). The peaks at 2982 and 1025 cm^{-1} are assigned to C–H stretching of CH_n (alkane) in cellulose component and indicated C-O-C stretching vibration of secondary alcohol in lignin and it is indicative of methoxy groups ($O\text{-}CH_3$), it confirmed the presence of pine cone in MNP-PCP composite (Bhaumik and Mondal, 2016, Lv et

al., 2007). The indication of iron oxide particle in MNP-PCP and Mn-MNP-PCP composites was observed at 560 cm^{-1}, due to vibrations (v1) band of Fe-O and the (v2) band of the Fe-O. For Mn-MNP-PCP functional groups, there was a decrease in the intensity between 500 and 350 cm^{-1}, this indicated the addition of manganese onto the magnetite-pinecone material as it was also observed by (Jiang et al., 2018). The FT-IR spectra of La-MNP-PCP, bands at 3425 cm^{-1} and 1642 cm^{-1} can be assigned to the O-H and C=O stretching and bending vibration of adsorbed water. Predominant peaks at 2982 and 1025 cm^{-1} correspond to C-H and C-O-C stretching on the washed pinecone powders surface. Magnetic stretching peak of FeO appeared intensively at 560 cm^{-1} indicating the presence of magnetite in La-MNP-PCP material. This band is interpreted as stretching vibrations of Fe^{2+} and Fe^{3+} ions in tetrahedral regions and Fe^{3+} ions in the octahedral areas of magnetite. A distinct peak observed on La-MNP-PCP at 400 cm^{-1} was assigned to the vibration modes of lanthanum, the observations indicate the doping on the MNP-PCP surface. At the same time, bands between 2250 and 2100 cm^{-1} in La-MNP-PCP adsorbent were assigned to C-N and C≡N stretch, respectively. This may be attributed to the cationic hydrogel in the La-MNP-PCP nanocomposites (Cao *et al*., 2014). The results obtained showed the successful synthesis of the La-MNP-PCP and Mn-MNP-PCP nanocomposite materials.

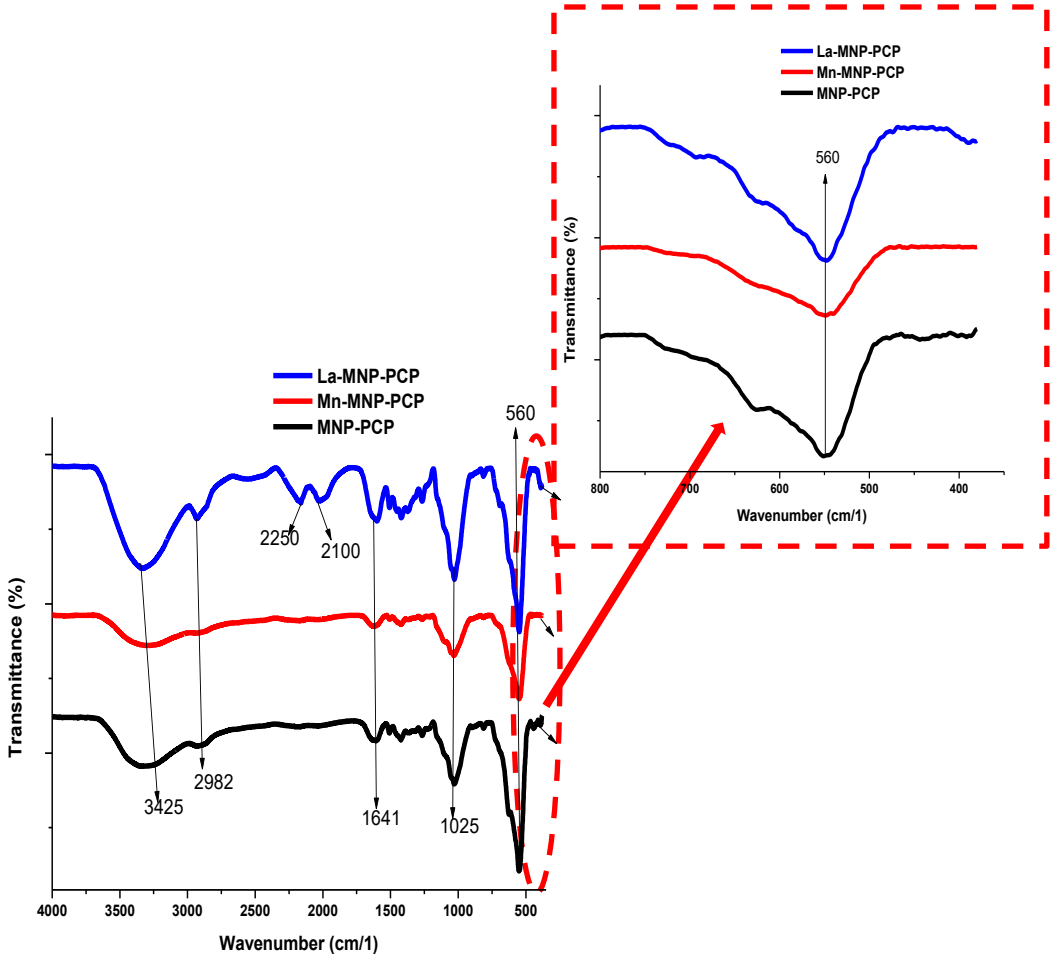

Figure 4.1: FTIR spectrum of MNP-PCP, Mn-MNP-PCP and La-MNP-PCP

4.3 THERMOGRAVIMETRIC ANALYSIS (TGA) AND DERIVATIVE THERMOGRAVIMETRIC ANALYSIS (DTA) OF MNP-PCP, MN-MNP-PCP and La-MNP-PCP

Thermogravimetric analysis (TGA) and differential thermal analysis (DTA) were carried out to determine the thermal stability of MNP-PCP, Mn-MNP-PCP and La-MNP-PCP and also to investigate their degradation profiles. The thermal analysis results of TGA and DTA curves obtained from MNP-PCP, Mn-MNP-PCP and La-MNP-PCP, were performed at a heating rate of 10 °C /min from 30 °C to 900 °C under inert conditions, and the results are shown in Figure 4.2 a-b. The thermal profile can be roughly divided into three stages in the following temperature ranges; 30–150 °C, 150–350 °C and 350–850 °C.

The MNP-PCP TGA profile and derivative weight loss percentage in Figure 4.2 a shows the first stage of weight loss of about 5.4 % at a temperature range of 30-150 °C, with a corresponding DTA curve of 360 °C. This weight loss can be attributed to the loss of surface adsorbed water (Roonasi and Holmgren, 2009). The second stage of weight loss was observed at a temperature range of 150-350 °C, which may be attributed to hemicellulose decomposition and cellulose decomposition (Sadeek et al., 2020). The final stage of decomposition was observed at a temperature range of 350-850 °C, attributed to the conversion of Fe_3O_4 to FeO (Roonasi and Holmgren, 2009, Liu et al., 2015).

The thermogram of Mn-MNP-PCP also indicated an initial weight loss at 30-150 °C, which was due to loss of surface adsorbed water. The sample weight loss continued at the temperature range of 150-350 °C; this step is usually related to the decomposition of uncoordinated carboxyl, hemicellulose, and hydroxyl groups from the pinecone. As shown by the cell parameters, there was a reduction and deoxidation at 717 °C due to manganese replacement of some iron sites in the crystal structure, resulting in a shift in the composition of magnetite crystals (Puerta and Valerga, 1990). The final derivative peak (750 °C) indicates the deoxidation of manganese oxide present in the doped sample (Liu et al., 2015). The DTA of Mn-MNP-PCP is slightly altered compared to MNP-PCP at temperatures above 500 °C, due to the addition of manganese onto the magnetite-pinecone material in Figure 4.2b.

Doping of lanthanum with magnetite pinecone nanocomposite depicted similar TGA behaviour as the Mn-MNP-PCP. Both the endothermic reactions and the weight loss at 30-150 °C are possibly attributed to removing water from the La-MNP-PCP material (Aghazadeh et al., Roonasi and Holmgren, 2009). The endothermic peak around 480 °C may be attributed to the complete decomposition of hydroxides and initiation of a complete formation of La-MNP-PCP (Ghosh et al., 2005).

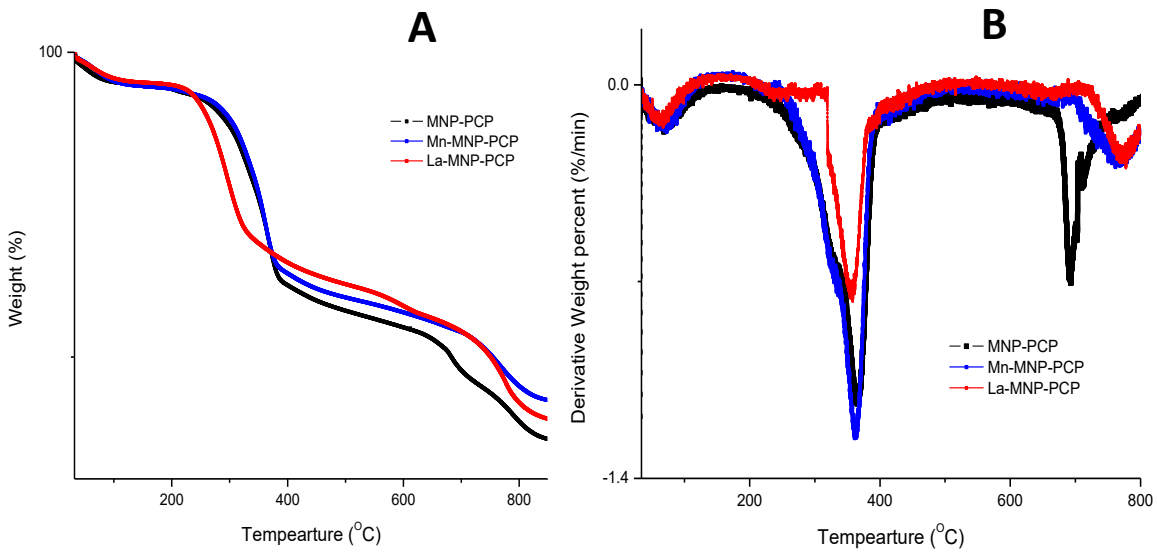

Figure 4.2: (a)Thermogravimetric and (b) differential thermal analysis curves for MNP-PCP, Mn-MNP-PCP and La-MNP-PCP

4.4 X-RAY DIFFRACTION (XRD) ANALYSIS

The X-ray diffraction of MNP-PCP, Mn-MNP-PCPand La-MNP-PCP, is shown in Figure 4.3. The diffraction peaks of MNP-PCP were observed around 2θ = 30.17°, 35.46°, 43.38°, 57.23° and 63.5° and are marked with their corresponding indices at (220), (311), (400), (422) and (440), as was also observed by Liu et al., (2015). The XRD of Mn-MNP-PCP exhibited new intense and sharp diffraction peaks around 39.2 ° and 47.5 °, this is attributed to the presence of manganese (Liu et al., 2015). The major reflections of all composition in the XRD patterns are indexed to $MnFe_2O_4$ (JCPDS10-0319) and Fe_3O_4 (JCPDS 75-1610) (Cui et al., 2013). The patterns match the standard diffraction pattern for synthetic magnetite and doped magnetite, confirming the synthesised nanoparticles inverse spinel structure (Aghazadeh et al., 2017). The presence or doping of Lanthanum onto MNP-PCP to be La-MNP-PCP did not generate any secondary, impurity-related reflections. Moreover, the diffraction intensity decreased of La-MNP-PCP, possibly indicating a decrease in crystallinity with the dopant's addition. It was established that La^{3+} acts similar to Fe^{2+} ions at the deposition and formation steps (Aghazadeh et al., 2017).

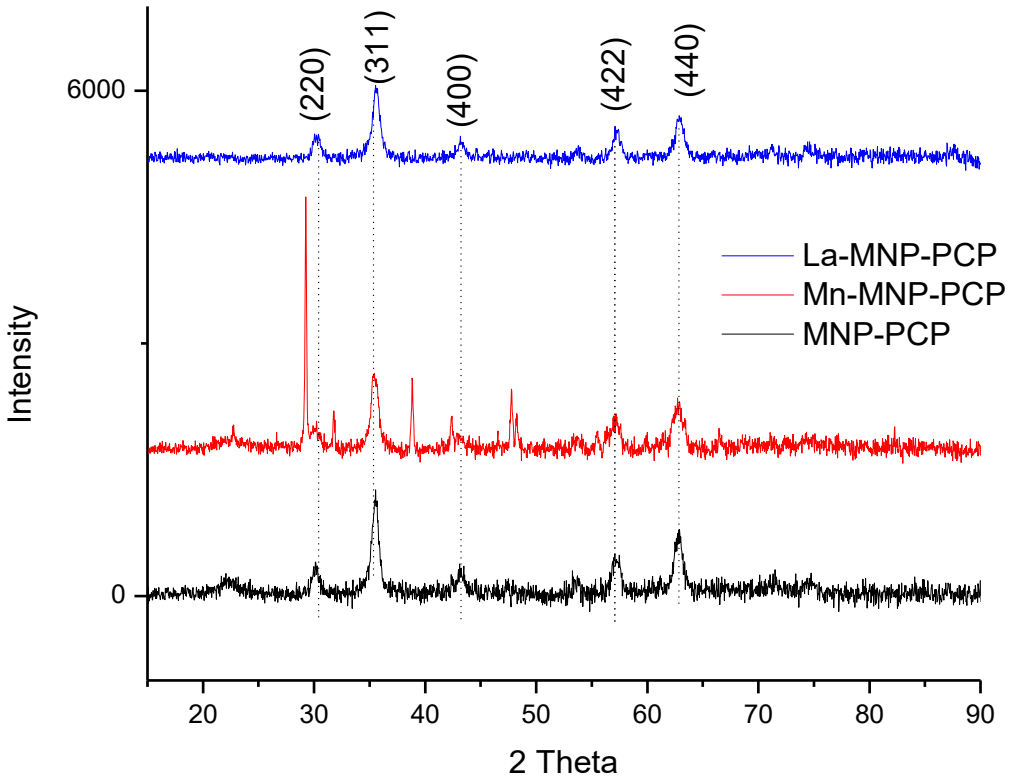

Figure 4.3: XRD diagram of MNP-PCP, Mn-MNP-PCP and La-MNP-PCP

4.5 TRANSMISSION ELECTRON MICROSCOPY IMAGING ANALYSIS

TEM analysis was conducted to investigate the morphology and particles size of MNP-PCP, Mn-MNP-PCP and La-MNP-PCP samples. The TEM micrograph and histograms of the size distribution are given in Figure 4.4 (a-c) and Figure 4.5 (a-c), respectively. The statistical analysis for the MNP-PCP, Mn-MNP-PCP and La-MNP-PCP samples were performed through counting several particles, using ImageJ software. The particle size distribution was fitted using the Gaussian function. The TEM micrographs of MNP-PCP in Figure 4.4 a) shows the particles to be spherical and had better separation as compared to Mn-MNP-PCP and La-MNP-PCP in Figure 4.4 b and c. MNP-PCP spherical nanostructures had an average particle size of approximately 13.8 nm. Mn-MNP-PCP particles in Figure 4.4(b), indicates that the presence of manganese inhibited the formation of nanostructures. The sample also consisted of agglomerates of primary particles with a spherical shape and an average size of 10.7 nm. Lastly, the TEM image of La–MNP-PCP in Figure 4.4(c) display well distributed and slightly agglomerated particles, which may

be attributed to magnetic statics interaction (Ganure et al., 2017). The average size particles of La-MNP-PCPC was estimated to be 12.6 nm. The histogram of MNP-PCP, Mn-MNP-PCP and La-MNP-PCP samples in Figure 4.5 (a-c) display a mean diameter of about 14, 10.9 and 125.5 nm, which is consistent with the result from TEM analysis.

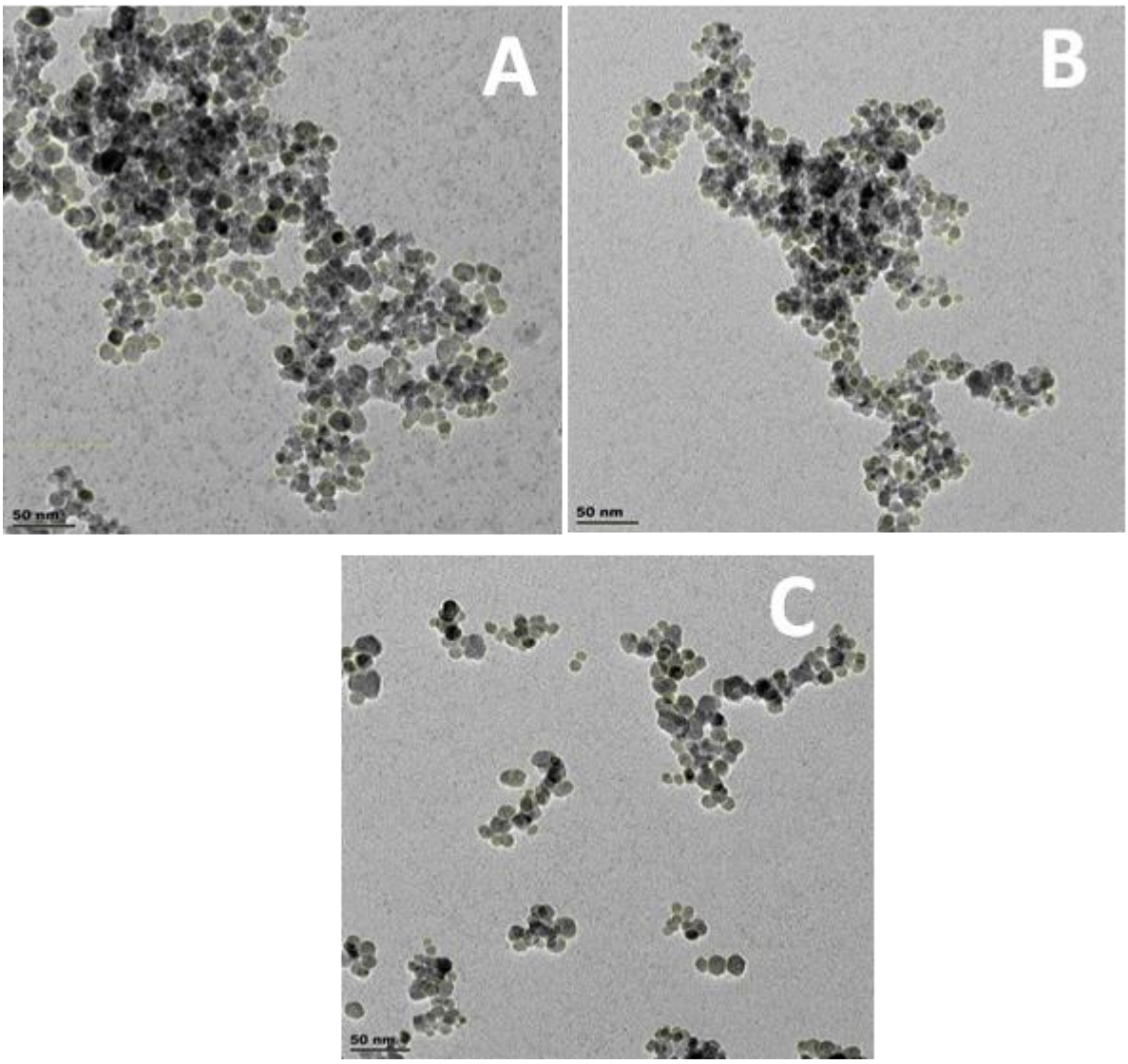

Figure 4.4: TEM micrographs of (a) MNP-PCP, (b) Mn-MNP-PCP and (c) La-MNP-PCP

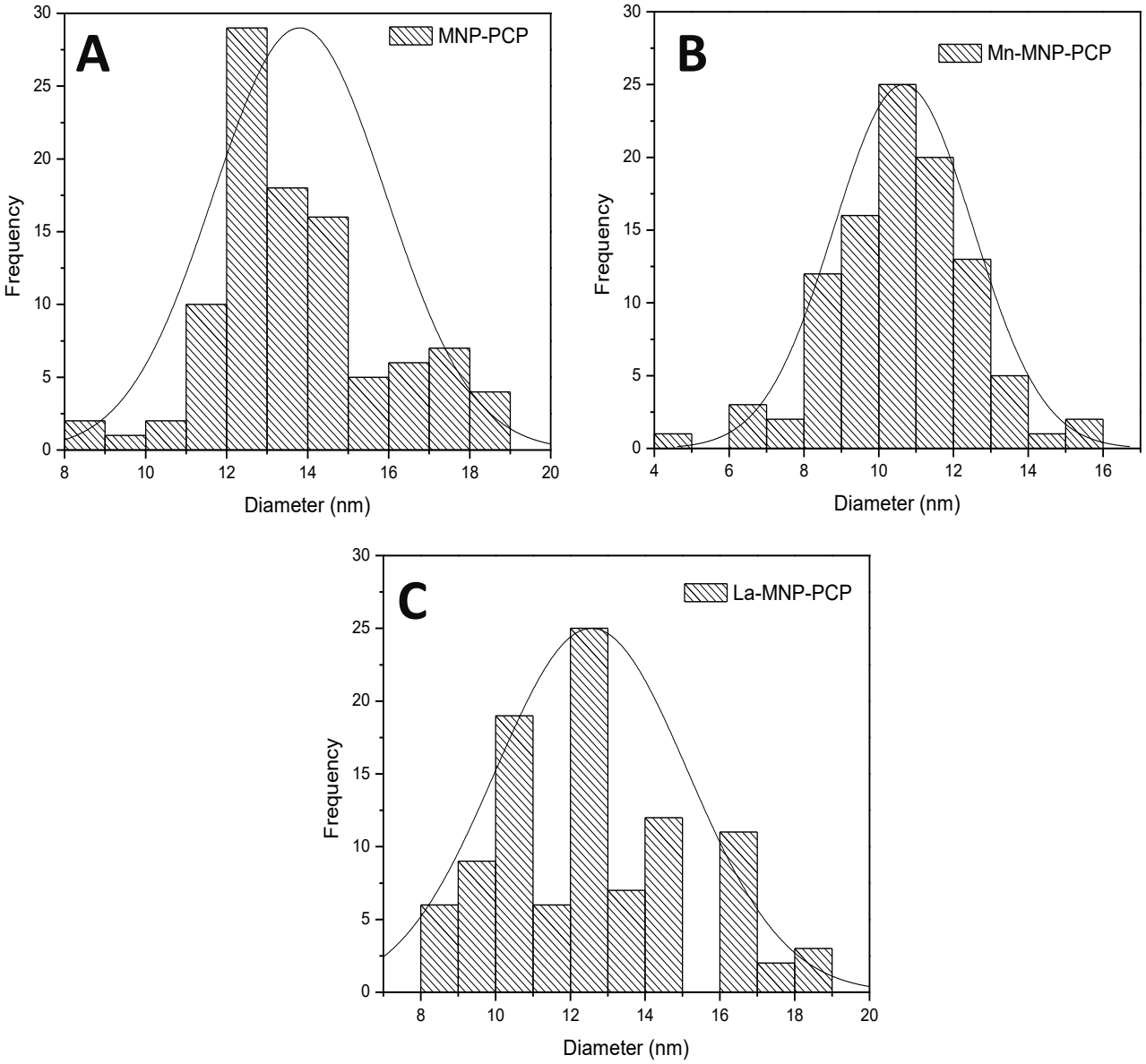

Figure 4.5: Size distribution of (a) MNP-PCP, (b) Mn-MNP-PCP and (c) La-MNP-PCP

4.6 SCANNING ELECTRON MICROSCOPY (SEM) AND ELECTRON DISPERSIVE SPECTROSCOPY (EDX)

The surface morphology of the synthesised MNP-PCP, Mn-MNP-PCP and La-MNP-PCP composites are shown in Figure 4.6 a-c. The surface of MNP-PCP in Figure 4.6(a) appears to have a spherical structure. The addition or doping of manganese led to an apparent change in the micro-morphology of Mn-MNP-PCP material in Figure 4.6b. Spherical particles were also observed on La-MNP-PCP in Figure 4.6c, and there was an increase in the size of the surface area of the material, which could be attributed to the presence of lanthanum dopant (Liang et al., 2018).

EDX spectroscopy was used to determine the elemental composition of MNP-PCP, Mn-MNP-PCP and La-MNP-PCP composites, and the results are presented in Table. 4.1. According to the EDX analysis results, the MNP-PCP had 17.33 % C, 17.5 % O and 65.17 % Fe; this confirms that the material was magnetite incorporated with pinecone powder. While Mn-MNP-PCP had 28.59 % C, 43.99 O, 25.73 % Fe and 1.69 % Mn, whilst La-MNP-PCP had 32.92 % C, 42.24 % O, 20.54 % Fe and 4.3 % La. The results show that the % Fe content for Mn-MNP-PCP and La-MNP-PCP composites was lower than that of MNP-PCP. This result can be attributed to the presence of the doping of manganese and lanthanum, respectively which affects the distribution of % Fe onto doped adsorbents.

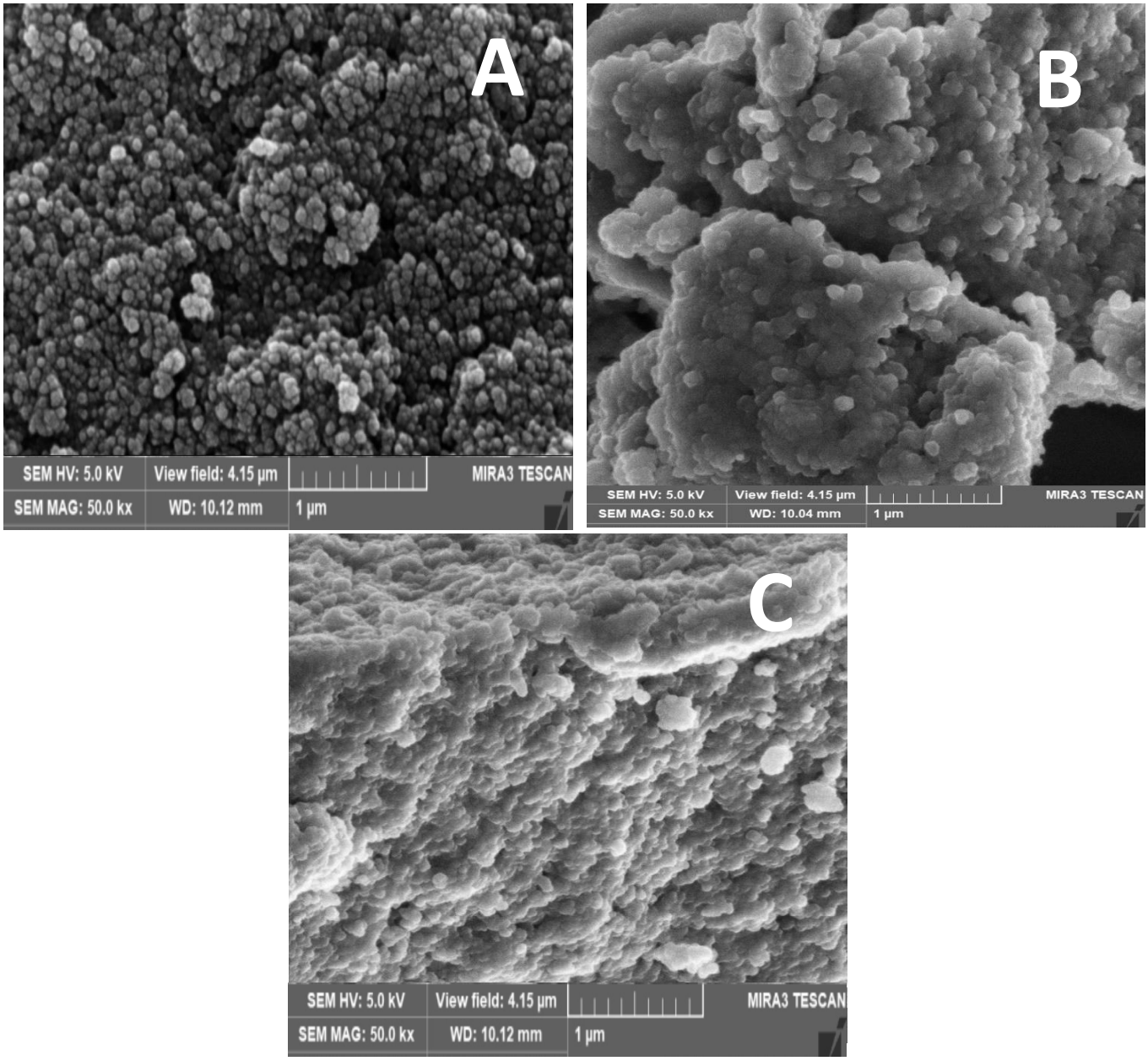

Figure 4.6: SEM images of (a) MNP-PCP, (b)Mn-MNP-PCP, (c) La-MNP-PCP

Table 4.1: Elemental analysis of MNP-PCP, Mn-MNP-PCP and La-MNP-PCP composites

	Weight (%)					
	C	O	Fe	Mn	La	Total
MNP-PCP	17.33	17.5	65.17	-	-	100
Mn-MNP-PCP	28.59	43.99	25.73	1.69	-	100
La-MNP-PCP	32.92	42.24	20.54	-	4.3	100

4.7 XPS SCANNING

X-ray photoelectron spectroscopy (XPS) is a versatile surface analysis technique used to analyse elements composition and chemical state of elements present on the MNP-PCP, Mn-MNP-PCP and La-MNP-PCP and the full range is shown in Fig.4.7a. The binding energy of various elements present and the surface states present in the prepared La-MNP-PCP sample was examined by XPS analysis in Figure 4.7a. Peaks corresponding to La 3d, F 2pe, O 1sand C 1s were observed on the La-MNP-PCP adsorbent with the binding energy at 830 and 850 eV for La, 700eV for Fe, 525 eV for O and 275 eV for C.

The Fe 2p XPS spectrum from La-MNP-PCP in Figure 4.7 b was deconvoluted into two peaks; at a binding energy of 710 and 723.5 corresponding to Fe $2p_{3/2}$, Fe $2p_{1/2}$ respectively which can be attributed to magnetite (Ouma et al., 2018). The high resolution XPS spectra of La in La-MNP-PCP was displayed in Figure 4.6c, and it indicated two peaks of La 3d5/2 at 833.3 eV, and 836.7 eV and one peak of La 3d3/2 centred at 852 eV (Wang et al., 2019), implying the incorporation of lanthanum with MNP-PCP. The deconvolved XPS spectrum of O 1s in Figure 4.7 d had three peaks at 530, 531 and 533 eV and the peaks were assigned to Fe-O-C in MNP-PCP, C-O and O-H from the NaOH washed pinecone powder (Mtshatsheni et al., 2019). The deconvolution of the C 1s peak shows the presence of three types of carbon bonds in Figure 4.6e at a binding energy of 284 eV, 286 eV and 289 eV corresponds to C-C bonds, C-O bonds and C=O from lignin and cellulose components of NaOH washed pinecone powder (Ouma et al., 2018).

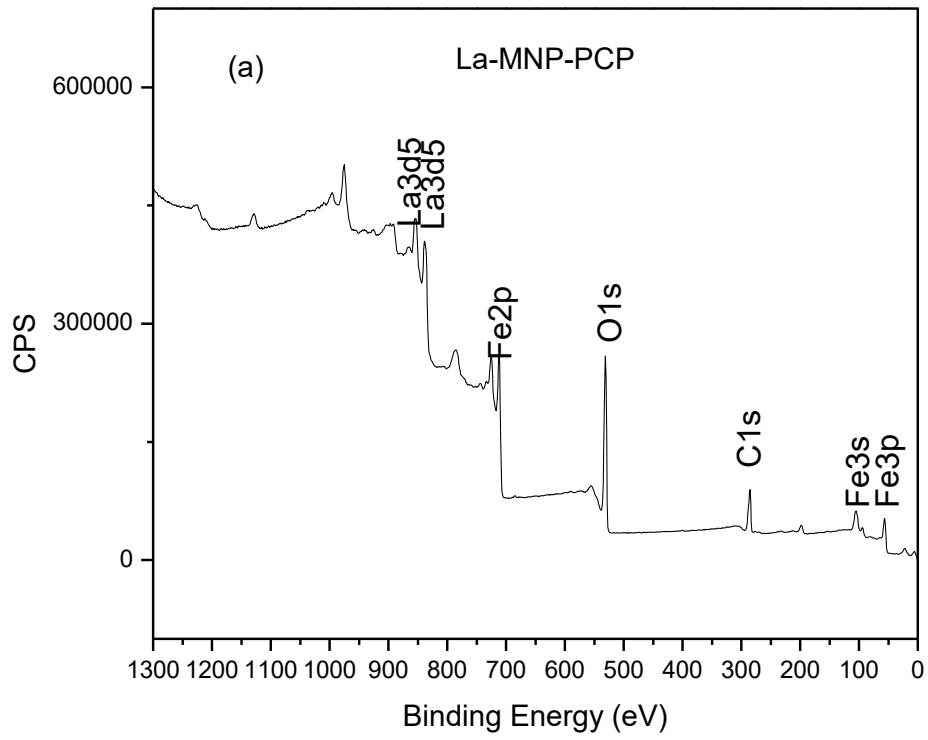

Figure 4.7a: XPS spectra of La-MNP-PCP

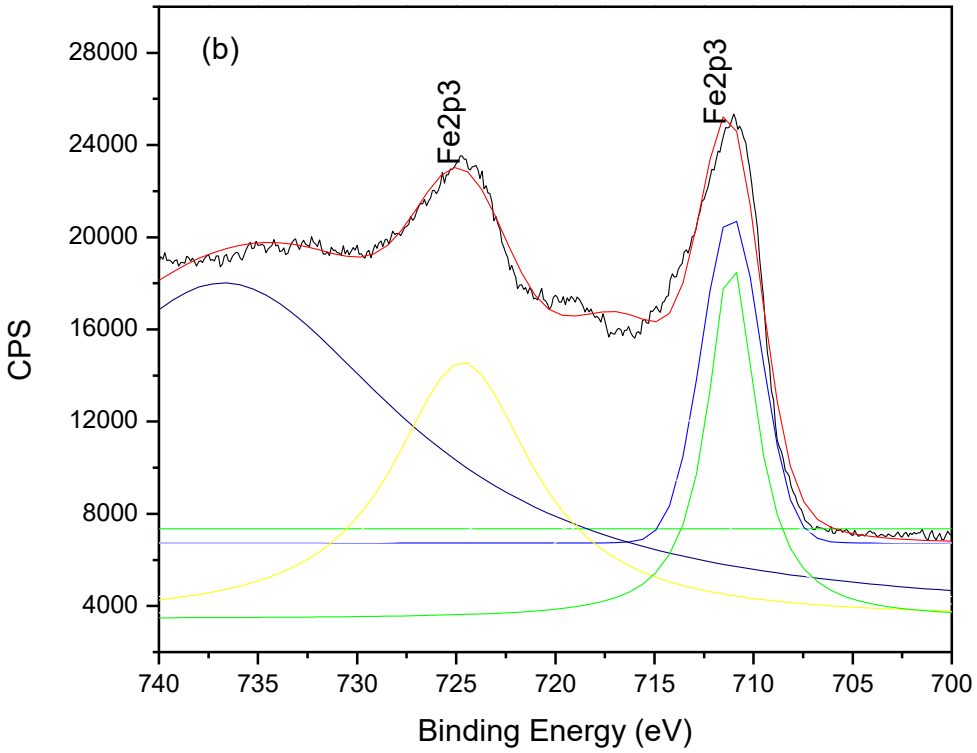

Figure 4.7b: XPS spectra of Fe2p

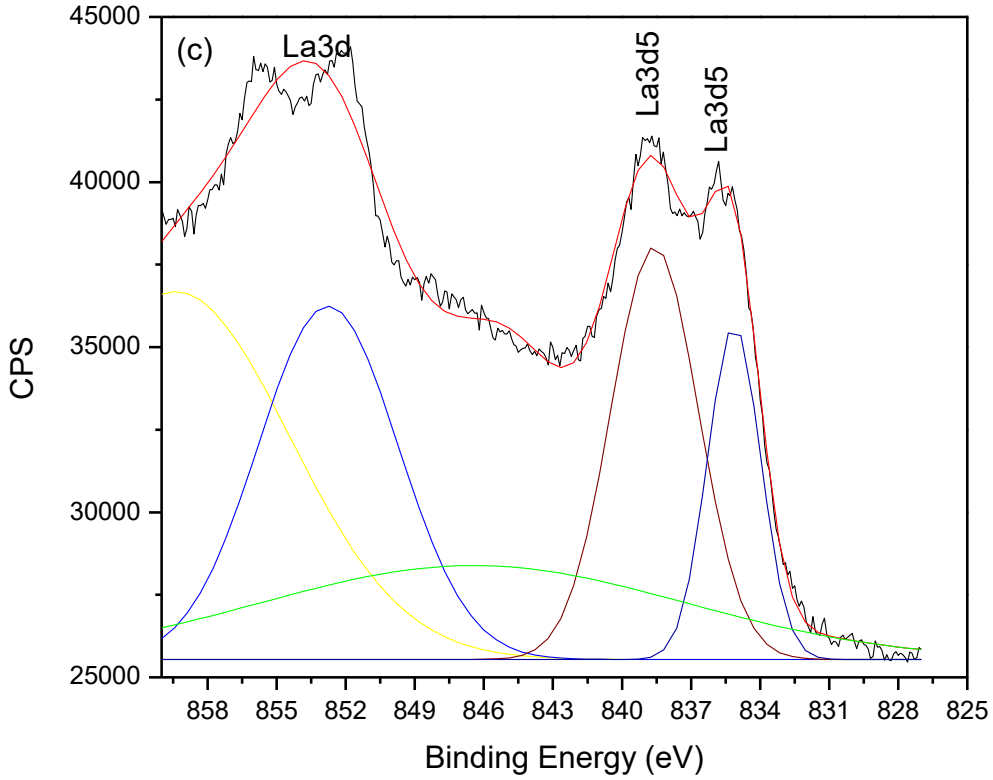

Figure 4.7c: XPS spectra of La3d

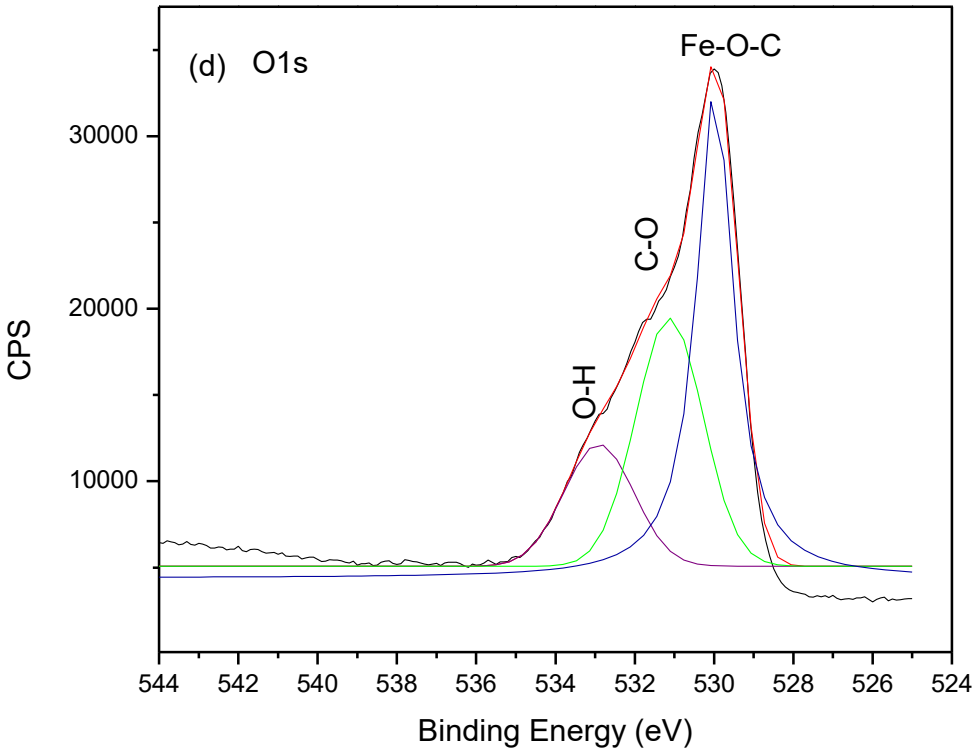

Figure 4.7d: XPS spectra of O1s

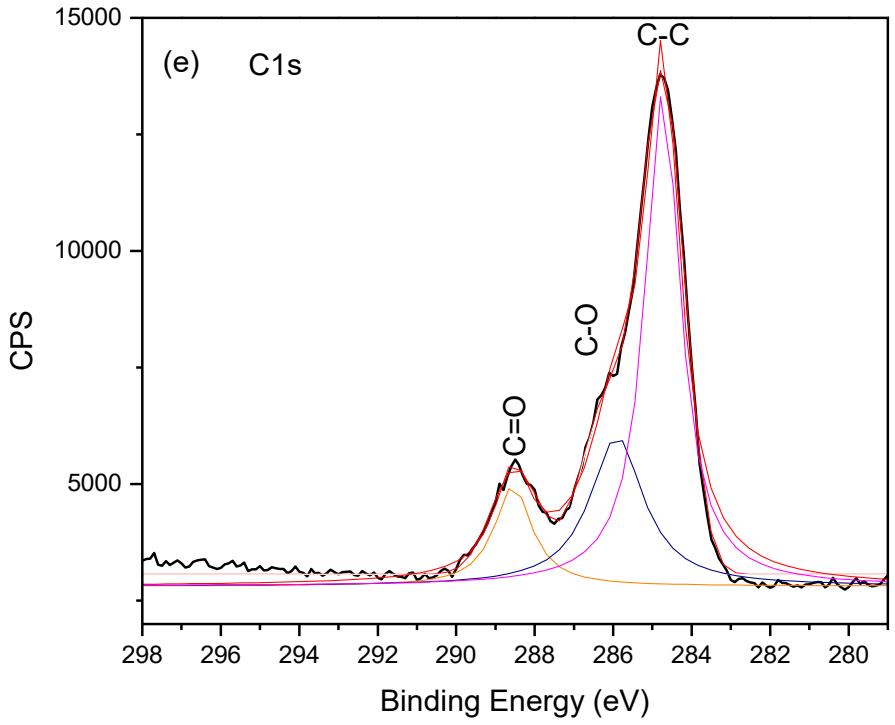

Figure 4.7e: XPS spectra of C1s

4.8 pH at point zero charge (pH*pzc*) STUDY

The surface charge of nanoparticles plays a crucial role in the kinetics of adsorption of contaminants on the surface of nanoparticles. pH at point zero charge was used to asses the surface charge. The adsorbent surface is negatively charged at pH > pHpzc, neutral at pH = pHpzc and a net positive charge at pH<pHpzc.

The pHpzc of the MNP-PCP, Mn-MNP-PCP and La-MNP-PCP sample composite were observed to be different, and the values are presented in Table 4.2. According to the data, the pHpzc value decreases from MNP-PCP to Mn-MNP-PCP and La-MNP-PCP composite. The pHpzc for MNP-PCP was 6.3, while the pHpzc for Mn-MNP-PCP and La-MNP-PCP was 6 and 5.4 . However, when the pH of a solution is less than pHpzc, the nanoparticle surface becomes positively charged and favours adsorption of anionic species.

Table 4.2: pHpzc values of MNP-PCP, Mn-MNP-PCP and La-MNP-PCP

	MNP-PCP	Mn-MNP-PCP	La-MNP-PCP
pHpzc	6.3	6	5.4

4.9 CONCLUSION

In summary, this chapter reports the successful synthesis of manganese and lanthanum doped magnetite pinecone powder nanocomposite adsorbent materials *via* co-precipitation method. The adsorbent materials were accordingly characterised using analytical instrumentation (FTIR, TGA, XRD, TEM SEM, EDX and XPS surface area). FTIR results obtained showed that the composite materials successfully synthesised. The morphological analysis of images showed the homogeneity of the synthesised spherical nanocomposites, while the EDX showed the incorporation of the lanthanum and manganese into the pinecone nanocomposite. All the adsorbent materials were thermally stable with MNP significantly improving the thermal stability and surface areas of Mn-MNP-PCP and La-MNP-PCP. The zeta potential analysis showed that the MNP-PCP surface area and the point of zero charge decreased after Mn and La doping. Manganese and lanthanum doping or modification also improved MNP-PCP properties for anion pollutants adsorption.

4.10 REFERENCES

AGHAZADEH, M., KARIMZADEH, I. & GANJALI, M. R. 2018. PVP capped Mn^{2+} doped Fe_3O_4 nanoparticles: A novel preparation method, surface engineering and characterization. *Materials Letters,* 228**,** 137-140.

AGHAZADEH, M., KARIMZADEH, I., GANJALI, M. R. & BEHZAD, A. 2017. Mn^{2+}-doped Fe_3O_4 nanoparticles: a novel preparation method, structural, magnetic and electrochemical characterizations. *Journal of Materials Science: Materials in Electronics,* 28**,** 18121-18129.

BHAUMIK, R. & MONDAL, N. K. 2016. Optimizing adsorption of fluoride from water by modified banana peel dust using response surface modelling approach. *Applied Water Science,* 6**,** 115-135.

ÇIFTÇI, H., ERSOY, B. & EVCIN, A. 2017. Synthesis, Characterization and Cr (VI) Adsorption Properties of Modified Magnetite Nanoparticles. *Acta Physica Polonica, A.,* 132**, 1-11**.

CUI, H.-J., SHI, J.-W., YUAN, B. & FU, M.-L. 2013. Synthesis of porous magnetic ferrite nanowires containing Mn and their application in water treatment. *Journal of Materials Chemistry A,* 1**,** 5902-5907.

GANURE, K. A., DHALE, L. A., KATKAR, V. T. & LOHAR, K. S. 2017. Synthesis and characterization of lanthanum-doped Ni-Co-Zn spinel ferrites nanoparticles via normal micro-emulsion method. *International Journal of Nanotechnology and Applications,* 11**,** 189-195.

GHOSH, A., SAHU, A., GULNAR, A. & SURI, A. 2005. Synthesis and characterization of lanthanum strontium manganite. *Scripta Materialia,* 52**,** 1305-1309.

JIANG, Y., CAI, W., TU, W. & ZHU, M. 2018. Facile Cross-Link Method To Synthesize Magnetic Fe_3O_4@ SiO_2–Chitosan with High Adsorption Capacity toward Hexavalent Chromium. *Journal of Chemical & Engineering Data,* 64**,** 226-233.

LIANG, P., AN, R., LI, R. & WANG, D. 2018. Comparison of La^{3+} and mixed rare earths-loaded magnetic chitosan beads for fluoride adsorption. *International Journal of Biological Macromolecules,* 111**,** 255-263.

LIU, Y., LUO, C., CUI, G. & YAN, S. 2015. Synthesis of manganese dioxide/iron oxide/graphene oxide magnetic nanocomposites for hexavalent chromium removal. *RSC Advances,* 5**,** 54156-54164.

LV, L., HE, J., WEI, M., EVANS, D. & ZHOU, Z. 2007. Treatment of high fluoride concentration water by MgAl-CO_3 layered double hydroxides: Kinetic and equilibrium studies. *Water Research,* 41**,** 1534-1542.

MTSHATSHENI, K., OFOMAJA, A. & NAIDOO, E. 2019. Synthesis and optimization of reaction variables in the preparation of pine-magnetite composite for removal of methylene blue dye. *South African Journal of Chemical Engineering,* 29**,** 33-41.

OUMA, I. L., NAIDOO, E. B. & OFOMAJA, A. E. 2018. Thermodynamic, kinetic and spectroscopic investigation of arsenite adsorption mechanism on pine cone-magnetite composite. *Journal of Environmental Chemical Engineering,* 6**,** 5409-5419.

PUERTA, M. & VALERGA, P. 1990. Thermal decomposition of a natural manganese dioxide: A laboratory experiment for undergraduate students. *Journal of Chemical Education,* 67**,** 344.

ROONASI, P. & HOLMGREN, A. 2009. A Fourier transform infrared (FTIR) and thermogravimetric analysis (TGA) study of oleate adsorbed on magnetite nano-particle surface. *Applied Surface Science,* 255**,** 5891-5895.

SADEEK, S. A., MOHAMMED, E. A., SHABAN, M., ABOU KANA, M. T. & NEGM, N. A. 2020. Synthesis, characterization and catalytic performances of activated carbon-doped transition metals during biofuel production from waste cooking oils. *Journal of Molecular Liquids***,** 11, 27-49.

SHAHID, M. K., PHEAROM, S. & CHOI, Y.-G. 2018. Synthesis of magnetite from raw mill scale and its application for arsenate adsorption from contaminated water. *Chemosphere,* 203**,** 90-95.

WANG, L., WANG, J., HE, C., LYU, W., ZHANG, W., YAN, W. & YANG, L. 2019. Development of rare earth element doped magnetic biochars with enhanced phosphate adsorption performance. *Colloids and Surfaces A: Physicochemical and Engineering Aspects,* 561**,** 236-243.

CHAPTER 5

5. RESULTS AND DISCUSSION

5.1 INTRODUCTION

The chapter covers the application of manganese-doped magnetite-coated pinecone (Mn-MNP-PCP) and lanthanum-doped magnetite-coated pinecone (La-MNP-PCP) adsorbents for nitrate and fluoride adsorption from aqueous solutions. Batch adsorption studies was carried out and the effect of solution pH, adsorbent dose and effect of contact time were conducted. Kinetic models such as the Lagergen's pseudo-first-order equation and pseudo-second-order equation were employed in modelling the uptake of NO_3^- and F^- ions onto Mn-MNP-PCP and La-MNP-PCP adsorbents. The equilibrium isotherm modelling results and thermodynamic parameters of the adsorption processes are also presented.

5.2 BATCH ADSORPTION STUDIES FOR THE REMOVAL OF NO_3^- AND F^- IONS

The effects of solution pH, adsorbent dose, initial solution concentrations and contact time on the adsorption of nitrate and fluoride ions using Mn-MNP-PCP and La-MNP-PCP were investigated varying one factor at a time while other factors were held constant. The adsorption capacity and percentage removal were calculated using the following equations.

Adsorption Capacity $q_e = \frac{(C_i - C_e)}{m} V$ (5.1)

Percentage removal $= \frac{(C_i - C_e)}{C_i}$ x 100 (5.2)

Ci is the initial concentration, Ce is the final concentration, m is the mass of the adsorbent (g), and V is the solution's volume (L).

5.2.1 Effect of solution pH on nitrate and fluoride adsorption

The effect of solution pH is the most important parameter in adsorption studies. It controls the adsorbent's surface properties, such as surface charges and ionic species in an aqueous medium. The solution pH effect for the adsorption of nitrate and fluoride onto manganese-doped magnetite (Mn-MNP-PCP) and lanthanum-doped magnetite nanocomposite (La-MNP-PCP) were examined

in the pH range 2-12. The results are given in Figure 5.1 a and b. From Figure 5.1a, the amount of nitrate adsorbed was observed to increase from 10.8 to 22.8 mg/g and from 33.9 to 37.5 mg/g as the solution pH increased from pH 2 to pH 4 for Mn-MNP-PCP and La-MNP-PCP, respectively. The amount of nitrate adsorbed reduced gradually as the solution pH increases from pH 4 to 12 for both adsorbent materials. La-MNP-PCP nanocomposite had the highest nitrate ion adsorption capacity as compared to Mn-MNP-PCP nanocomposite. The removal of the ions by both adsorbents was favoured at acidic conditions. At low solution pH, the adsorbent surface is protonated, leaving the nitrates ions (NO_3^-) in solution. Therefore, high adsorption capacity at low solution pH may be due to electrostatic interaction between the protonated Mn-MNPPCP and La-MNPPCP with the negatively charged nitrate ions (Rezaei Kalantary et al., 2016). The decrease in the concentration of nitrates adsorbed as the solution pH increases from solution pH 4-12 may be due to higher competition between nitrate and hydroxyl ions for the same sites on adsorbent's surface (Hafshejani et al., 2016). The results from Rezaei Kalantary et al. show that the maximum adsorption efficiency of nitrate obtained was about 17.1 mg/g at pH 3.0 using magnetite and the adsorption efficiency dropped with an increase of pH (Rezaei Kalantary et al., 2016). Other researchers have reported similar results whereby a continual decrease in nitrate ions adsorption with increasing pH was observed using Magnetite magnetic nanoparticles (Karthikeyan *et al.*, 2019; Wu *et al*., 2019).

The effect of solution pH on the fluoride adsorption in Figure 5.1b shows that higher amount of F^- ions was adsorbed at low solution pH. The amount of F^- adsorbed at solution pH 2 was 46.20 mg/g for Mn-MNP-PCP and 44.77 mg/g for La-MNP-PCP, which decreased gradually as solution pH increases from pH 2 to 12. These findings can be explained by considering the pH at point of zero-charge (pH_{pzc}) values of both adsorbents. pH_{pzc} is the pH where the adsorbent surface exhibited a neutral charge. The pH_{pzc} of Mn-MNP-PCP was observed to be 6.0 while that of La-MNP-PCP was found to be 5.63. The pH_{pzc} values at surfaces of the Mn-MNP-PCP and La-MNP-PCP adsorbents revealed a net positive charge below pH_{pzc} and negative charge above the pH_{pzc}. Lower amount of F^- ions were removed at higher solution pH, due to the abundance of OH^- ions resulting in strong electrostatic repulsion between the adsorbent materials negative surfaces and the F^- ions. There are several H^+ ions at low solution pH, protonating the negatively charged groups on the adsorbent surface that bind by electrostatic attraction to the F^- ions. (Li et al., 2017; Nagaraj et al., 2017; Sobeih et al., 2020). Research from Aigbe at al indicated the amount of fluoride adsorbed

was observed to increase from 36.3 to 37.2 mg/g between 2 pH to 6 pH by Magnetite (Aigbe et al., 2019).

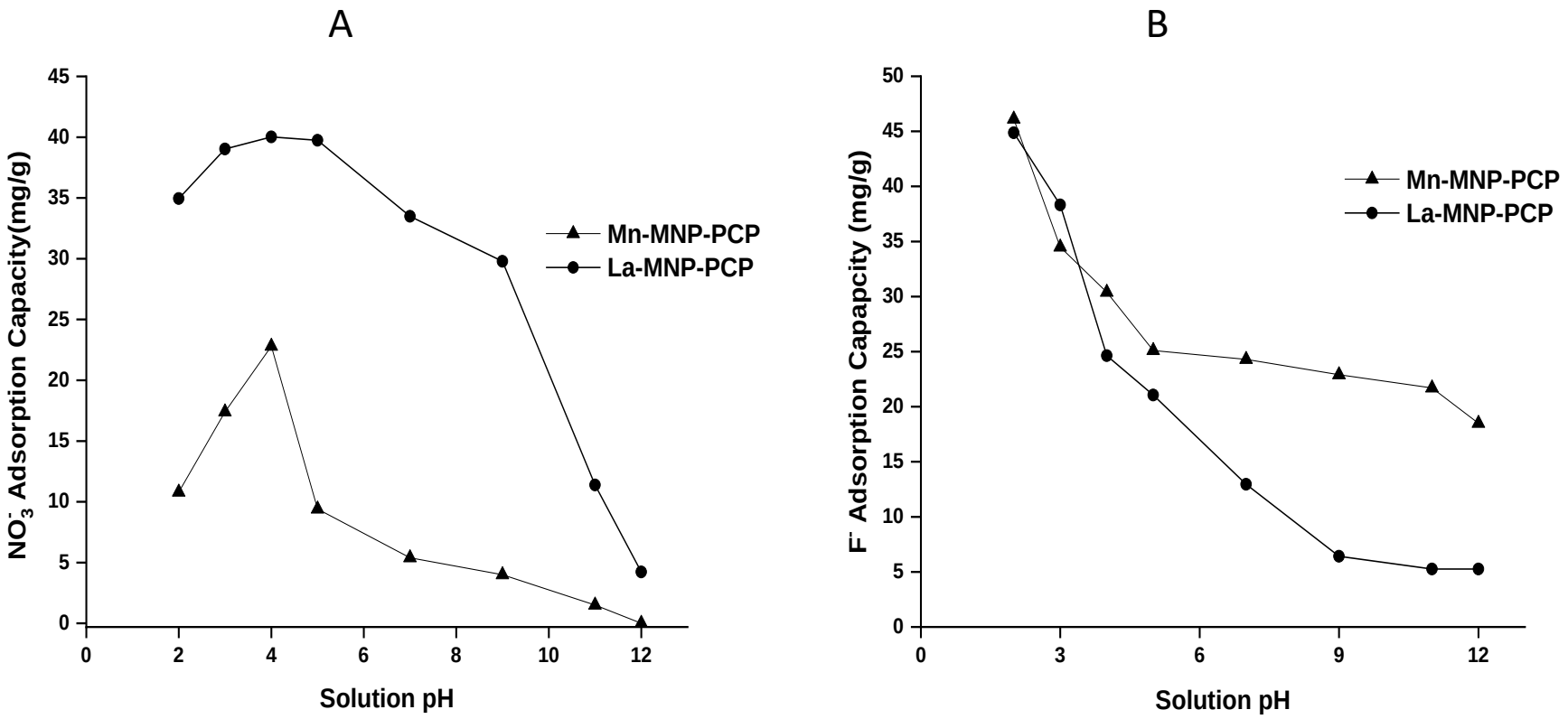

Figure 5.1: The effect of solution pH on the adsorption of (a) NO_3^- ions using Mn-MNP-PCP and La-MNP-PCP and (b) F^- ions onto Mn-MNP-PCP and La-MNP-PCP (adsorbent dosage = 1 g/L, initial nitrate concentration = 50 mg/ L, contact time = 2 hrs, temperature = 25 ± 1 ^oC).

5.3 EFFECT OF ADSORBENT DOSE

Adsorbent dosage is a significant variable in removing pollutants from aqueous solutions since it could change the system's adsorbent–adsorbate equilibrium. To study the effect of La-MNP-PCP and Mn-MNP-PCP dose on nitrate and fluoride ions adsorption, different amounts of adsorbent materials were varied from 0.25-2.5 g. An initial nitrate concentration of 50 mg/L and solution pH of pH 4 for NO_3^- ions and pH 2 for F^- at a temperature of 26 °C were used while agitating the solution system at 200 rpm for 2 h, and the results are shown in Figure 5.2 a-b and 5.3 a-b. Figure 5.2a-b showed reduction in the nitrate adsorption capacity from 78.00 to 11.04 mg/g and 152.4 to 16.46 mg/g as the adsorbent dosage increased from 0.25-2.5 g for Mn-MNP-PCP and La-MNP-PCP nanocomposites, respectively. However, nitrate percentage removal abruptly increased with an increase in adsorbent dosage from 39.0 to 55.2 % and 76.2 to 81.0 % for Mn-MNP-PCP and La-MNP-PCP nanocomposites, respectively. Rezaei Kalantary et al represented in their study that the nitrate percentage removal increased with an increase in adsorbent dosage from 18 to 42 % (Rezaei Kalantary et al., 2016). At low adsorbent dose, the less active site of the adsorbents are available which can be occupied by the nitrate ions excess in solution, inducing surface exhaustion and generating a greater adsorption capacity (EL-Mekkawi et al., 2016, Isagba et al., 2017, Nodeh et al., 2017). The significant increase in the nitrate percentage removal as the adsorbent dosage increases for both adsorbents is due to the more active sites availability.

Figure 5.3 a-b indicated that with an increase in adsorbent dosage from 0.25 g/L to 2.5 g/L, the fluoride removal efficiency (%) increased from 91.2 % to 92.3 % and the adsorption capacity decreased from 182.4 to 18.47 mg/g for Mn-MNP-PCP. Whereas the increase in La-MNP-PCP adsorbent dosage, the percentage of fluoride removal efficiency increased from 61.56% to 92.46%, and the adsorption capacity decreased from 123.12 to 18.49 mg/g., respectively. Perhaps, the changes were due to the higher availability of surface and pore volume at higher doses (Bhaumik and Mondal, 2016; Tang and Zhang, 2016; Nagaraj et al., 2017). Therefore, the optimal dose for further nitrate and fluoride adsorption studies was considered to be 0.5 g. Aigbe at al had 34.5-81.5% of fluoride removal using magnetite (Aigbe et al., 2019).

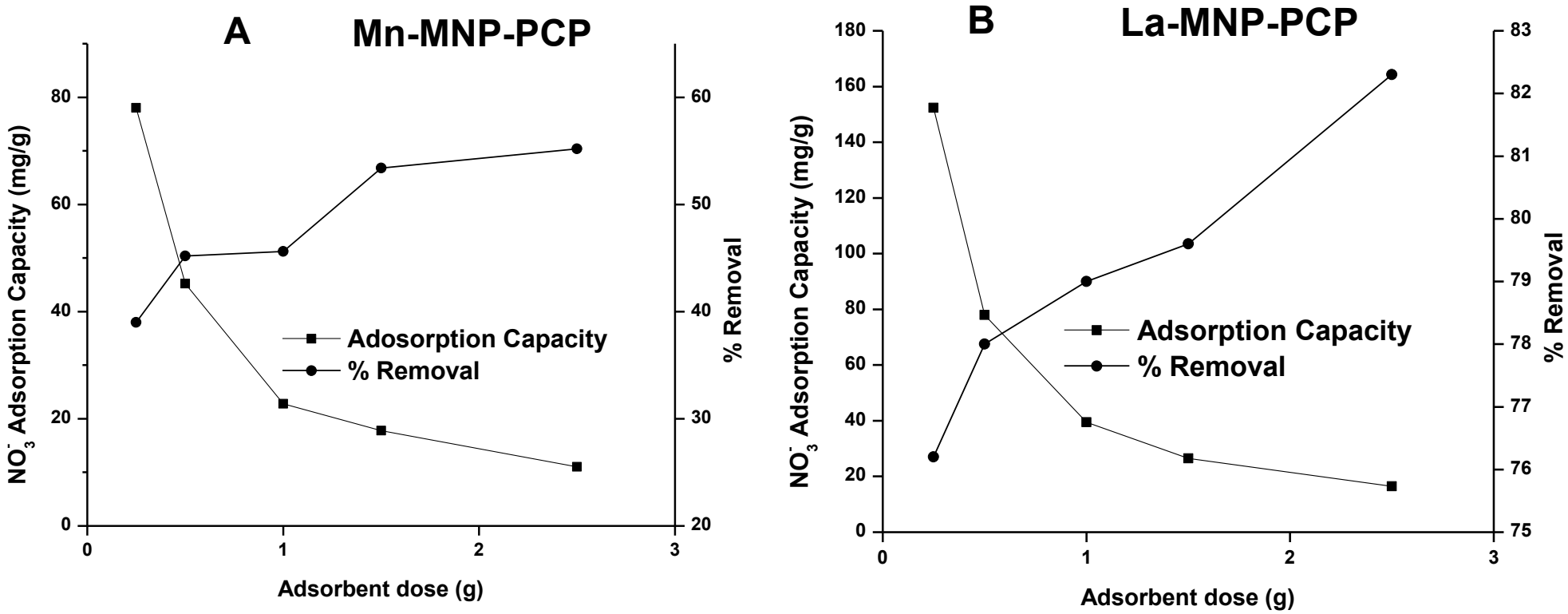

Figure 5.2: Effect of adsorbent dosage for nitrate adsorption onto (a) Mn-MNP-PCP and (b) La-MNP-PCP (initial pH = 4, initial nitrate concentration = 50 mg/L, contact time = 2 h, temperature = 25 ±1 ^oC).

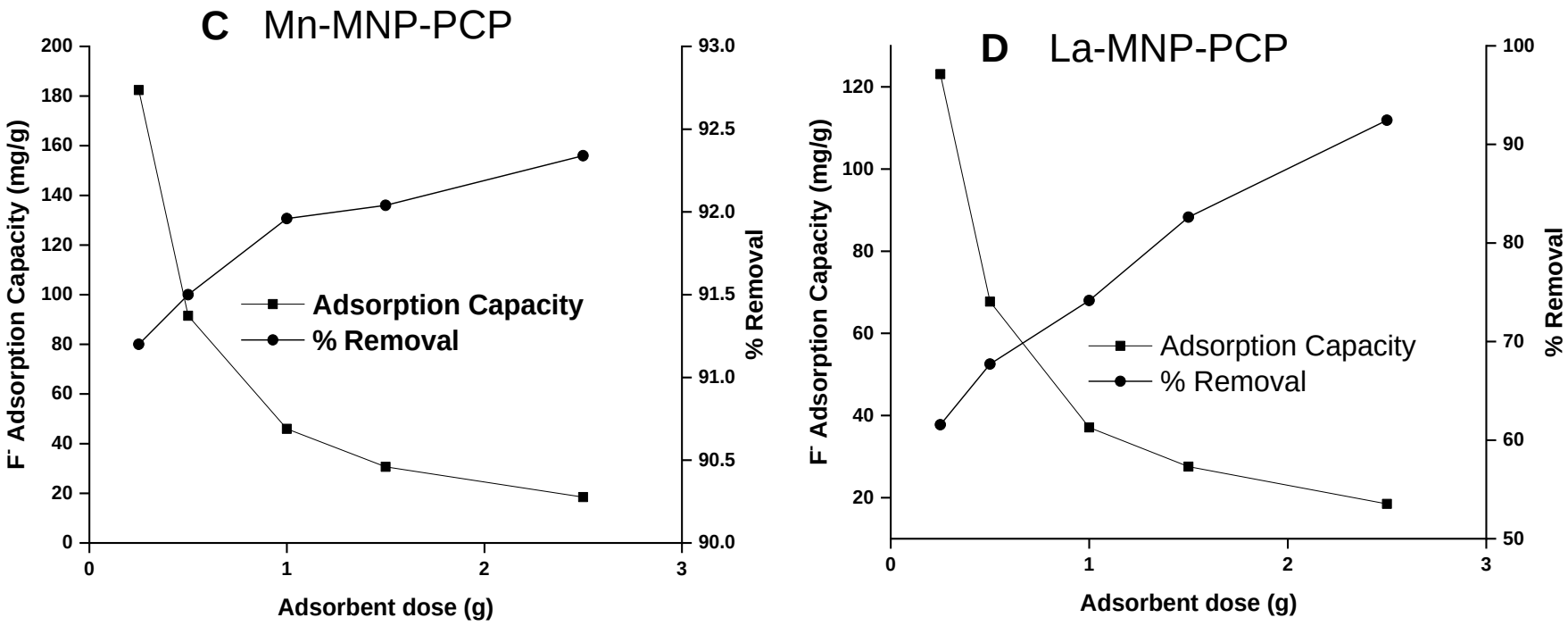

Figure 5.3: Effect of adsorbent dosage for fluoride adsorption onto (c) Mn-MNP-PCP and (d) La-MNP-PCP (initial pH = 2, initial nitrate concentration = 50 mg/L, contact time = 2 h, temperature = 25 ±1 °C).

5.4 EFFECT OF CONTACT TIME

The effect of contact time on the adsorption of nitrate and fluoride ions onto Mn-MNP-PCP and La-MNP-PCP nanocomposites were investigated at different contact times (0.5, 1, 2, 5, 10, 20, 30, 60 and 120 min) with concentration ranging from 10 to 100 mg/dm^3 and the results are presented in Figure 5.4 a-b and 5.5 a-b. Studies show that the amount of NO_3^- and F^- ions adsorbed increased rapidly at the initial adsorption stage during the first 15 min for fluoride ions and 20 minutes for nitrate ions. Then, the adsorption rate becomes slow adsorption rate until the system reaches a saturated adsorption capacity due to the full occupation of available active sites. Rapid adsorption rate at the onset of adsorption process may be due to the presence of a greater number of active sites on both adsorbents surfaces for the adsorption of NO_3^- and F^- ions while the surface of the adsorbents was saturated with NO_3^- and F^- ions at the end of the adsorption process (Rezaei Kalantary et al., 2016). Here, the adsorption capacities of both Mn-MNP-PCP and La-MNP-PCP increased with increasing initial NO_3^- and F^- ions concentrations. La-MNP-PCP showed the highest NO_3^- ions removal, while Mn-MNP-PCP had the highest F^- ions removal. Inferentially, the findings can be attributed to the extent of driving force of the concentration gradients as the NO_3^- and F^- ions concentrations increase (Bhatnagar et al., 2010). Similar results on nitrate adsorption have been reported by other researchers and contact time showed a direct proportional increase, which after reaching equilibrium time, the adsorption remained constant (Hu et al., 2015; Hafshejani et al., 2016; Liu et al., 2016; Rajeswari et al., 2016). The optimal contact time for further nitrate and fluoride adsorption studies was considered to be 1 h.

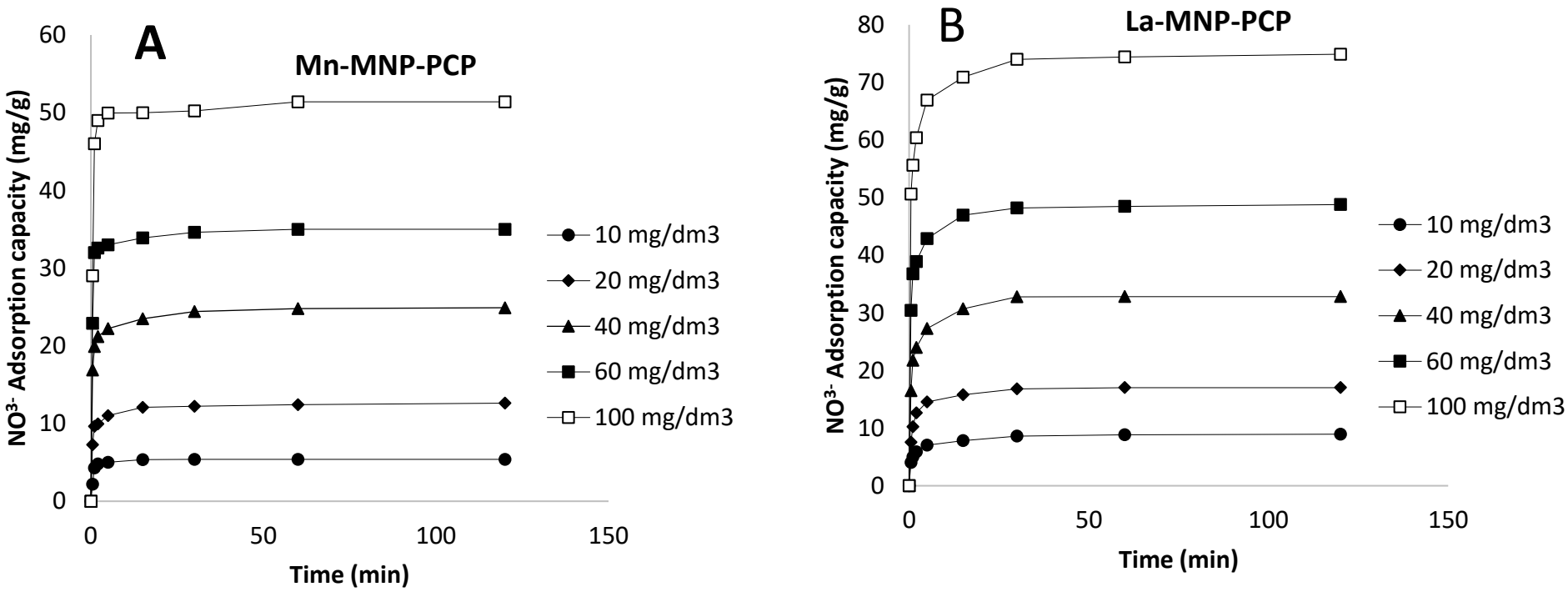

Figure 5.4: Effect of contact time on the adsorption of nitrate ions onto (a) Mn-MNP-PCP and (b) La-MNP-PCP at different initial concentrations (initial pH = 4, adsorbent dosage = 1 g/L, temperature = 25 ±1 °C).

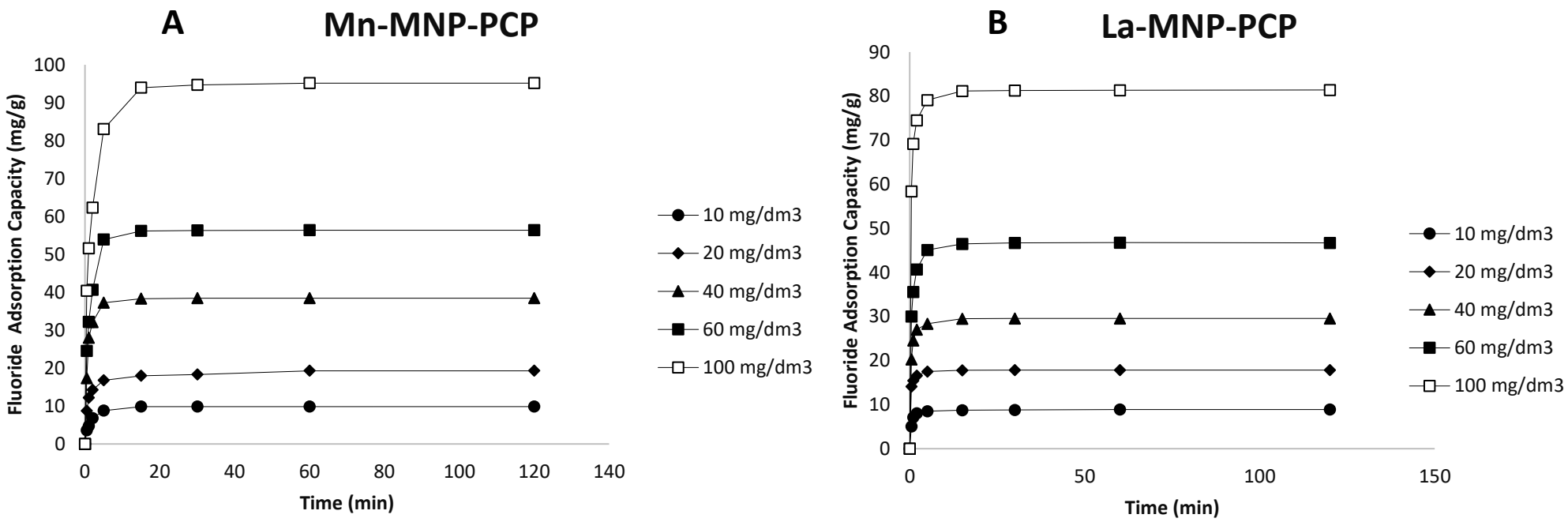

Figure 5.5: Effect of contact time on the adsorption of fluoride ions onto (A) Mn-MNP-PCP and (B) La-MNP-PCP at different initial concentrations (initial pH = 2, adsorbent dosage = 1 g/L, temperature = 25 ±1 °C).

5.5 KINETICS STUDIES - EFFECT OF CONCENTRATION

5.5.1 Kinetic modelling

Adsorption kinetics demonstrates the adsorbent adsorption rate and is one of the most significant variables reflecting adsorbents adsorption performance and thereby deciding their possible applications.

5.5.1.1 Pseudo first and pseudo second order models

To further investigate the adsorption rate and mechanism of NO_3^- and F^- ions adsorption onto Mn-MNP-PCP and La-MNP-PCP nanocomposites, kinetic studies were conducted using the pseudo-first and pseudo-second-order kinetic models. The pseudo-first-order kinetic model can be used to understand adsorption kinetics, which occurs by diffusion across a boundary layer. In contrast, the pseudo-second-order model describes adsorption processes that proceed by surface chemisorption. The ***pseudo-first-order kinetic model*** is expressed by the following equation (Lagergren, 1898):

$$\log(q_e - q_t) = \log(q_e) - \frac{k_1}{2.303}t \qquad (5.3)$$

The nonlinear form of the pseudo-first order model is given as:

$$q_t = q_e\left(1 - e^{-kt}\right) \qquad (5.4)$$

Where q_t and q_e are, the amount adsorbed (mg/g) at time t (Kong et al., 2019) and at equilibrium and k_1 is the rate constant of the pseudo-first-order kinetic model (min^{-1}). Plots of log (q_e-q_t) versus t give a straight line for pseudo-first-order kinetics, which allows the computation of the adsorption rate constant, k_1 and the equilibrium capacity, q_e.

The ***pseudo-second-order*** accounts for adsorption processes that proceed for surface chemisorption and the linear equation are given as (Ho, 1995):

$$\frac{t}{q_t} = \frac{1}{k_2 q_e^2} + \frac{1}{q_e}t \qquad (5.5)$$

Where k_2 is the rate constant (g/mg min). On re-arrangement, the non-linear form of the pseudo-second-order model is obtained:

$$q_t = \frac{k_2 q_e^2 t}{1 + k_2 q_e t} \quad (5.6)$$

Where the initial adsorption rate (mg/g min), h, is given by:

$$h = k_2 q_e^2 \quad (5.7)$$

Table 5.1 a-d presented the pseudo-first-order, pseudo-second-order kinetic parameters and error measurements for nitrate and fluoride ions' adsorption.

The results reveal that the experimental adsorption capacities of both Mn-MNP-PCP and La-MNP-PCP increased with increasing initial NO_3^- and F^- ions concentration. Higher NO_3^- adsorption capacities were observed for La-MNP-PCP than for Mn-MNP-PCP at all initial concentrations while Mn-MNP-PCP had the highest F^- ions adsorption capacities than La-MNP-PCP at all initial concentrations. The pseudo-second-order correlation coefficients, r^2, were close to unity and in the range 0.9702-0.9949 and 0.9839-0.9978 for NO_3^- ions removal and 0.9914-0.9975 and 0.9944-0.9998 for F^- ions removal by Mn-MNP-PCP and La-MNP-PCP, respectively. Moreover, the errors determination, % variables were observed to be lower for pseudo-second-order and in the range 0.1202-8.9380 and 0.0821-6.4551 for NO_3^- ions and 0.0619-8.5219 and 0.0146-0.2009 for F^- ions removal by Mn-MNP-PCP and La-MNP-PCP, respectively.

The adsorption capacity values, q_e, obtained from the pseudo second order were much closer to the experimental results for both adsorbents for NO_3^- and F^- ions removal. The kinetic models fit the experimental data were also tested by plotting the predicted adsorption capacities for each model against the experimental data (Figure 5.6 a-b and Figure 5.7 a-b). The findings were found to be in line with what was anticipated by the methods of error calculation. It can also be observed from the results that the pseudo second-order kinetic model suited the experimental data better than the pseudo first-order kinetics, as shown from the higher correlation coefficient values, r^2 and lower % variable error values.

In this study, pseudo-second order (PSO) model suggests that $NO3^-$ or F^- uptake onto the adsorbent occur through surface complexation with the charged ions on Mn-MNP-PCP and La-MNP-PCP through electron sharing (covalent bonds) or exchange of electrons (Huong *et al.*, 2019; Min *et al*., 2019; Esmaeili Bidhendi *et al.*, 2020). This finding confirms the interaction mechanism was a rate-limiting step chemisorption for the anion removal. This result is further corroborated with the free

energy (ΔG) findings, which showed that the negative ΔG were increased with increased temperature.

.

Table 5.1a: Kinetic data for the adsorption of nitrate ions onto Mn-MNP-PCP

Kinetic model	10 mg/dm^3	20 mg/dm^3	40 mg/dm^3	60 mg/dm^3	100 mg/dm^3
Mn-MNPPCP					
Pseudo-first order					
Exp. q (mg/g)	5.39	12.82	24.90	35.00	51.40
Model q (mg/g)	5.31	11.83	24.49	34.18	50.72
k_1 (min^{-1})	1.3114	1.7098	2.2581	2.3219	1.8986
r^2	0.9854	0.9668	0.9744	0.9940	0.9936
Variable Error	0.0589	0.6158	1.8038	0.8946	2.1781
Pseudo-second order					
Exp. q (mg/g)	5.39	12.82	24.90	35.00	51.40
Model q (mg/g)	5.52	12.32	24.29	35.07	52.15
k_2 (g/mg min)	0.3856	0.2347	0.1771	0.1408	0.0714
h (mg/g min)	11.7494	35.6233	104.5758	173.1706	194.1810
r^2	0.9702	0.9926	0.9949	0.9867	0.9735
Variable Error	0.1202	0.1372	0.3621	1.9866	8.9380

Table 5.1b: Kinetic data for the adsorption of nitrate ions onto La-MNP-PCP

Kinetic model	10 mg/dm^3	20 g/dm^3	40 g/dm^3	60 mg/dm^3	100 mg/dm^3
La-MNPPCP					
Pseudo-first order					
Exp. q (mg/g)	8.95	17.02	32.82	46.9	74.90
Model q (mg/g)	8.20	16.15	30.83	45.98	70.26
k_1 (min^{-1})	0.9058	0.9893	1.2001	1.8178	2.0456
r^2	0.9353	0.9714	0.9491	0.9608	0.9548
Variable Error	0.6322	1.0634	6.7240	10.8633	28.8953
Pseudo-second order					
Exp. q (mg/g)	8.95	17.02	32.82	46.9	74.90
Model q (mg/g)	8.63	16.92	32.33	47.86	73.01
k_2 (g/mg min)	0.1556	0.0895	0.0574	0.0653	0.0500
h (mg/g min)	11.6020	25.6226	59.9961	149.5748	266.5230
r^2	0.9839	0.9978	0.9896	0.9926	0.9899
Variable Error	0.1574	0.0821	1.3781	2.0565	6.4551

Table 5.1c: Kinetic data for the adsorption of fluoride ions onto Mn-MNP-PCP

Kinetic model	10 mg/dm^3	20 g/dm^3	40 g/dm^3	60 mg/dm^3	100 mg/dm^3
Mn-MNPPCP					
Pseudo-first order					
Exp. q (mg/g)	9.85	19.28	38.44	56.36	95.15
Model q (mg/g)	9.69	18.16	37.95	55.58	92.32
k_1 (min^{-1})	0.6698	1.0635	1.2070	0.8534	0.7558
r^2	0.9877	0.9730	0.9935	0.9827	0.9653
Variable Error	0.1779	1.2538	1.3090	7.7102	43.5555
Pseudo-second order					
Exp. q (mg/g)	9.85	19.28	38.44	56.36	95.15
Model q (mg/g)	10.16	19.00	39.45	57.92	96.68
k_2 (g/mg min)	0.0990	0.0874	0.0504	0.0236	0.0121
h (mg/g min)	10.2193	31.5514	78.477	79.1715	113.0990
r^2	0.9957	0.9975	0.9914	0.9935	0.9932
Variable Error	0.0619	0.1157	1.7249	2.8959	8.5219

Table 5.1d: Kinetic data for the adsorption of fluoride ions onto La-MNP-PCP

Kinetic model	10 mg/dm^3	20 g/dm^3	40 g/dm^3	60 mg/dm^3	100 mg/dm^3
La-MNPPCP					
Pseudo first-order					
Exp. q (mg/g)	8.88	17.83	29.55	46.69	81.4
Model q (mg/g)	8.71	17.46	29.10	45.58	79.52
k_1 (min^{-1})	1.6911	2.9933	2.2054	1.8007	45.4518
r^2	0.9961	0.9896	0.9912	0.9823	0.8921
Variable Error	0.0388	0.3953	0.9334	4.7280	84.4358
Pseudo second-order					
Exp. q (mg/g)	8.88	17.83	29.55	46.69	81.4
Model q (mg/g)	8.99	17.89	29.75	47.12	81.89
k_2 (g/mg min)	0.3440	0.3960	0.1502	0.0711	0.0625
h (mg/g min)	27.8021	126.7406	132.9364	157.8629	419.1233
r^2	0.9944	09996	0.9996	0.9992	0.9998
Variable Error	0.0552	0.0146	0.0396	0.2009	0.1594

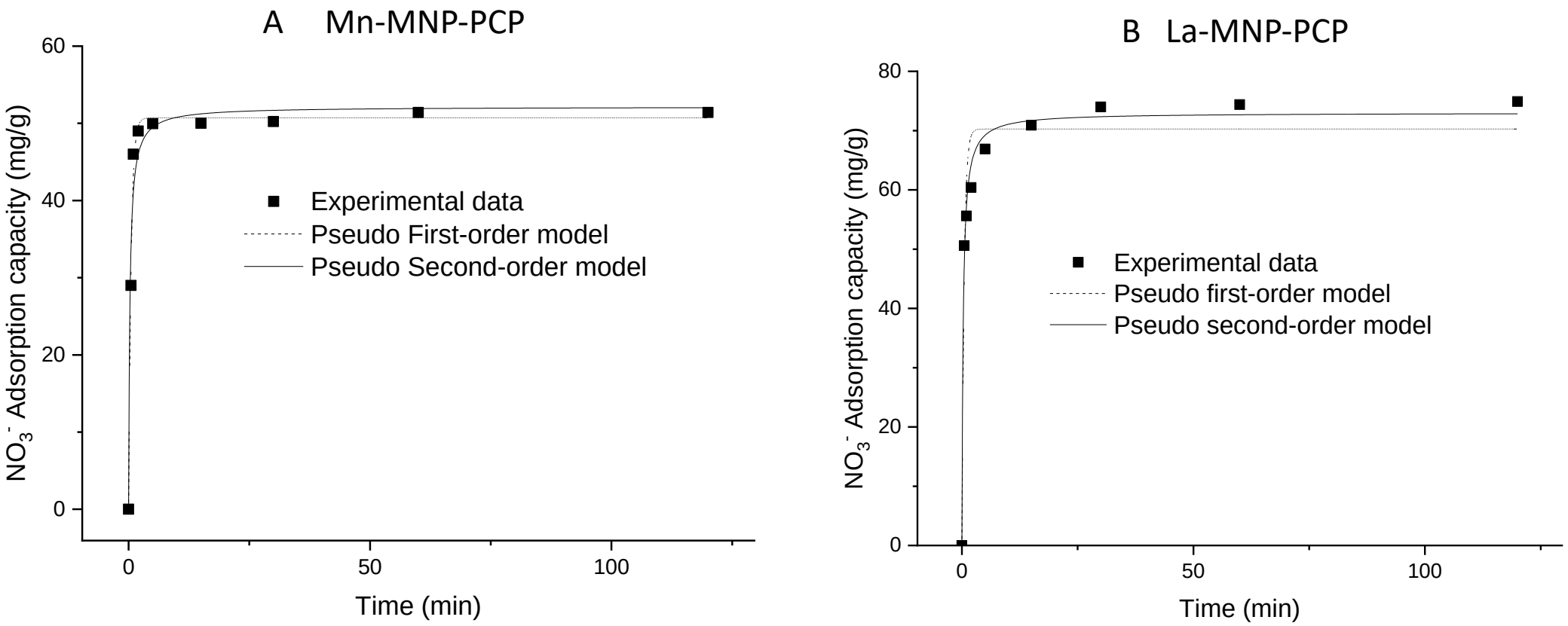

Figure 5.6: Fitting of experimental data with Pseudo first- and pseudo second-order kinetic models for the nitrate ions adsorption by (a) Mn-MNP-PCP and (b) La-MNP-PCP.

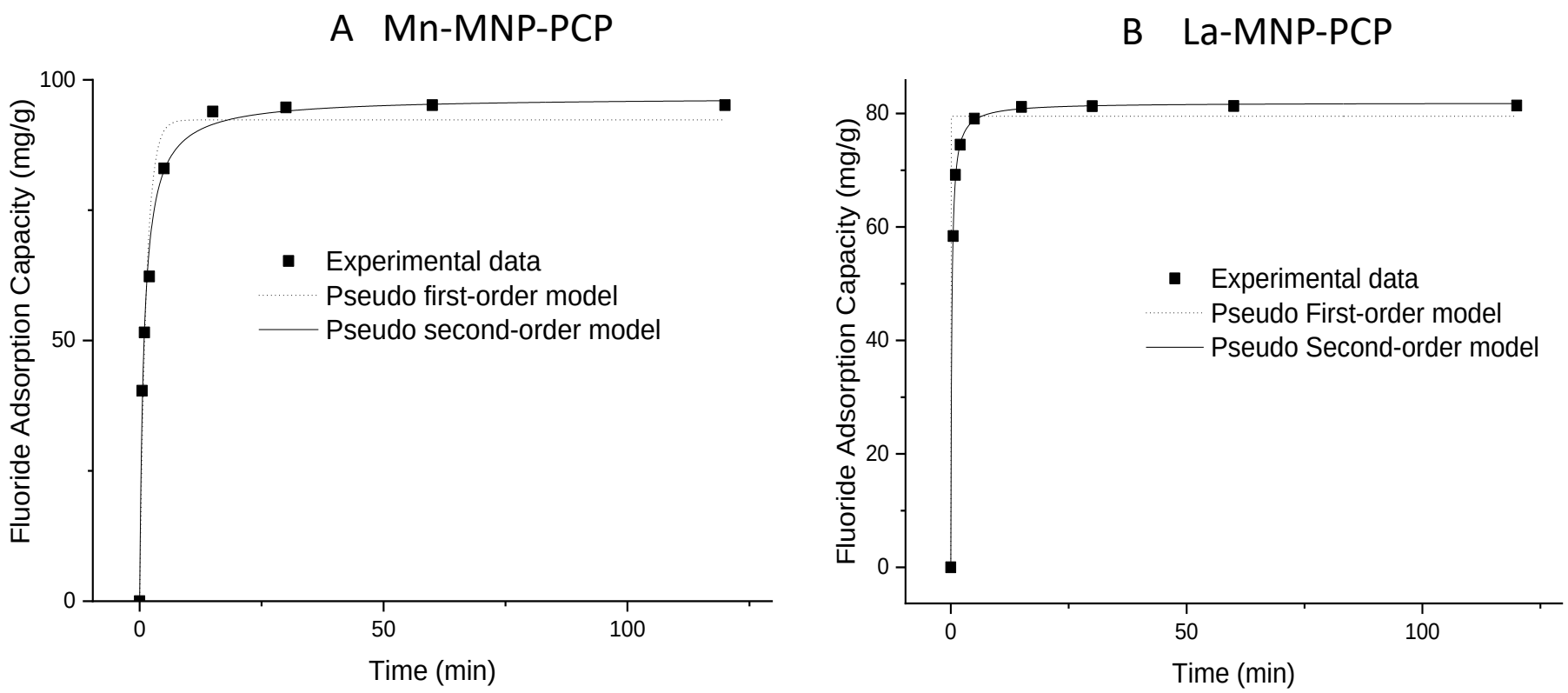

Figure 5.7: Fitting of experimental data with Pseudo first- and pseudo second-order kinetic models for the fluoride ions adsorption by (a) Mn-MNP-PCP and (b) La-MNP-PCP.

5.6 EQUILIBRIUM ISOTHERM

The equilibrium isotherm modelling can give significant information on the adsorbent's affinity for the adsorbate, the surface properties, and the adsorption mechanism. Three isotherm models were plotted with the equilibrium data to obtain the relationship between the adsorbed nitrate and fluoride ions at their equilibrium concentrations. These include the Langmuir, Freundlich, and Dubinin–Radushkevich (DR) isotherms whose non-linear expressions are presented below.

Langmuir isotherm: $q_e = \frac{q_m K_a C_e}{1 + K_a C_e}$ (5.8)

Freundlich isotherm $q_e = K_F C_e^{1/n}$ (5.9)

Dubinin–Radushkevich isotherm $q_e = q_s \exp\left(-\beta\varepsilon^2\right)$ (5.10)

Where q_e (mol/g) is the amount of adsorbate concentrated on the adsorbent surface at equilibrium, q_s is the theoretical adsorbent saturation capacity (mol/g), and C_e is the equilibrium concentration left in solution. (Kalaruban et al., 2016). The monolayer capacity and the equilibrium constant are expressed by the Langmuir isothermal constants q_m and K_a, while the Freundlich constants n and K_F are related to the adsorption affinity and the adsorbent capacity. Moreover, β and ε are the adsorption energy and ε the polyanion potential of the D-R isotherm.

Equilibrium adsorption studies conducted for the removal of NO_3^- and F^- ions onto Mn-MNP-PCP and La-MNP-PCP adsorbents were carried out at different temperatures (298, 303, 308, 313 and 318 K) and initial concentration ranging from 10-100 mg/dm^3 stirred for 2 h to obtain equilibrium. The equilibrium plots of NO_3^- and F^- ions adsorption capacity versus equilibrium concentration for Mn-MNP-PCP and La-MNP-PCP adsorbents are shown in Figure 5.8 a-b and 5.9 a-b, respectively. The NO_3^- and F^- ions adsorption capacity increased with increasing equilibrium concentration until attaining an almost constant value, due to increasing adsorption driving force for all adsorbents.

The amount of NO_3^- ions adsorption capacity was also observed to increase with increase in temperature from 298 to 318 K. This might be, with an increasing temperature, the NO_3^- ions escape from the solid phase to the bulk phase, thus weakening the attraction forces between NO_3^- ions and the nanocomposite adsorbent. Moreover, the nitrate uptake by La-MNP-PCP was greater than Mn-MNP-PCP nanocomposite.

The amount of F^- uptake in Figure 5.9a by Mn-MNP-PCP was seen to increase with increase in concentration and temperature from 299 to 318 K. However, F^- uptake by La-MNP-PCP was observed to have a different trend. Figure 5.9b showed that the F^- adsorption capacity increased with increasing temperature from 298 to 303 K. Furthermore, the fluoride adsorption reduced as the temperature increased from 303 to 318 K.The results showed that increasing temperature favoured the removal of F^- ions by Mn-MNP-PCP, and low temperature favoured the F^- ions removal by Ln-MNP-PCP. Similar results have been reported by (Tang and Zhang, 2016; Zhang *et al*., 2016; Nabbou *et al*., 2019).

.

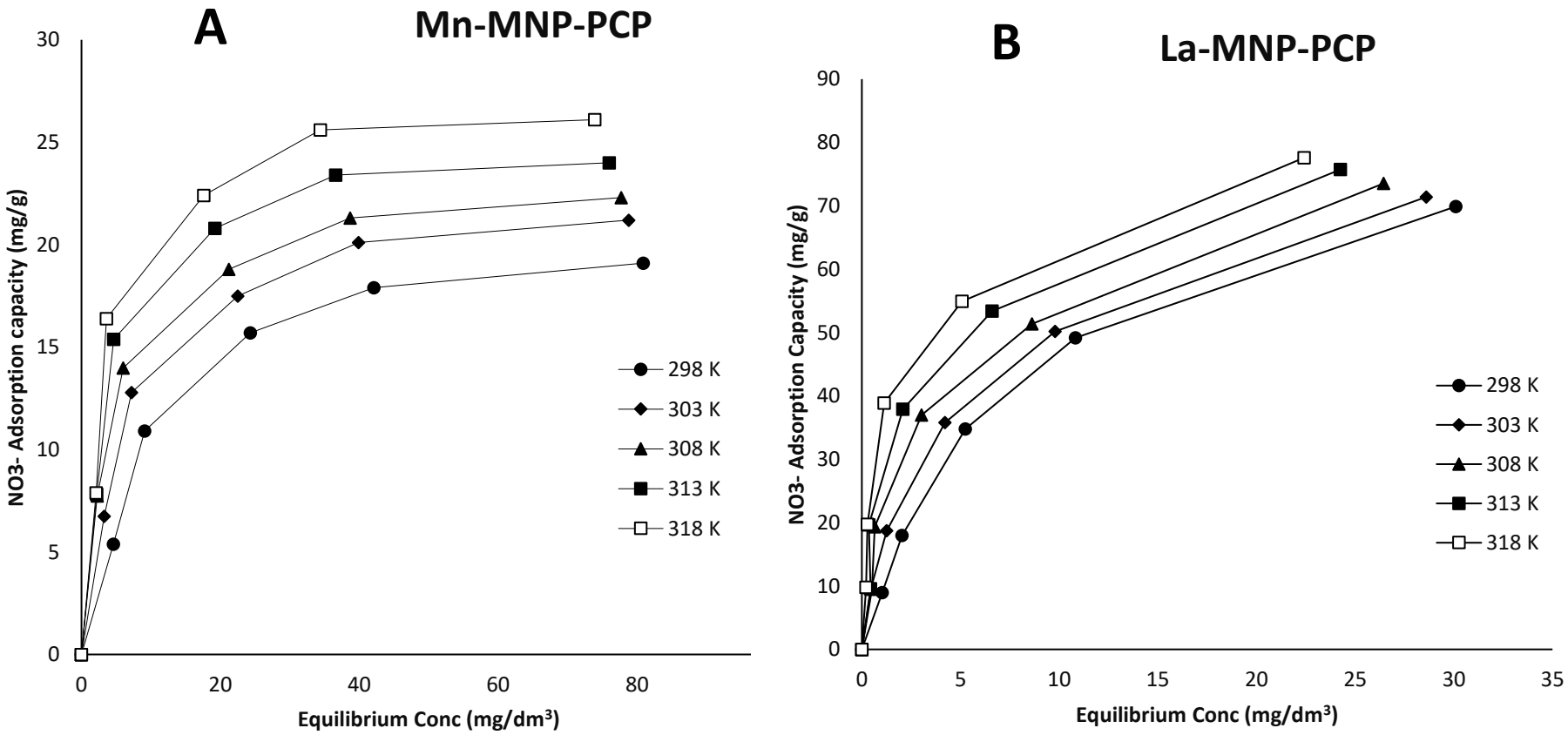

Figure 5.8: Equilibrium adsorption of nitrate ions onto (a) Mn-MNP-PCP and (b) La-MNPPCP

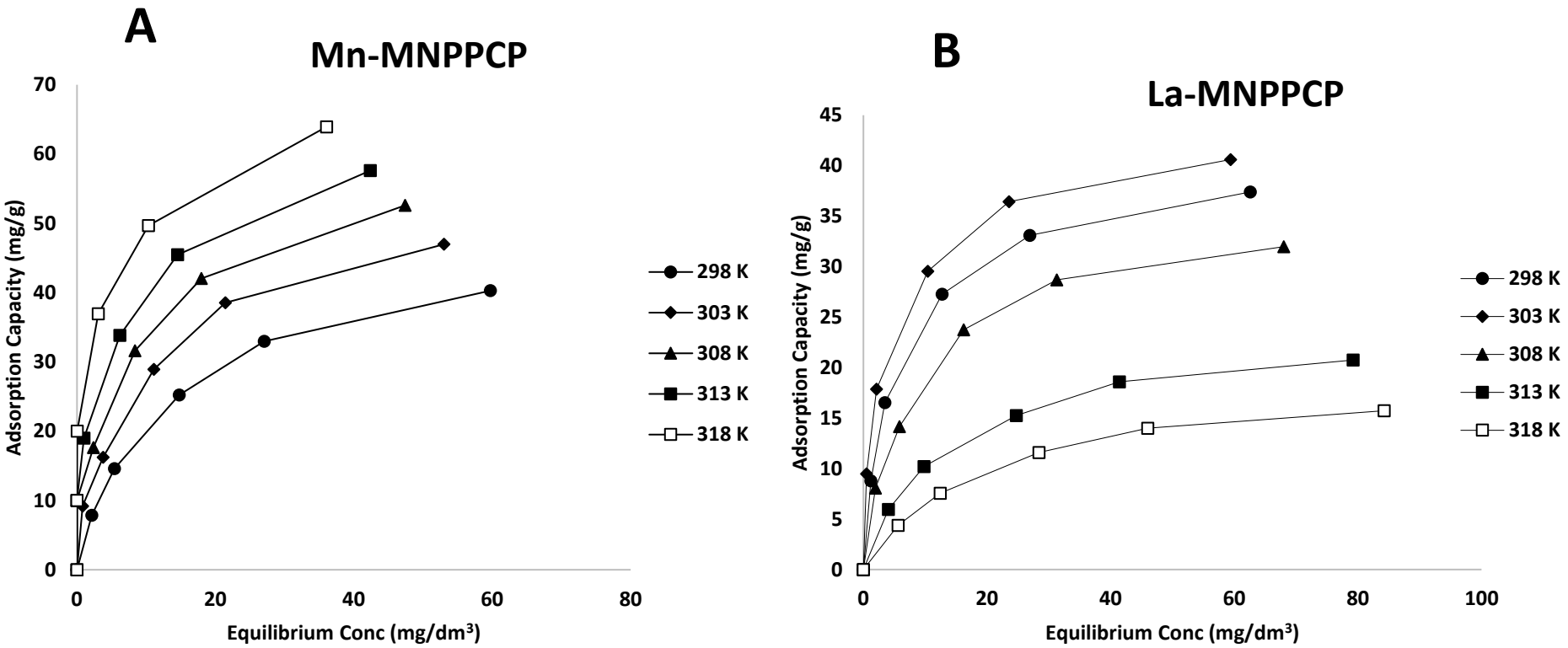

Figure 5.9: Equilibrium adsorption of fluoride ions onto (a) Mn-MNP-PCP and (b) La-MNPPCP

The values of the equilibrium constants obtained for the isotherm models along with values of the correlation coefficient (r^2) and errors determination were calculated for both nanocomposites adsorbents as presented in Table 5.2 a-d. The r^2 values of Langmuir model were in the range of 0.9820–0.9923 and 0.9989-0.9996 for NO_3^- ions removal and 0.9972-0.9984 and 0.9932-0.9979 for F^- ions removal by Mn-MNP-PCP and La-MNP-PCP, respectively. According to correlation coefficient (R^2) in Table 5.6a and Table 5.6b; adsorption of nitrate and fluoride ions onto Mn-MNP-PCP and La-MNP-PCP well fitted with Langmuir isotherm model, respectively. The findings reveal that the adsorption process is governed by the monolayer and homogeneous adsorption (Saleh *et al*., 2018).

The separation factor indicates that the adsorption dependent on Langmuir adsorption is favourable. R_L value > 1 implies unfavourable adsorption, while R_L = 1 indicates a linear adsorption process. When the R_L value is > 0 and < 1, the adsorption process is considered favourable while R_L = 0 means that it is irreversible (Saleh *et al*., 2018, Hu *et al*., 2018). All the separation values at different temperatures and initial concentrations for NO_3^- ions are between 0.2186-0.2489 and 0.8792-0.9065. For F^- ions are between 0.5518-0.7509 and 0.3069-0.4358 using Mn-MNP-PCP and La-MNP-PCP, respectively. Findings indicated that the removal of NO_3^- and F^- ions onto both adsorbent materials are favourable.

Isotherm model data from Dubinin-Raduschkevich allowed the determination of the adsorption process mean free energy to be determined. It, therefore, articulate whether the adsorption process was the physical or chemical. The mean free energy values calculated using both adsorbents to remove NO_3^- ions scale from 0.31 and 2.47 kJ mol^{-1}. Contrastingly, 0.29 and 7.00 kJ mol^{-1} was obtained for F^- ions. The results implied that the adsorption of NO_3^- and F^- ions onto Mn-MNP-PCP and La-MNP-PCP, occurred by physical adsorption since all values were < 8 kJ mol^{-1}.

Table 5.2 a: Equilibrium data for nitrate adsorption onto Mn-MNP-PCP

Isotherm model	298 K	303 K	308 K	313 K	318 K
Mn-MNPPCP					
Langmuir					
q (mg/g)	24.82	27.41	28.16	30.85	34.23
K_a (dm^3/mg)	0.0373	0.0408	0.0460	0.0452	0.0416
r^2	0.9852	0.9913	0.9923	0.9849	0.9820
%Variable Error	1.0325	0.7492	0.7311	1.7316	2.5079
Separation factor (RL)	0.2489	0.2373	0.2186	0.2255	0.2454
Freundlich					
n	0.4155	0.3978	0.3729	0.3764	0.934
$K_F (mg/g)(dm^3/mg)^{1/n}$	3.0000	3.6648	4.3210	4.6371	4.6842
r^2	0.9481	09601	0.9615	0.9471	0.9423
%Variable Error	3.6207	3.4527	3.6613	6.1034	8.0159
Dubinin–Radushkevich					
q_s (mol/g)	48.31	45.11	55.40	54.23	61.06
β (mol^2/J^2)	5.11×10^{-6}	2.37×10^{-6}	1.11×10^{-6}	1.12×10^{-6}	1.09×10^{-6}
E (kJ/mol)	0.31	0.46	0.67	0.67	0.68
r^2	0.9711	0.9534	0.9296	0.979	0.9885

Table 5.2 b: Equilibrium data for nitrate adsorption onto La-MNP-PCP

Isotherm model	298 K	303 K	308 K	313 K	318 K
La-MNPPCP					
Langmuir					
q (mg/g)	225.66	221.0128	229.96	240.11	249.05
K_a (dm^3/mg)	0.0045	0.0048	0.0047	0.0047	0.0046
r^2	0.9993	0.9996	0.9996	0.9992	0.9989
Separation factor (RL)	0.8807	0.8792	0.8894	08976	0.9065
Freundlich					
n	0.8159	0.8056	0.8084	0.8128	0.8161
$K_F (mg/g)(dm^3/mg)^{1/n}$	1.6631	1.7792	1.8074	1.8294	1.8476
r^2	0.9963	0.9968	0.9968	0.9960	0.9954
%Variable Error	3.2226	2.8856	3.0916	4.1207	4.9196
Dubinin–Radushkevich					
q_s (mol/g)	48.30	45.11	55.40	54.23	61.06
β (mol^2/J^2)	6.53×10^{-7}	2.08×10^{-7}	2.28×10^{-7}	1.33×10^{-7}	8.19×10^{-8}
E (kJ/mol)	0.88	1.55	1.48	1.94	2.47
r^2	0.8788	0.8171	0.9228	0.7385	0.9451

Table 5.2 c: Equilibrium data for fluoride adsorption onto Mn-MNPPCP

Isotherm model	298 K	303 K	308 K	313 K	318 K
Mn-MNPPCP					
Langmuir					
q (mg/g)	71.09	85.60	99.34	114.04	135.18
K_a (dm^3/mg)	0.0136	0.0127	0.0116	0.0105	0.0092
R^2	0.9980	0.9972	0.9983	0.9984	0.9978
% Variable Error	0.5892	1.1471	0.8677	0.9916	1.6467
Separation factor (RL)	0.5518	0.5976	0.6452	0.6921	0.7509
Freundlich					
n	0.62	0.64	0.65	0.67	0.70
K_F (mg/g)$(mg/dm^3)^{1/n}$	2.3772	2.6138	2.6919	2.6763	2.6215
R^2	0.9862	0.9859	0.9890	0.9894	0.9888
%Variable Error	4.0909	5.6925	5.4801	6.3732	8.3505
Dubinin–Radushkevich					
q_s (mol/g)	33.2017	39.3817	43.2199	45.3904	48.9011
β (mol^2/J^2)	2.51×10^{-6}	1.89×10^{-6}	1.14×10^{-6}	2.65×10^{-7}	1.02×10^{-8}
E (kJ/mol)	0.45	0.51	0.66	1.37	7.00
R^2	0.9547	0.9591	0.9516	0.9393	0.9419

Table 5.2 d: Equilibrium data for fluoride adsorption onto La-MNPPCP

Isotherm model	298 K	303 K	308 K	313 K	318 K
La-MNPPCP					
Langmuir					
q (mg/g)	55.99	61.27	47.21	28.76	22.05
K_a (dm^3/mg)	0.0220	0.0218	0.0233	0.0279	0.0268
R^2	0.9945	0.9932	0.9937	0.9979	0.9979
% Variable Error	1.4734	2.1645	1.2227	0.1638	0.1006
Separation factor (RL)	0.4207	0.4358	0.3869	0.3114	0.3069
Freundlich					
n	0.53	0.53	0.51	0.47	0.48
K_F (mg/g)$(mg/dm^3)^{1/n}$	3.5460	3.8275	3.2295	2.4828	1.8080
R^2	0.9719	0.9697	0.9707	0.9796	0.9789
%Variable Error	7.4577	9.6167	5.7111	1.6045	0.9583
Dubinin–Radushkevich					
q_s (mol/g)	29.5830	31.4689	25.1737	16.9777	13.0137
β (mol^2/J^2)	5.73×10^{-7}	1.71×10^{-7}	1.05×10^{-6}	3.35×10^{-6}	6.12×10^{-6}
E (kJ/mol)	0.93	1.71	0.69	0.39	0.29
R^2	0.8571	0.8232	0.8141	0.8580	0.8730

5.7 THERMODYNAMIC PARAMETERS OF ADSORPTION

The evaluation of the thermodynamic feasibility and temperature influence on the adsorption process of nitrate and fluoride ions onto Mn-MNP-PCP and La-MNP-PCP are essential in this study. Thermodynamic parameters such as a change in free energy ΔG*, entropy *ΔS** and enthalpy *ΔH** were determined to derive the following equations' parameters.

$$\Delta G^* = -RT \ln K_L \tag{5.11}$$

Where K_L is calculated from the ratio of nitrate and fluoride on the adsorbent surface at equilibrium to the C_r left in solution.

$$\ln K_L = -\frac{\Delta G^*}{RT} = -\frac{\Delta H^*}{RT} + \frac{\Delta S^*}{R} \tag{5.12}$$

Multiply Eq.**(5.)** with - *RT*:

$$\Delta G^* = \Delta H^* - T\Delta S^* \tag{5.13}$$

The *R* is the gas constant (8.314 J/mol K), *T* is the absolute temperature (K), *ΔH** and *ΔS** could be obtained from the slope and intercept of *ΔG** versus *1/T,* respectively.

The thermodynamic analysis was investigated at five different temperatures 298, 303, 308, 311 and 318 K. Tables 5.7 a and b presented the nitrate and fluoride adsorption parameters using Mn-MNP-PCP and La-MNP-PCP, respectively. The values of free energy change, *ΔG** of nitrate adsorption were calculated to range from -7.51 to -10.14 kJ/mol for Mn-MNP-PCP and from -11.29 to -16.27 kJ/mol for La-MNP-PCP as adsorption temperature increased from 298 to 318 K as shown in Table 5.7 a. The values of *ΔG** were observed to increase with an increase in temperature and were all negative, suggesting that nitrate's adsorption onto Mn-MNP-PCP and La-MNP-PCP is spontaneous and the spontaneity increases with temperature. The *ΔG** results also show that the spontaneity was more for La-MNP-PCP than for Mn-MNP-PCP. The values of entropy *ΔS** and enthalpy *ΔH** for Mn-MNP-PCP were calculated to be 134.29 J/K mol and 32.2 kJ/mol 2, respectively and 251.38 J/K mol and 63.77 kJ/mol for La-MNP-PCP, respectively. The positive values of enthalpy *ΔH** for both adsorbents materials suggested the endothermic nature of the adsorption process and supported the increase in adsorption capacity with an increase in temperature. The positive values of entropy *ΔS*,* on the other hand, suggest

increasing randomness during the adsorption process, which was higher for La-MNP-PCP than Mn-MNP-PCP nanocomposite.

The ΔG^* values become more negative (-3.21 to -30.44 kJ/mol) with increasing temperature, suggesting that higher temperature makes the adsorption easier. The negative ΔG^* values of fluoride ion adsorption onto Mn-MNP-PCP at various temperatures indicate the spontaneous nature of the adsorption. The positive value of ΔH^* implies the endothermic nature of the fluoride adsorption by Mn-MNP-PCP, and the positive value of ΔS^* suggests that the process is entropy-driven and increases the randomness at the solid-solution interface during the adsorption process (Nabbou et al., 2019).

The negative value of ΔG^* on fluoride adsorption increased from -4.91 to -0.65 kJ/mol with increasing temperature from 298 to 318 K for La-MNP-PCP, suggesting the adsorption process is unfavourable and non-spontaneous at a higher temperature as shown in Table 5.7b. The negative value of ΔH^* and ΔS^* for La-MNP-PCP; indicates no structural changes and supports the physical adsorption on La-MNP-PCP surface after fluoride adsorption (Zhang et al., 2016).

Table 5.7a: Thermodynamic parameters of Nitrate ions adsorption onto Mn-MNP-PCP and La-MNP-PCP

Sample	Temp. (K)	ΔG*(kJ/mol)	ΔH*(kJ/mol)	ΔS*(J/ K mol)
Mn-MNPPCP	298	-7.51		
	303	-8.54		
	308	-9.65	32.22	134.29
	313	-9.90		
	318	-10.14		
La-MNPPCP	298	-11.29		
	303	-12.27		
	308	-13.53	63.77	251.38
	313	-14.90		
	318	-16.27		

Table 5.7b: Thermodynamic parameters of Fluoride ions adsorption onto Mn-MNPPCP and La-MNPPCP

Sample	Temp. (K)	ΔG*(kJ/mol)	ΔH*(kJ/mol)	ΔS*(J/ K mol)
Mn-MNPPCP	298	-3.21		
	303	-6.16		
	308	-20.61	429.11	1448.02
	313	-23.97		
	318	-30.44		
La-MNPPCP	298	-4.91		
	303	-7.31		
	308	-3.66	-109.20	-344.02
	313	-1.01		
	318	-0.65		

5.8 EFFECT OF COMPETING IONS

Drinking water and underground water polluted by nitrate and fluoride ions usually contain along with it several other anions such as PO_4^{3-}, CO_3^{2-}, SO_4^{2-} and Cl^-, which can influence the nitrate and fluoride ion adsorption. The influence of these anions on nitrate and fluoride ions adsorption was investigated by contacting 0.1 g of Mn-MNP-PCP and La-MNP-PCP nanocomposites with 100 mg/dm^3 of nitrate or fluoride ion solution containing 0.1 mg/dm^3 of each anion. The impact of competing anions are illustrated in Figure 5.10 and Figure 5.11. Figure 5.10 indicates that the presence of competing ions had both positive and negative effects on the nitrate ions removal using both Mn-MNP-PCP and La-MNP-PCP. The carbonates positively affected the nitrate ion removal followed by chlorides, while the sulphates and phosphates negatively affected the removal of nitrate ions by Mn-MNP-PCP. On the other hand, the presence of competing ions on the removal of nitrate ions by La-MNP-PCP showed a positive effect following the order $CO_3^{2-} > Cl^- > SO_4^{2-} > PO_4^{3-}$.

Furthermore, the reduction in fluoride adsorption capacity by Mn-MNP-PCP in Figure 5.11 was highest for carbonates, followed by chloride. Simultaneously, phosphate and sulphate had a minimal effect compared to the adsorption of fluoride onto Mn-MNP-PCP. While the co-existence of other anions following the order carbonate, sulphate and phosphate ions influenced the fluoride adsorption onto La-MNP-PCP, there was no significant change in the presence of chloride ion. In general, the decrease in nitrate and fluoride removal efficiency by increasing initial concentration of other anions may have resulted from the competition between nitrate and fluoride anions because the other anions form chelates with active sites of the adsorbents via electrostatic repulsion (Fan and Zhang, 2018). The literature works reported that multi-valent anion with higher charge density is more readily adsorbed than monovalent anion. Other researchers have reported similar results where multivalent and mono charge anions have shown more and less adsorption trend, respectively (Rajeswari et al., 2016).

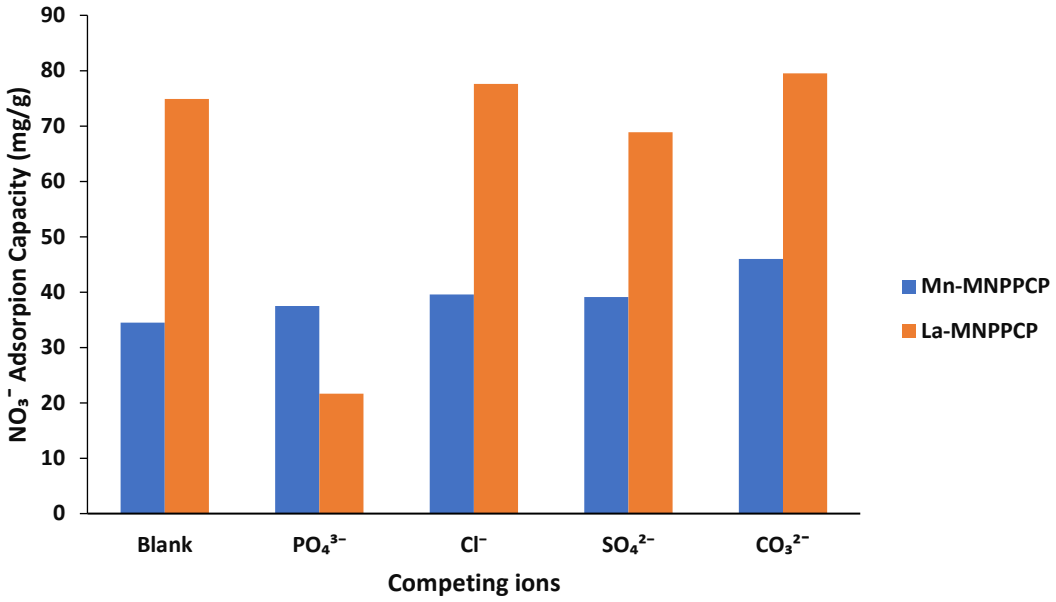

Figure 5.10: Effect of competing anions on NO_3^- uptake onto Mn-MNP-PCP and La-MNP-PCP nanocomposite.

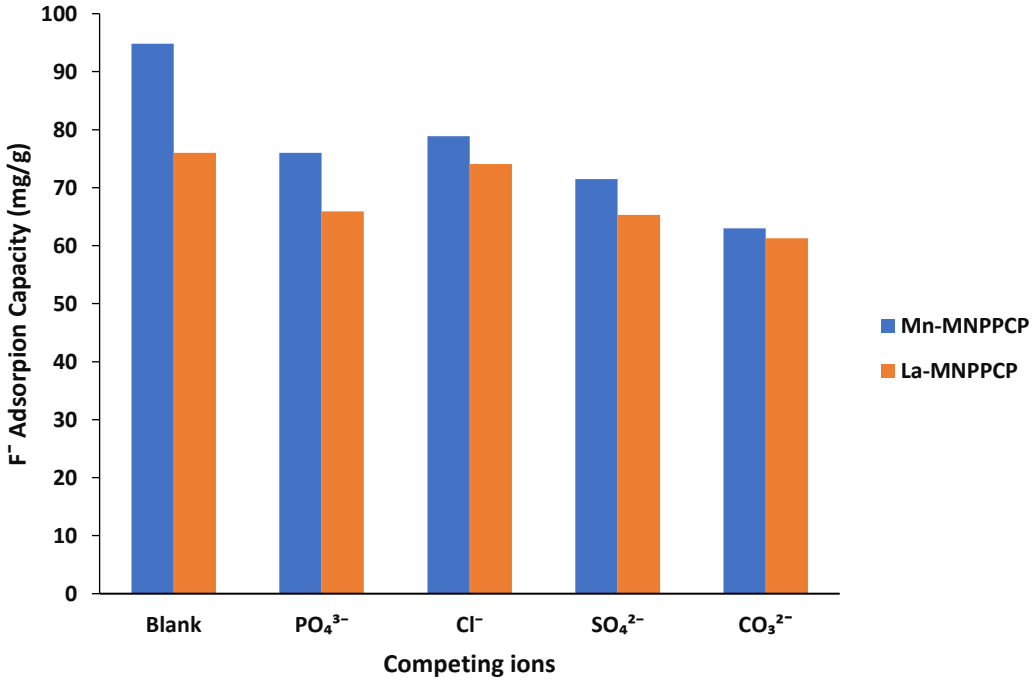

Figure 5.11: Effect of competing anions on F^- uptake onto Mn-MNP-PCP and La-MNP-PCP nanocomposite.

5.9 DETERMINATION OF THE MECHANISM OF NITRATE AND FLUORIDE ONTO Mn-MNP-PCP AND La-MNP-PCP AS A MODEL ADSORBENT

5.9.1 FTIR

FTIR spectroscopy was conducted on the Mn-MNP-PCP and La-MNP-PCP adsorbents before and after nitrate and fluoride adsorption

To elucidate functional groups responsible for their removal and to reveal the adsorption mechanism, and the results are shown in Figure 5.12 a-b and Figure 5.13 a-b. Comparison of the FTIR spectra of Mn-MNP-PCP adsorbent before and after nitrate adsorption in Figure 5.12a shows that the predominate peaks at 3425, 1641, 1025 cm^{-1} and around 560 cm^{-1} corresponds to the –OH stretching, C=O stretching of carboxylic acid, C-O-C stretching and Fe-O and Mn-O bonds, respectively. The nitrate ions adsorbed onto the Mn-MNP-PCP adsorbent revealed the new FTIR peak at 1354 cm^{-1}, assigned to the vibration modes of nitrate anions. Figure 5.12b FTIR spectra after adsorption of nitrate ions indicate the presence of nitrate on La-MNP-PCP adsorbent by the decreased peaks at 2250, 2100 and 1025 cm^{-1} a peak shifting around 560 cm-1. Moreover, there was a new sharp, strong peak at 1354 cm^{-1}, which was assigned to the vibration modes of nitrate anions. These observations confirm the successful loading of nitrate ions onto Mn-MNP-PCP and La-MNP-PCP adsorbents.

For the pristine Mn-MNP-PCP in Figure 5.13a, the peaks at 3425, 1641, 1447 and 1025 cm^{-1} can be ascribed to the stretching and bending vibration of adsorbed water, OH bending, C-O bending and the peak around 560-450 cm^{-1} indicated the presence of magnetite pinecone powder and manganese material. There was a significant decrease of intensity at peak 1447 cm^{-1} and an addition of a peak at 600 cm^{-1} After fluoride adsorption which indicated that the hydroxyl groups on the adsorbent were involved in the adsorption process of fluoride.

The FT-IR spectra of La-MNP-PCP before and after fluoride adsorption in Figure 5.13b indicate the broad IR peaks around 3425, 2982, 1641, 1025 and 560 cm^{-1} for all of the samples were the O-H bond stretching modes of free water, C-H stretching, C=O stretching, C-O-C stretching and La-Fe oxides. Moreover, the bands at 2250, 2100, 1425 and 1025 cm^{-1} after fluoride adsorption become less intense due to the disturbance of the local symmetry through fluoride uptake by La-MNP-PCP adsorbent material.

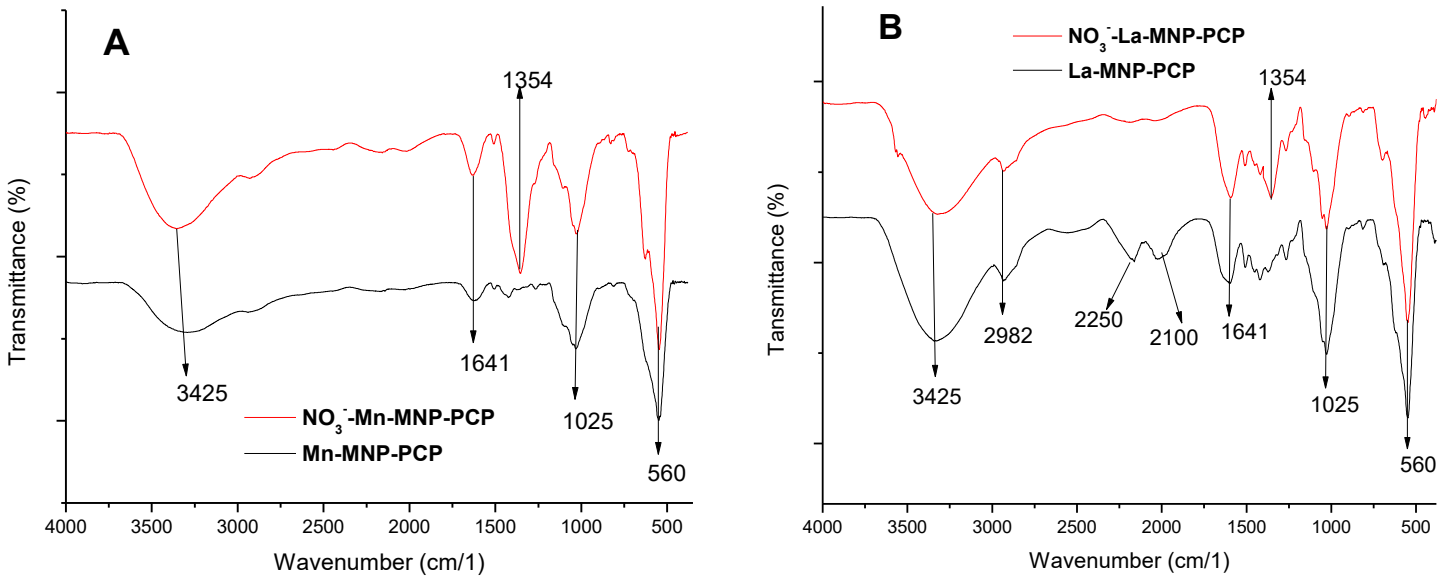

Figure 5.12: FTIR spectra of (a) Mn-MNP-PCP and (b) La-MNP-PCP; before and after nitrate adsorption.

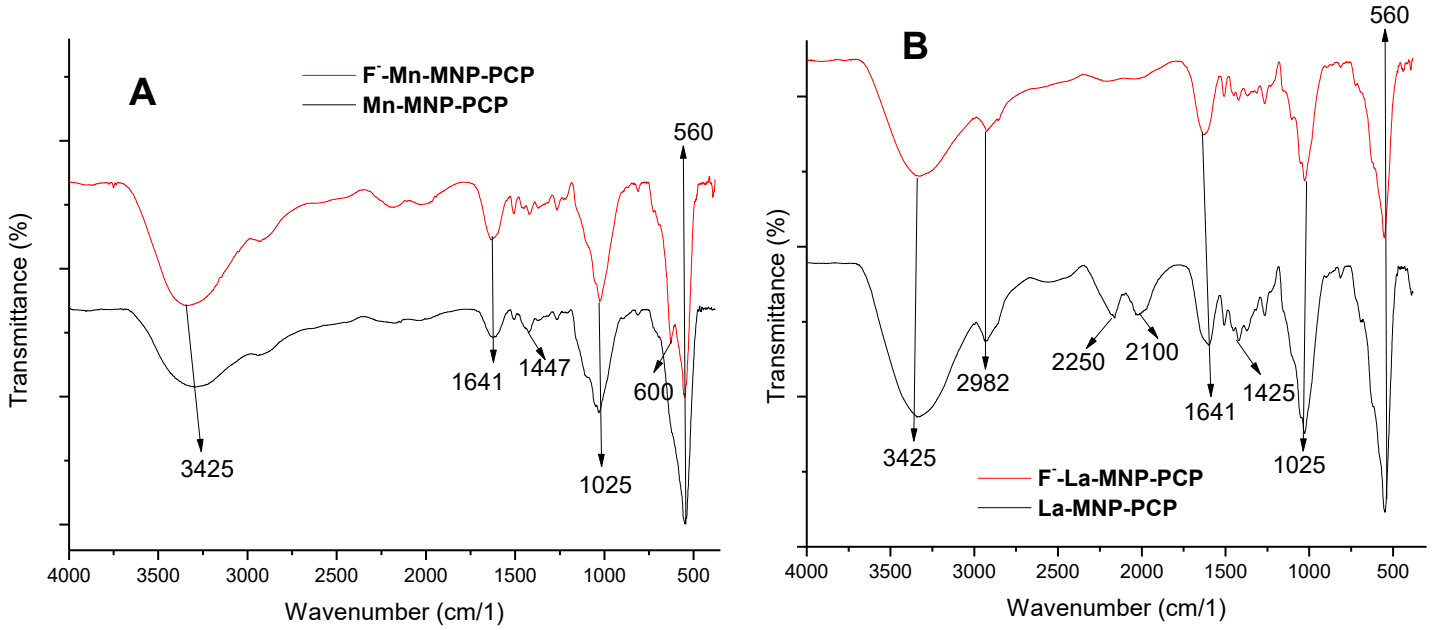

Figure 5.13: FTIR spectra of (a) Mn-MNP-PCP and (b) La-MNP-PCP, before and after fluoride adsorption

5.9.2 Scanning Electron Microscopy-Energy Dispersive X-ray spectroscopy (SEM-EDX)

The SEM images of Mn-MNP-PCP and La-MNP-PCP pre- and post-adsorption of the nitrate and fluoride are illustrated in Figure 5.14 a-d and 5.15 a-d. The findings indicate that although Mn-MNP-PCP materials morphology in Figure 5.14a remained slightly unchanged with some irregular outline same even after nitrate adsorption in 5.14b where there was also an expansion in the surface of the particle. In Figure 5.14c. Unused La-MNP-PCP material possessed a larger surface area and porous diameter, while in Figure 5.14 d, a decrease of the particle size morphology were observed after nitrate adsorption, which indicated the presence of nitrate on its surface.

In the comparison to Figure 5.15a, Mn-MNP-PCP before fluoride adsorption and Figure 5.15b Mn-MNP-PCP after fluoride adsorption; there was a change in aggregation and morphology of the surface area. By comparing the surface morphology and the particle size of La-MNP-PCP before and after fluoride adsorption in Figure 5.15c and 5.15d, the structure surface had significantly changed after adsorption of fluoride.

EDS was performed to analyze the element compositions on the samples surface before and after adsorption, and the elemental compositions are shown in Table 5.9a and b. The results are the adsorbent surface points and are not average content.

Table. 5.9 a shows the energy dispersive X-ray (EDX) analysis micrograph of Mn-MNP-PCP and La-MNP-PCP before and after nitrate ion adsorption. The elements C, O, Fe, Mn and C, O, Fe, La, were detected from Mn-MNP-PCP and La-MNP-PCP before and after nitrate adsorption

There was an apparent nitrate content in the composition after adsorption in both adsorbents elemental composition, which confirmed nitrate adsorption.

The elemental composition of Mn, C, O and Fe and La, C, O and Fe appeared in the EDS spectrum of Mn-MNP-PCP and La-MNP-PCP before fluoride adsorption. A new fluoride element appeared in the EDX of Mn-MNP-PCP and La-MNP-PCP after fluoride adsorption in Table 5.9b, which illustrated that adsorbent materials were efficient for the fluoride ion adsorption.

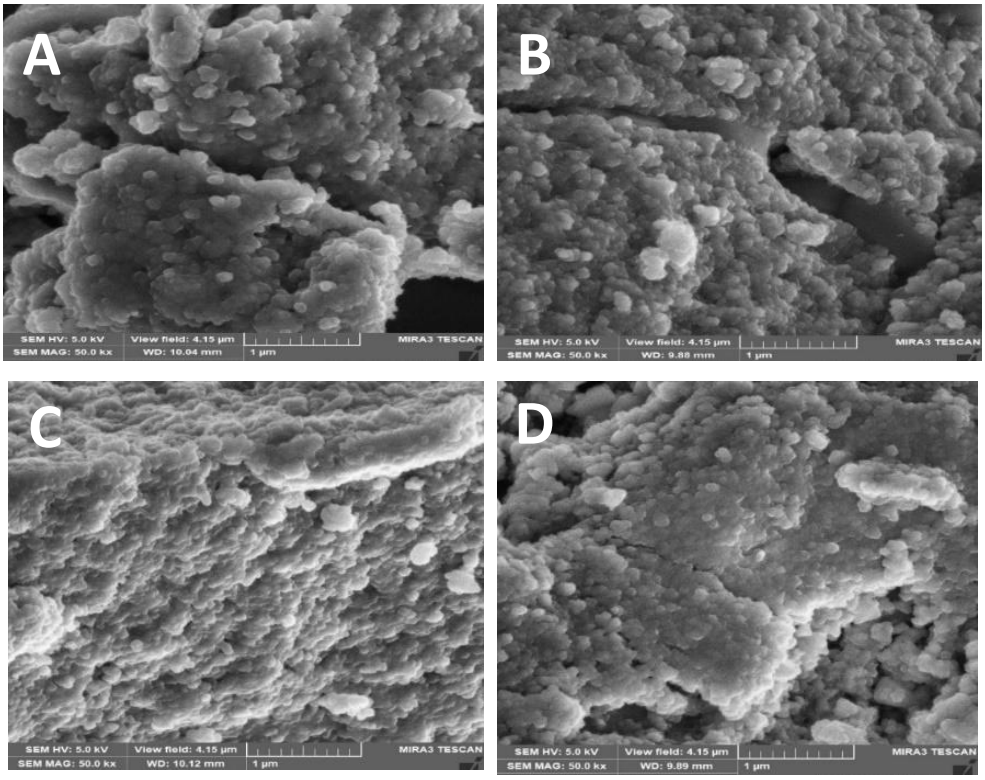

Figure 5.14: SEM images of (a) Mn-MNP-PCP before and (b) Mn-MNP-PCP after nitrate adsorption; (c) La-MNP-PCP before and (d) La-MNP-PCP after nitrate adsorption.

Table 5.9a: EDX micrographs of Mn-MNP-PCP and La-MNP-PCP before and after nitrate absorption

	Weight (%)						
	C	O	Fe	Mn	La	N	Total
Mn-MNP-PCP (Before)	28.59	43.99	25.73	1.69			100
Mn-MNP-PCP (After)	21.72	39.78	24.78	2.06		11.7	100
La-MNP-PCP (Before)	32.92	42.24	20.54		4.3		100
La-MNP-PCP (After)	29.08	31.55	18.54		3.19	17.6	100

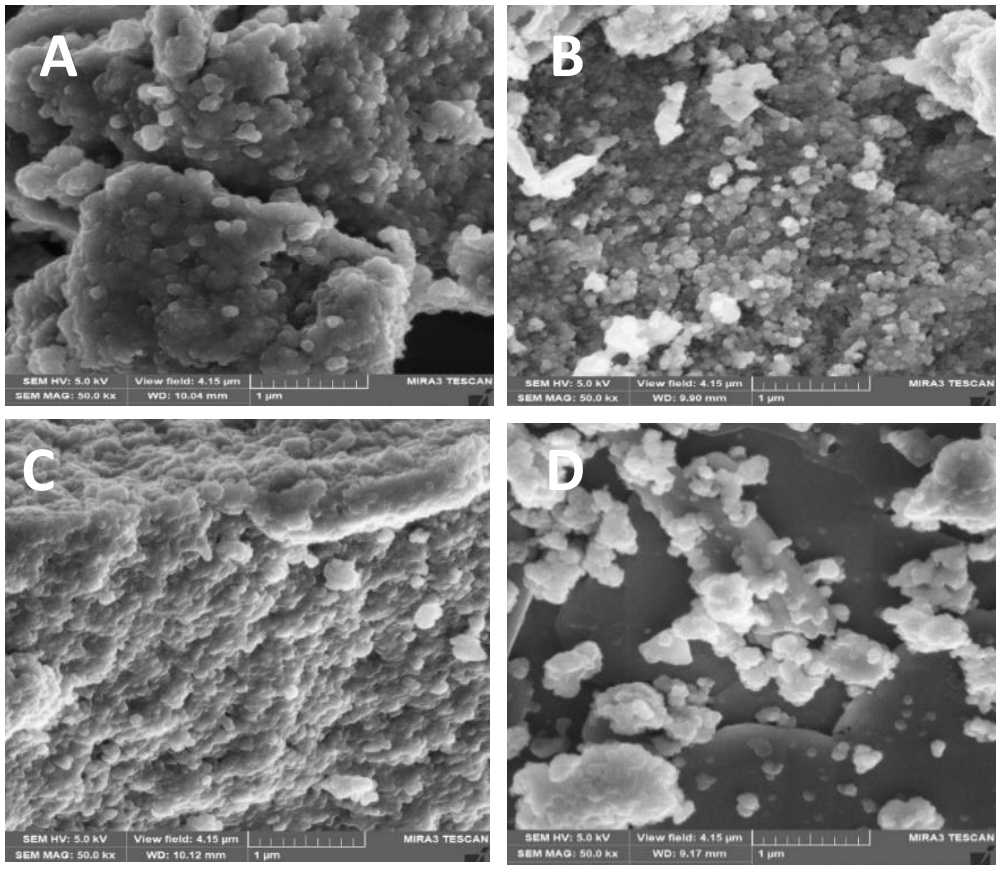

Figure 5.15: SEM images of (a) Mn-MNP-PCP before, (b) Mn-MNP-PCP after fluoride adsorption, (c) La-MNP-PCP before and (d) La-MNP-PCP after fluoride adsorption.

Table 5.9b: EDX micrographs of Mn-MNP-PCP and La-MNP-PCP before and after fluoride adsorption

	Weight (%)						
	C	O	Fe	Mn	La	F	Total
Mn-MNP-PCP (Before)	28.59	43.99	25.73	1.69			100
Mn-MNP-PCP (After)	22.49	38.56	24.78	1.95		12.2	100
La-MNP-PCP (Before)	32.92	42.24	20.54		4.3		100
La-MNP-PCP (After)	25.76	34.37	17.43		2.22	20.2	100

5.10 COMPARISON OF Mn-MNP-PCP AND La-MNP-PCP WITH OTHER FABRICATED ADSORBENTS ON NITRATE AND FLUORIDE ADSORPTION

Adsorption study from various literature of different adsorbent on nitrate and fluoride was shown in Table 5.10 a-b. The comparison was done based on adsorbent dosage, contact time, and adsorption capacity used for nitrate and fluoride adsorption with the various adsorbent.

It was evident that Lanthanum-modified activated carbon was superior to the majority of the adsorbents along with newly synthesized Mn-MNP-PCP and La-MNP-PCP used in this study reported in Table 5.10 a. Even though literature indicates that Lanthanum-modified activated carbon did not use the same materials and synthesis process. Synthesized Mn-MNP-PCP and La-MNP-PCP adsorbents had a relatively high sorption capacity compared to Fe_3O_4 dispersed on Douglas fir biochar and graphene oxide-induced boron-doped iron oxide adsorbents.

Table 5.10b indicates that manganese carbonate ($MnCO_3$) had a better adsorption capacity on fluoride removal than other adsorbents, including the current Mn-MNP-PCP and La-MNP-PCP adsorbents, respectively. Although Mn-MNP-PCP and La-MNP-PCP had lower maximum adsorption capacity, the adsorption capacity was sufficient for F^- adsorption and the percentage F^- removal was above 92 % at evaluated pH values (2‑12). Therefore Mn-MNP-PCP and La-MNP-PCP were found to be comparable with other adsorbents for both nitrate and fluoride adsorption.

Table 5.10a: Comparison of different adsorption capacities of different adsorbents for nitrate removal

Adsorbent	pH	Initial nitrate (mg/L)	Adsorption capacity (mg/g)	Reference
Organic-modified aluminum-manganese bimetal oxide (OABO)	6	2	56.65	Wu *et al*., (2019)
Synthetic activated carbon magnetic nanoparticles (MNP)	3	50	17.1	(Rezaei Kalantary et al., 2016)
Lanthanum hydroxide doped-magnetic reduced graphene oxide (MG@La)	6	20	64	Nodeh *et al*., (2017)
Lanthanum-modified activated carbon	7	50	40	Huong *et al*., (2019)
Graphene oxide-induced boron-doped iron oxide	5	20	20	Han *et al*., (2020)
Mn-MNP-PCP	4	50	22.8	Present Study
La-MNP-PCP	4	50	37.5	Present Study

Table 5.10b: Comparison of different adsorption capacities of different adsorbents for fluoride removal

Adsorbent	pH	Initial fluoride (mg/L)	Adsorption capacity (mg/g)	Reference
MnO_2 coated Na bentonite	8	5	2.4	Mudzielwana *et al*., (2017)
Fe-La composite oxide (MG@La)	6	10	4.98	Wang *et al*., (2018)
Manganese Carbonate (MnCO3)	7	100	46.8	Zhang and Jia, (2018)
Removal of fluoride ions using a polypyrrole magnetic nanocomposite influenced by a rotating magnetic field	6	10	37.2	(Aigbe et al., 2019)

Lanthanum-doped nanocomposites (La@MgAl)	6	50	51.03	Kong *et al*., (2019)
Iron oxide nanoparticles modified with ionic liquid (IL-iron oxide)	7	10	22	Pillai *et al*., (2020)
Mn-MNP-PCP	2	50	46.2	Present Study
La-MNP-PCP	2	50	44.7	Present Study

5.11 CONCLUSION

Application of the synthesized La-MNP-PCP and Mn-MNP-PCP nanocomposites and their comparison for the removal of both nitrate and fluoride is well reported in this chapter. From batch adsorption optimization study, the optimum pH for the adsorption of nitrate onto both adsorbents was found to be pH 4, respectively, with the maximum adsorption capacity of 22.8 mg/g and 37.5 mg/g on nitrate uptake. The maximum fluoride's adsorption using La-MNP-PCP and Mn-MNP-PCP nanocomposites was optained at pH 2, with the 46.20 mg/g and 44.77 mg/g adsorption capacity. The optimum adsorbent dosage was determined as 0.1 g/dm^3 for both Mn-MNP-PCP and La-MNP-PCP adsorbents. The experimental data fitted well with pseudo-second-order kinetic model in all nitrate and fluoride experiments by both Mn-MNP-PCP and La-MNP-PCP. The Langmuir isotherm described the experimental results better than other isotherm models on both nitrate and fluoride adsorption.

Thermodynamic study suggests that nitrate adsorption is favourable, endothermic and stable in terms of binding energy with all nanocomposites. Adsorption of fluoride onto Mn-MNP-PCP nanocomposite was spontaneous, endothermic and accompanied with an increase in entropy. On the hand fluoride adsorption onto La-MNP-PCP was exothermic and the adsorption process is unfavourable at as you increase the temperature. The reduction in adsorption capacity of nitrate was found to be highest for phosphate and sulphate, while the presence of carbonate and chloride had positive nitrate adsorption onto both Mn-MNP-PCP and La-MNP-PCP nanocomposites. The presence of all competitive ions significantly decreased the fluoride adsorption onto Mn-MNP-PCP and La-MNP-PCP nanocomposites. FTIR, SEM and EDX were used to elucidate adsorption

mechanism, the results showed that the adsorbents could be utilised for the adsorption of nitrate and fluoride.

This study suggests that the La-MNP-PCP adsorbent is an effective adsorbent for the nitrate adsorption and Mn-MNP-PCP is an effective adsorbent for the fluoride adsorption from aqueous solution.

5.12 REFERENCES

AIGBE, U. O., ONYANCHA, R. B., UKHUREBOR, K. E. & OBODO, K. O. 2019. Removal of fluoride ions using a polypyrrole magnetic nanocomposite influenced by a rotating magnetic field. Rsc Advances, 10, 595-609.

BHATNAGAR, A., KUMAR, E. & SILLANPÄÄ, M. 2010. Nitrate removal from water by nano-alumina: Characterization and sorption studies. *Chemical Engineering Journal,* 163**,** 317-323.

BHAUMIK, R. & MONDAL, N. K. 2016. Optimizing adsorption of fluoride from water by modified banana peel dust using response surface modelling approach. *Applied Water Science,* 6**,** 115-135.

DEWAGE, N. B., LIYANAGE, A. S., PITTMAN JR, C. U., MOHAN, D. & MLSNA, T. 2018. Fast nitrate and fluoride adsorption and magnetic separation from water on α-Fe_2O_3 and Fe_3O_4 dispersed on Douglas fir biochar. *Bioresource Technology,* 263**,** 258-265.

EL-MEKKAWI, D. M., IBRAHIM, F. A. & SELIM, M. M. 2016. Removal of methylene blue from water using zeolites prepared from Egyptian kaolins collected from different sources. *Journal of Environmental Chemical Engineering,* 4**,** 1417-1422.

ESMAEILI BIDHENDI, M., ASADI, Z., BOZORGIAN, A., SHAHHOSEINI, A., GABRIS, M. A., SHAHABUDDIN, S., KHANAM, R. & SAIDUR, R. 2020. New magnetic Co_3O_4/Fe_3O_4 doped polyaniline nanocomposite for the effective and rapid removal of nitrate ions from ground water samples. *Environmental Progress & Sustainable Energy,* 39**,** 13306.

FAN, C. & ZHANG, Y. 2018. Adsorption isotherms, kinetics and thermodynamics of nitrate and phosphate in binary systems on a novel adsorbent derived from corn stalks. *Journal of Geochemical Exploration,* 188**,** 95-100.

HAFSHEJANI, L. D., HOOSHMAND, A., NASERI, A. A., MOHAMMADI, A. S., ABBASI, F. & BHATNAGAR, A. 2016. Removal of nitrate from aqueous solution by modified sugarcane bagasse biochar. *Ecological Engineering,* 95**,** 101-111.

HAN, L., LI, B., TAO, S., AN, J., FU, B., HAN, Y., LI, W., LI, X., PENG, S. & YIN, T. 2020. Graphene oxide-induced formation of a boron-doped iron oxide shell on the surface of NZVI for enhancing nitrate removal. *Chemosphere***,** 126496.

HU, Q., CHEN, N., FENG, C. & HU, W. 2015. Nitrate adsorption from aqueous solution using granular chitosan-Fe_3^+ complex. *Applied Surface Science,* 347**,** 1-9.

HU, Q., LIU, Y., FENG, C., ZHANG, Z., LEI, Z. & SHIMIZU, K. 2018. Predicting equilibrium time by adsorption kinetic equations and modifying Langmuir isotherm by fractal-like approach. *Journal of Molecular Liquids,* 268**,** 728-733.

HUONG, P. T., JITAE, K., GIANG, B. L., NGUYEN, T. D. & THANG, P. Q. 2019. Novel lanthanum-modified activated carbon derived from pine cone biomass as ecofriendly bio-sorbent for removal of phosphate and nitrate in wastewater. *Rendiconti Lincei. Scienze Fisiche e Naturali,* 30**,** 637-647.

ISAGBA, E., KADIRI, S. & ILABOYA, I. 2017. Yam Peels as Adsorbent for the Removal of Copper (Cu) and Manganese (Mn) in Waste Water. *Nigerian Journal of Environmental Sciences and Technology (NIJEST) Vol,* 1**,** 28-41.

KALARUBAN, M., LOGANATHAN, P., SHIM, W., KANDASAMY, J., NAIDU, G., NGUYEN, T. V. & VIGNESWARAN, S. 2016. Removing nitrate from water using iron-modified Dowex 21K XLT ion exchange resin: Batch and fluidised-bed adsorption studies. *Separation and Purification Technology,* 158**,** 62-70.

KARTHIKEYAN, P., BANU, H. A. T. & MEENAKSHI, S. 2019. Synthesis and characterization of metal loaded chitosan-alginate biopolymeric hybrid beads for the efficient removal of phosphate and nitrate ions from aqueous solution. *International Journal of Biological Macromolecules,* 130**,** 407-418.

KONG, L., TIAN, Y., PANG, Z., HUANG, X., LI, M., YANG, R., LI, N., ZHANG, J. & ZUO, W. 2019. Synchronous phosphate and fluoride removal from water by 3D rice-like lanthanum-doped La@ MgAl nanocomposites. *Chemical Engineering Journal,* 371**,** 893-902.

LAGERGREN, S. 1898. Zur theorie der sogenannten adsorption gelöster stoffe, Kungliga Svenska Vetenskapsakademiens. *Handlingar,* 24**,** 1-39.

LI, L., ZHU, Q., MAN, K. & XING, Z. 2017. Fluoride removal from liquid phase by Fe-Al-La trimetal hydroxides adsorbent prepared by iron and aluminum leaching from red mud. *Journal of Molecular Liquids,* 237**,** 164-172.

LIU, Q., HU, P., WANG, J., ZHANG, L. & HUANG, R. 2016. Phosphate adsorption from aqueous solutions by Zirconium (IV) loaded cross-linked chitosan particles. *Journal of the Taiwan Institute of Chemical Engineers,* 59**,** 311-319.

MIN, X., WU, X., SHAO, P., REN, Z., DING, L. & LUO, X. 2019. Ultra-high capacity of lanthanum-doped UiO-66 for phosphate capture: Unusual doping of lanthanum by the reduction of coordination number. *Chemical Engineering Journal,* 358**,** 321-330.

NABBOU, N., BELHACHEMI, M., BOUMELIK, M., MERZOUGUI, T., LAHCENE, D., HAREK, Y., ZORPAS, A. A. & JEGUIRIM, M. 2019. Removal of fluoride from groundwater using natural clay (kaolinite): Optimization of adsorption conditions. *Comptes Rendus Chimie,* 22**,** 105-112.

NAGARAJ, A., SADASIVUNI, K. K. & RAJAN, M. 2017. Investigation of lanthanum impregnated cellulose, derived from biomass, as an adsorbent for the removal of fluoride from drinking water. *Carbohydrate Polymers,* 176**,** 402-410.

NODEH, H. R., SERESHTI, H., AFSHARIAN, E. Z. & NOURI, N. 2017. Enhanced removal of phosphate and nitrate ions from aqueous media using nanosized lanthanum hydrous doped on magnetic graphene nanocomposite. *Journal of Environmental Management,* 197**,** 265-274.

RAJESWARI, A., AMALRAJ, A. & PIUS, A. 2016. Adsorption studies for the removal of nitrate using chitosan/PEG and chitosan/PVA polymer composites. *Journal of Water Process Engineering,* 9**,** 123-134.

REZAEI KALANTARY, R., DEHGHANIFARD, E., MOHSENI-BANDPI, A., REZAEI, L., ESRAFILI, A., KAKAVANDI, B. & AZARI, A. 2016. Nitrate adsorption by synthetic activated carbon magnetic nanoparticles: kinetics, isotherms and thermodynamic studies. *Desalination and Water Treatment,* 57**,** 16445-16455.

SALEH, T. A., ADIO, S. O., ASIF, M. & DAFALLA, H. 2018. Statistical analysis of phenols adsorption on diethylenetriamine-modified activated carbon. *Journal of Cleaner Production,* 182**,** 960-968.

SOBEIH, M. M., EL-SHAHAT, M., OSMAN, A., ZAID, M. & NASSAR, M. Y. 2020. Glauconite clay-functionalized chitosan nanocomposites for efficient adsorptive removal of fluoride ions from polluted aqueous solutions. *RSC Advances,* 10**,** 25567-25585.

TANG, D. & ZHANG, G. 2016. Efficient removal of fluoride by hierarchical Ce–Fe bimetal oxides adsorbent: thermodynamics, kinetics and mechanism. *Chemical Engineering Journal,* 283**,** 721-729.

WANG, J., WU, L., LI, J., TANG, D. & ZHANG, G. 2018. Simultaneous and efficient removal of fluoride and phosphate by Fe-La composite: Adsorption kinetics and mechanism. *Journal of Alloys and Compounds,* 753**,** 422-432.

WU, K., LI, Y., LIU, T., HUANG, Q., YANG, S., WANG, W. & JIN, P. 2019. The simultaneous adsorption of nitrate and phosphate by an organic-modified aluminum-manganese bimetal oxide: adsorption properties and mechanisms. *Applied Surface Science,* 478**,** 539-551.

ZHANG, Y.-X. & JIA, Y. 2018. Fluoride adsorption on manganese carbonate: Ion-exchange based on the surface carbonate-like groups and hydroxyl groups. *Journal of Colloid and Interface Science,* 510**,** 407-417.

ZHANG, Y., LIN, X., ZHOU, Q. & LUO, X. 2016. Fluoride adsorption from aqueous solution by magnetic core-shell Fe_3O_4@ alginate-La particles fabricated via electro-coextrusion. *Applied Surface Science,* 389**,** 34-45.

6. CONCLUSION AND RECOMMENDATIONS

Doping of Magnetite pinecone powder nanocomposite by manganese and lanthanum was examined in the study. The doped magnetite pinecone nanocomposite adsorbents were applied in the adsorption of nitrate and fluoride. The conclusion of the findings of the present research are summarised, and some recommendations for future work are proposed

6.1 CONCLUSION

The global health issue that affects all kinds of living organisms is the excessive release of water toxins such as nitrate and fluoride into natural habitats and marine environments. Numerous techniques have been reported in the research for wastewater treatment, and adsorption has been recognized as the ideal procedure that minimizes the contamination while being environmentally friendly and efficient. Adsorption uses adsorbents that can be extracted from various materials to ensure effectiveness and reduce the cost of treatment. Different types of new adsorbents for the removal of water contaminants have been developed so far, especially composites made of metal oxide or hydroxide that are incorporated into the surface or into a porous support material channel.

The main goal of this study was to dope magnetite incorporated pinecone adsorbent with La and Mn material/s using co-precipitation method. The doped nanocomposites were investigated for its possible adsorption application. The most appropriate parameters were examined to obtain the material's highest performance to remove nitrate and fluoride from aqueous samples.

The magnetite pinecone nanocomposite was successfully doped with manganese and lanthanum. The materials were also duly characterized with FTIR, TGA, XRD, TEM, SEM and EDX. The TEM images showed that all adsorbent materials were spherical. SEM and EDS showed the homogeneity of the synthesised spherical nanocomposites and the successful incorporation of the lanthanum and manganese into the pinecone nanocomposite. The pHpzc of magnetite pinecone nanocomposite decrease after doping of manganese and lanthanum. The pHpzc was 6.3 for the magnetite pinecone nanocomposite, 6 for manganese doped magnetite pinecone nanocomposite composite and 5.4 for lanthanum magnetite pinecone nanocomposite.

Mn-MNP-PCP and La-MNP-PCP were successfully applied for the adsorption of nitrate and fluoride. The optimum pH for the adsorption of nitrate and fluoride was determined to be pH 4 for nitrate and pH 2 for fluoride. La-MNP-PCP gave the highest adsorption capacity for nitrate and Mn-MNP-PCP gave the highest adsorption capacity for fluoride.

Pseudo second-order model better fitted the adsorption kinetics processes of the nitrate and fluoride. Adsorption of NO_3^- and F^- ions at temperatures between 298 to 318 K and 299 to 318 K showed that adsorption was more favourable on Mn-MNP-PCP for nitrate and La-MNP-PCP adsorbent, respectively. The Langmuir isotherm model better predicted the equilibrium data of nitrate and fluoride adsorption by all adsorbents. The results indicated that monolayer and homogeneous adsorption governed the adsorption processes. The separation factor findings suggested that the removal of NO_3^- and F^- ions onto both adsorbent materials were favourable.

Thermodynamic data indicated that the nitrate adsorption processes were endothermic and spontaneous for both adsorbents. The results also show that the spontaneity was more for La-MNP-PCP than for Mn-MNP-PCP for nitrate adsorption. fluoride adsorption processes were endothermic and spontaneous for Mn-MNP-PCP and unfavourable and non-spontaneous at a higher temperature for La-MNP-PCP.

This study results offer a new strategy to tune the properties of doped metal oxides and other environmental materials to develop high efficient adsorbent for the treatment of wastewater samples by selective adsorption of nitrate and fluoride pollutants in water bodies.

RECOMMENDATIONS

Based on this research's findings, further work may be carried out to continue the scientific development and generation of knowledge about environmental remediation. Adsorption of real wastewater from industries should be evaluated on the adsorbent materials to assess their adsorption properties in the presence of multiple pollutants. The use of other synthesis methods, such as thermal decomposition, and microemulsion could, therefore, be investigated to synthesize the manganese-doped magnetite-coated pinecone and lanthanum-doped magnetite-coated pinecone composite. Column adsorption (or continuous fixed-bed column) studies may also be carried out to improve the adsorption process and better utilize the adsorbent materials. A few of the continuous fixed-bed column advantages over the batch adsorption include the use of small adsorbent mass (mg/g), little or no adsorbent wastage since the absorbate solution flows through

the bed without changing at different concentrations during adorption-desorption stage, probable removal of these anions below threshold levels before the adsorbent is disposed, among others. More kinetic models and isotherms may be conducted to better understand the adsorption mechanism for all pollutants investigated. The models include intraparticle diffusion and Elovish fittings. The intraparticle diffusion and Elovish models have been widely applied to model kinetic uptake of nitrate and fluoride ions unto surfaced metal-functionalised adsorbents in aqueous solutions as in this study. Both models can be used to confirm the diffusive probability of ntrae and fluoride ions unto the adsorbent and activation energy for chemisorption vacant site if the model will be suitable as pseudo-second order.